

**DESIGN, MODELING AND ANALYSIS OF LOW
VOLTAGE DC MICROGRID**

BY

AHMAD ABDULAZIZ AL-HARBI

A Dissertation Presented to the
DEANSHIP OF GRADUATE STUDIES

KING FAHD UNIVERSITY OF PETROLEUM & MINERALS

DHAHRAN, SAUDI ARABIA

In Partial Fulfillment of the
Requirements for the Degree of

DOCTOR OF PHILOSOPHY

In

ELECTRICAL ENGINEERING

APRIL, 2018

KING FAHD UNIVERSITY OF PETROLEUM & MINERALS

DHAHRAN- 31261, SAUDI ARABIA

DEANSHIP OF GRADUATE STUDIES

This thesis, written by **Ahmad Abdulaziz Al-Harbi** under the direction of his thesis advisor and approved by his thesis committee, has been presented and accepted by the Dean of Graduate Studies, in partial fulfillment of the requirements for the degree of **DOCTOR OF PHILOSOPHY IN ELECTRICAL ENGINEERING.**



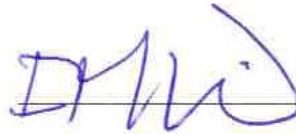
Dr. Ali Al-Shaikhi
Department Chairman



Dr. Salam A. Zummo
Dean of Graduate Studies



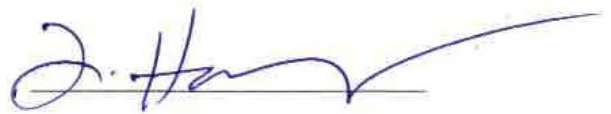
10/5/18
Date



Dr. Ibrahim ElAmin
(Advisor)



Dr. Mohammad Abido
(Member)



Dr. Zakariya Al-Hamouz
(Member)



Dr. Ibrahim Habiballah
(Member)



Dr. Mahmoud Kassas
(Member)

© Ahmad Abdulaziz Al-Harbi

2018

إهداء

إلى والديّ الغاليين .. أسأل الله أن يحفظكما .. و يطيل أعماركما على طاعته ..

إلى زوجتي العزيزة .. التي كانت عوناً لي بعد الله لإنجاز هذا العمل ..

إلى أبنائي .. أسأل الله أن يحفظكم .. و يصلحكم .. و ينبتكم نباتاً حسناً ..

إلى من أحبّ .. إخواني .. و أخواتي ..

إلى كل من ساندني .. برأي .. أو نصيحة .. أو دعوة صادقة ..

ACKNOWLEDGMENT

First of all, I thank and pray to Allah for his guidance and protection throughout my life, including the years of this study. Peace and blessings of Allah be on his last Messenger, Muhammad.

I would like to thank my parent for their encouragements and support, my wife who was very patient in supporting me to finish this work, and all of my brothers, sisters and friends for their support.

I am very thankful to Royal Commission of Yanbu for giving me this opportunity to continue my higher education.

Acknowledgment is due to King Fahd University of Petroleum & Minerals for making such high quality environment of education and research.

I am deeply indebted to my dissertation advisor Prof. Ibrahim El-Amin for his constant guidance, support, encouragement throughout the course of this research. He made my pursuit of higher education a truly enjoyable and unforgettable experience.

I also wish to thank the other members of my dissertation committee, Dr. Mohammad Abido, Dr. Zakariya Al-Hamouz, Dr. Ibrahim Habiballah and Dr. Mahmoud Kassas for their cooperation, encouragement and help.

Special thanks are to Engr. Sami Al-Alwani for his help in explaining and clarifying to me many issues in PV solar systems.

Lastly but not the least, thanks to everyone helped me by giving any idea, suggestion, support, encouragement and supplication.

TABLE OF CONTENTS

ACKNOWLEDGMENT	v
TABLE OF CONTENTS.....	vi
LIST OF TABLES.....	xii
LIST OF FIGURES.....	xv
LIST OF ABBREVIATIONS.....	xix
ABSTRACT	xx
ملخص الرسالة.....	xxii
CHAPTER 1 INTRODUCTION.....	1
1.1 Overview and Historical Background.....	1
1.2 Dissertation Motivations	2
1.2.1 Emergence of DC Appliances in the Existing Network	2
1.2.2 Use of Variable Speed Drives Motors in Various Household Appliances.....	3
1.2.3 Availability of DC Appliances.....	3
1.2.4 DC Nature of Renewable Energy Sources	4
1.2.5 Proper DC Voltage Selection	4
1.2.6 Energy Saving Opportunities and Cost Analysis.....	4
1.3 Dissertation Objectives	5
1.4 Dissertation Organization.....	6
CHAPTER 2 LITERATURE REVIEW.....	8
2.1 Overview.....	8
2.2 Research on DC Systems and Existing Applications.....	9

2.2.1	Shipboards	9
2.2.2	Data Centers	10
2.2.3	Commercial Facilities	11
2.2.4	Telecommunication	12
2.2.5	Lighting Systems	13
2.3	Analysis of Different Aspects of DC Systems	13
2.3.1	Modeling and Maximum Power Point Tracking of PV systems	14
2.3.2	Modeling of Household Appliances	15
2.3.3	Protection and Fault Analysis in DC Systems	16
2.4	DC Grid Research Challenges	17

CHAPTER 3 MATHEMATICAL MODELS FOR PERFORMANCE CHARACTERIZATION OF PV SYSTEMS 22

3.1	Introduction	22
3.2	EUREQA Software: General Overview [99, 100]	24
3.3	General Mathematical-Based Models for Characterization of PV Module Performance	25
3.3.1	Proposed Methodology	26
3.3.2	Simulation Results and Models Assessment	35
3.4	Application of the Proposed Models for MPPT of PV Systems	50
3.4.1	Proposed MPPT Methodology	51
3.4.2	Study Case#1: Application to 100 kW Grid-Connected PV system [105]	52
3.4.3	Study Case#2: Application to 400 kW Grid-Connected PV system [105]	56
3.5	Summary and Conclusions of the Chapter	60

CHAPTER 4 DEVELOPMENT OF MODELS FOR MAJOR AC AND DC HOUSEHOLD APPLIANCES 62

4.1	Introduction	62
-----	--------------------	----

4.2	Methodology.....	63
4.3	Experimental Set-up and Measurements Process.....	64
4.3.1	AC and DC Appliances under Study	64
4.3.2	Measured Electrical Parameters.....	65
4.3.3	Instrument used in Measurements	65
4.3.4	Process of Measurements	66
4.4	Proposed Modeling Approaches.....	67
4.4.1	Modeling using Mathematical Representation	67
4.4.2	Modeling using Circuit Representation	68
4.5	AC and DC Appliances Models Building	71
4.5.1	Category I: Appliances with Constant Operating Characteristics	71
4.5.2	Category II: Appliances with Pulsating Operating Characteristics	73
4.6	AC and DC Appliances Models Validation and Assessments	80
4.7	Summary and Conclusions of the Chapter	83
 CHAPTER 5 AC AND DC DISTRIBUTION ARCHITECTURES FOR A STANDALONE HOUSE.....		86
5.1	Introduction	86
5.2	Design and Architectures of the Standalone House	87
5.2.1	Layout of the Proposed Standalone House.....	87
5.2.2	DC Appliances Voltage Selection and Specifications.....	88
5.2.3	Proposed Power System Configurations for the Standalone House.....	90
5.3	AC and DC Sources Sizing.....	96
5.3.1	Diesel Generator Sizing	96
5.3.2	PV and Batteries Sizing Approach.....	98
5.4	Peak Sun Hours in Dhahran City	100

5.5	Required Components Preparation and Architectures Sizing.....	101
5.5.1	Sizing, Required Components and Costs of Architecture I	103
5.5.2	Sizing, Required Components and Costs of Architecture II	104
5.5.3	Sizing, Required Components and Costs of Architecture III	106
5.5.4	Sizing, Required Components and Costs of Architecture IV	108
5.6	Energy Saving Opportunities and Capital Cost Analysis	112
5.7	Economic Analysis over the Entire Life Cycle	115
5.7.1	Life Cycle Cost of the PV-Batteries Systems.....	116
5.7.2	Life Cycle Cost of the Diesel Generator Systems.....	117
5.8	Systems Comparisons Based on Total Life Cycle Cost	120
5.9	Sensitivity Analysis	124
5.9.1	Reduction in DC Appliances Prices	124
5.9.2	Increasing Days of Autonomy for PV-Batteries Systems	125
5.9.3	Increasing Diesel Generator Lifespan	127
5.10	Summary and Conclusions of the Chapter	128
 CHAPTER 6 MICROGRID DESIGN: SYSTEM CONFIGURATIONS AND COMPARATIVE STUDY		130
6.1	Introduction	130
6.2	Design of the Power System Network under Study	132
6.2.1	Demand Side.....	132
6.2.2	Supply Side	134
6.2.3	Selection of DC Grid Distribution Voltage.....	135
6.3	Proposed Network Schemes.....	136
6.3.1	System # 1: AC Source Supplying the AC Grid Area.....	136
6.3.2	System # 2: AC Source Supplying the DC Grid Area.....	137

6.3.3	System # 3: DC Source Supplying the AC Grid Area.....	138
6.3.4	System # 4: DC Source Supplying the DC Grid Area	139
6.4	Cost Analysis of the Proposed Schemes.....	140
6.4.1	Cost of Generation Sources	140
6.4.2	Diesel Generator Fuel Consumption Estimation	142
6.4.3	O&M Costs.....	143
6.4.4	Annual Load Profiles for the AC and DC Microgrids	143
6.4.5	Required Land Area for PV Systems	149
6.5	Life Cycle Cost Analysis and Systems Comparisons	149
6.6	Summary and Conclusions of the Chapter	152
CHAPTER 7 PROTECTION SCHEME FOR DC MICROGRID		154
7.1	Introduction	154
7.2	DC Microgrid System Description	155
7.3	Proposed Fault Detection and Locating Methodology and Resultant Mathematical Model.	156
7.4	Simulation Results and Analysis	159
7.4.1	Model Accuracy Verification	159
7.4.2	Online Monitoring and Simulations of the Proposed Protection Scheme	159
7.4.3	System Simulations and Performance under Different Fault Conditions	165
7.5	Summary and Conclusions of the Chapter	174
CHAPTER 8 CONCLUSIONS AND FUTURE WORK		176
8.1	Conclusions	176
8.1.1	Modeling and Control of One of the Essential DC Sources: PV System	176
8.1.2	Modeling of Major AC and DC Home Appliances.....	177
8.1.3	Energy and Cost Assessments for a Standalone House Configurations	177

8.1.4	Proposing a Microgrid with Different Configurations for Analysis and Study	179
8.1.5	Designing a Simple and Efficient Protection Scheme for DC Microgrid	180
8.2	Future Work	180
	REFERENCES.....	182
	APPENDIX.....	196
	VITAE	199

LIST OF TABLES

Table 3.1: Ten key points on I-V curve to be predicted	26
Table 3.2: Input and output variables employed in the proposed models	28
Table 3.3: Specifications of PV modules selected in training process	30
Table 3.4: Impact of changing operators on the accuracy of maximum power models ...	33
Table 3.5: PV modules specifications selected for models assessments	36
Table 3.6: Selected commercial PV modules employed in models assessment	42
Table 3.7: PV module specifications at STC used in [102] for methods assessments	46
Table 3.8: Measured maximum power data at different conditins [102].....	47
Table 3.9: Maximum power evaluation using the proposed model and [102]	47
Table 3.10: Measured maximum power values at different conditions [103]	48
Table 3.11: Maximum power evaluation using the proposed model and [103]	48
Table 3.12: PV module specifications at STC used in [104] for methods assessments ...	49
Table 3.13: Parameters evaluation using the proposed model and [104]	50
Table 4.1: Specifications of the appliances under study.....	65
Table 4.2: Measurements duration of the appliances under study.....	67
Table 4.3: Power and current values for mathematical models of category I appliances.	72
Table 4.4: Circuit elements values for appliances under category I.....	73
Table 4.5: Circuit elements values for category II AC appliances	79
Table 4.6: Circuit elements values for category II DC appliances	80
Table 4.7: Proposed models performance compared to the measurements (category I) ..	82
Table 4.8: Air conditioners and refrigerators energy comparisons to measurements.....	83
Table 5.1: Appliances locations in the proposed standalone house.....	88

Table 5.2: Appliances common DC voltage levels available in the market	89
Table 5.3: System DC voltages based on 100 A maximum current [109]	89
Table 5.4: Specifications of the selected appliances.....	90
Table 5.5: Common daily load profile for all configurations	102
Table 5.6: Power and energy characteristics of all appliances for architecture I	103
Table 5.7: Diesel generator specifications selected for configuration I.....	104
Table 5.8: Costs of all components required for architecture I.....	104
Table 5.9: Power and energy characteristics of all appliances for architecture II	105
Table 5.10: Diesel generator specifications selected for configuration II	106
Table 5.11: AC/DC converters specifications selected for configuration II.....	106
Table 5.12: Costs of all components required for architecture II	106
Table 5.13: Selected inverter specifications for configuration III	107
Table 5.14: Specifications of the selected PV module and battery for architecture III ..	108
Table 5.15: Costs of all components required for architecture III.....	108
Table 5.16: Power and energy characteristics of all appliances for architecture IV.....	109
Table 5.17: Selected PV module and battery data for architecture IV (48 V _{DC} system)	109
Table 5.18: Selected charge controller data for configuration IV (48 V _{DC} system).....	110
Table 5.19: Selected PV module and battery data for architecture IV (12 V _{DC} system)	111
Table 5.20: Selected charge controller data for configuration IV (12 V _{DC} system).....	111
Table 5.21: DC-DC converters required for configuration IV (12 V _{DC} system).....	111
Table 5.22: Costs of all components required for architecture IV	112
Table 5.23: Total energy consumption and capital cost summary of all configurations	113
Table 5.24: Fuel consumption in liters per hour at different loading conditions.....	119

Table 5.25: Parameters values used in total cost calculations	121
Table 5.26: Life cycle costs of all configurations.....	121
Table 6.1: Specifications of the selected 200 kW diesel generator	136
Table 6.2: Specifications of the selected 140 kW diesel generator	137
Table 6.3: Cost of all components of the AC and DC microgrids at supply side.....	141
Table 6.4: Approximate fuel consumption based on generator size and loading [137] .	142
Table 6.5: Cost of all components of the AC and DC microgrids at supply side.....	143
Table 6.6: Total generation costs for systems 1 and 2 for the first year	149
Table 6.7: Total life cycle cost calculations for systems 1 and 2	150
Table 6.8: Total life cycle cost calculations for systems 3 and 4	150
Table 6.9: Diesel prices of GCC countries in 2018 [142].....	151
Table 7.1: Parameters values of the DC microgrid components	156
Table 7.2: Sample data collected from SIMULINK simulations	157
Table 7.3: Results of model testing at new input data	159

LIST OF FIGURES

Figure 3.1: Basic function of EUREQA	24
Figure 3.2: Summary of steps followed in EUREQA to build mathematical models	25
Figure 3.3: The ten key points on the I-V curve	27
Figure 3.4: Summary of proposed methodology for building the predictive models	29
Figure 3.5: Temperature and irradiance points adopted in training process	31
Figure 3.6: Steps of mathematical operators adjustments and selecting the best model ..	32
Figure 3.7: I-V curves of PV module # 1 at the indicated weather conditions	37
Figure 3.8: I-V curves of PV module # 2 at the indicated weather conditions	37
Figure 3.9: I-V curves of PV module # 3 at the indicated weather conditions	38
Figure 3.10: I-V curves of PV module # 4 at the indicated weather conditions	38
Figure 3.11: I-V curves of PV module # 5 at the indicated weather conditions	39
Figure 3.12: I-V curves of PV module # 6 at the indicated weather conditions	39
Figure 3.13: I-V curves of PV module # 7 at the indicated weather conditions	40
Figure 3.14: I-V curves of PV module # 8 at the indicated weather conditions	40
Figure 3.15: I-V curves of PV module # 9 at the indicated weather conditions	41
Figure 3.16: I-V curves of PV module # 10 at the indicated weather conditions	41
Figure 3.17: I-V curves of 245 W S-energy module:(a) T=25°C and different G (b) G=1000 W/m ² and different T	43
Figure 3.18: I-V curves of 305 W SunPower module:(a)T=25°C and different G	
(b) G=1000 W/m ² and different T	44
Figure 3.19: I-V curves of 425 W SunPower module:(a) T=25°C and different G (b) G=1000 W/m ² and different T	45

Figure 3.20: Proposed MPPT algorithm	52
Figure 3.21: Scheme of the 100 kW grid-connected PV system	53
Figure 3.22: Temperature and irradiance profiles applied to the 100 kW system.....	54
Figure 3.23: proposed model and INC: (a) complete profiles (b) extracted period.....	55
Figure 3.24: Scheme of the 400 kW grid-connected PV system	56
Figure 3.25: Temperature and irradiance profiles for each PV array	58
Figure 3.26: Extracted maximum power profiles for each PV array	59
Figure 3.27: Extracted maximum power for the entire system:.....	60
Figure 4.1: Parallel <i>RLC</i> circuit used for appliances models.....	69
Figure 4.2: Evaluated circuit elements for the AC TV	73
Figure 4.3: Power profiles for the air conditioners and refrigerators	75
Figure 4.4: AC air conditioner SIMULINK model using circuit representation	79
Figure 4.5: AC fan power: (a) complete power profile (b) extracted interval.....	81
Figure 4.6: AC air conditioner power: (a) complete power profile (b) extracted period..	81
Figure 4.7: DC air conditioner: (a) complete power profile (b) extracted interval.....	82
Figure 5.1: Standalone house AC appliances supplied by AC source	91
Figure 5.2: Standalone house DC appliances supplied by AC source	92
Figure 5.3: Experimental set up for AC-DC configuration (DC air conditioner case).....	93
Figure 5.4: Standalone house AC appliances supplied by DC source	94
Figure 5.5: Standalone house DC appliances supplied by DC source	95
Figure 5.6: Experimental set up for DC-DC configuration (12 V _{DC} appliances case)	96
Figure 5.7: Peak sun hours variation per month for Dhahran [125]	101
Figure 5.8: Energy and capital cost comparison of all architectures	113

Figure 5.9: Components cost summary of the DC system: (a) components contribution (b) appliances contribution in total appliances cost.....	115
Figure 5.10: Fuel consumption trend for the 2 kW generator.....	119
Figure 5.11: Fuel consumption trend for the 3 kW generator.....	120
Figure 5.12: Life cycle costs comparisons for all configurations.....	121
Figure 5.13: Capital and future expenses comparison	122
Figure 5.14: Contribution of capital and future expenses in total life cycle cost	123
Figure 5.15: (a) Impact of reduction in DC appliances prices (b) life cycle costs at equal AC and DC appliances prices	125
Figure 5.16: (a) Impact of days of autonomy variation (b) life cycle costs at four days of autonomy.....	126
Figure 5.17: (a) Impact of diesel generator lifespan variation (b) life cycle costs at 5-year lifespan.....	128
Figure 6.1: Electrical layout of the proposed DC house.....	133
Figure 6.2: Hourly load profile of the AC load area.....	133
Figure 6.3: Hourly load profile of the DC load area.....	134
Figure 6.4: Layout of the diesel generator supplying the AC grid load area.....	137
Figure 6.5: Layout of the diesel generator feeding the DC grid load area.....	138
Figure 6.6: Layout of the PV array and battery bank supplying the AC grid load area .	139
Figure 6.7: Layout of the PV array and battery bank feeding the DC grid load area	140
Figure 6.8: Cost comparisons of supply side components.....	141
Figure 6.9: Hourly load profile for a residential area in Dhahran, 2005 [138].....	144
Figure 6.10: Load profiles at the designated hours for the area in Dhahran, 2005 [138]	145

Figure 6.11: Percent profiles at hours 12.00-15.00 with respect to the peak load value	146
Figure 6.12: Scaled AC load profiles for the hours 12.00-15.00	146
Figure 6.13: Scaled DC load profiles for the hours 12.00-15.00	147
Figure 6.14: Final hourly load profiles over the year (a) AC town (b) DC town	148
Figure 6.15: Life cycle costs comparison for all proposed configurations	150
Figure 6.16: Life cycle cost comparisons for GCC countries for all proposed schemes	152
Figure 7.1: Layout of the DC microgrid under study	155
Figure 7.2: Single line diagram of the DC microgrid under study	156
Figure 7.3: SIMULINK model of the DC microgrid protection scheme for one feeder	161
Figure 7.4: Algorithm of the IGBTs switching and controlling block	162
Figure 7.5: Proposed protection scheme process	163
Figure 7.6: Complete DC microgrid incorporated with proposed protection scheme	164
Figure 7.7: Fault distance evaluation under fault at feeder # 4 (case # 1)	167
Figure 7.8: Response of the signals sent to the IGBT's (case # 1)	168
Figure 7.9: Load supplied by each feeder (case # 1)	169
Figure 7.10: Total load supplied by the main generation source (case # 1)	170
Figure 7.11: Fault distance evaluation under faults at feeders # 2 and 5 (case # 2)	171
Figure 7.12: Response of the signals sent to the IGBTs (case # 2)	172
Figure 7.13: Load supplied by each feeder (case # 2)	173
Figure 7.14: Total load supplied by the main generation source (case # 2)	174

LIST OF ABBREVIATIONS

DG	:	Distributed Generation
GCC	:	Gulf Cooperation Council
INC	:	Incremental Conductance
LED	:	Light Emitting Diode
LVDC	:	Low Voltage DC
MPPT	:	Maximum Power Point Tracking
MVDC	:	Medium Voltage DC
P&O	:	Perturb and Observe
PV	:	Photovoltaic Panel
STC	:	Standard Test Conditions
VSD	:	Variable Speed Drive

ABSTRACT

Full Name : Ahmad Abdulaziz Al-Harbi
Thesis Title : Design, Modeling and Analysis of Low Voltage DC Microgrid
Major Field : Electrical Engineering
Date of Degree : April, 2018

In recent years, DC distribution systems have gained a special attention by various research studies. This dissertation discusses the design, modeling and analysis of a low voltage DC microgrid involving different DC sources and DC appliances. Mathematical-based models are first proposed to predict the maximum power parameters and the I-V curves for any PV module by just the knowledge of the module data sheet and temperature and irradiance values. The models are then employed for tracking the maximum power of PV systems under different weather conditions. The models effectiveness is compared with SIMULINK simulations, commercial PV module specifications from data sheet and with some published research. The proposed models have shown more efficient performance in parameters estimation and computation time than the other reported algorithms. Having modeled the DC source, major household AC and DC appliances are then adopted in this dissertation for analysis and study. Two approaches are proposed for the modeling. The simulation results are compared with the experimental data and the models effectiveness has been verified.

Four configurations for a small standalone house have been proposed in this study. The configurations represent complete AC system, complete DC system and two hybrid systems. The configurations are extensively analyzed and compared in terms of energy assessments and life cycle cost analysis. The results have shown that the complete DC

system has shown promising results for energy and money savings over a life cycle of 20 years.

The idea of this small house is then generalized to build a complete microgrid representing a small town of 100 houses. The life cycle cost of the DC system is also compared with different schemes considering capital costs, future expenses and revenues, in the utility company perspective. The results have shown that the complete DC system in this case is not recommended to be considered in Saudi Arabia due to the current low diesel prices in the Kingdom that make the diesel generator systems more cost effective. However, for other GCC countries, where the diesel prices are higher, the DC system is considered as one of the most economical solutions.

A protection scheme is then proposed and applied to the proposed DC microgrid. The proposed model can effectively and rapidly determine the fault distance as well as the faulty feeder by reading the load value in kW, source current at fault and fault resistance. The scheme is incorporated with insulated-gate bipolar transistors (IGBTs) used as circuit breakers for isolating the faulty feeder without affecting the load supplied by other feeders.

ملخص الرسالة

الاسم الكامل: أحمد عبدالعزيز مبيريك الصبحي الحربي

عنوان الرسالة: تصميم و نمذجة و تحليل نظام شبكة جهد منخفض نظام التيار المستمر

التخصص: هندسة كهربائية

تاريخ الدرجة العلمية: أبريل 2018

اكتسبت مؤخرا أنظمت التوزيع ذات التيار المستمر اهتماما خاصا من قبل العديد من البحوث و الدراسات. هذه الرسالة تناقش تصميم و نمذجة و تحليل نظام شبكة جهد منخفض على نظام التيار المستمر و التي تشمل على عدة مصادر و أحمال كهربائية تعمل على التيار المستمر. هذه الرسالة تعرض في البداية مقترح لعمل عدة نماذج رياضية لغرض التنبؤ بعناصر القدرة القصوى بالإضافة إلى منحنيات التيار-الجهد بمجرد معرفة بيانات درجة الحرارة و الإشعاع الشمسي إضافة إلى البيانات المطبوعة على كل لوح شمسي عند الظروف القياسية. تم استخدام هذه النماذج لتتبع أقصى قدرة للأنظمة الشمسية عند ظروف جوية مختلفة. تمت مقارنة أداء هذه النماذج مع عدة ألواح شمسية من برنامج السيمولنك و من عدة ألواح شمسية متوفرة تجاريا بالإضافة إلى بعض الطرق المقترحة في عدة أبحاث منشورة. أظهرت النماذج المقترحة أداء أكثر دقة و فعالية من ناحية تقدير قيمة العناصر و الزمن المطلوب لإيجاد قيمة هذه العناصر.

بعد عمل نموذج لمصدر تيار مستمر, تم عمل نماذج لبعض الأجهزة الرئيسية بنوعيتها: ذات تيار متردد و تيار مستمر باستخدام طريقتين. أظهرت النتائج فعالية هذه النماذج عند مقارنتها مع النتائج العملية. ثم تم اقتراح أربعة أنظمة مختلفة لتصميم منزل صغير معزول عن الشبكة الكهربائية. تم تحليل هذه الأنظمة و مقارنة خصائصها من ناحية الاستهلاك الكهربائي و الجدوى الاقتصادية على مدى 20 عام. أظهرت النتائج أنّ نظام التيار المستمر هو الأوفر في الاستهلاك والأجدى اقتصاديا خلال هذه الفترة.

تم تعميم فكرة هذا المنزل الصغير لإنشاء نظام كامل لمدينة صغيرة مكونة من 100 منزل و تمت دراسة الجدوى الاقتصادية من وجهة نظر الشركة المزودة للكهرباء باعتبارات التكاليف الرأسمالية للمشروع و النفقات المستقبلية و الإيرادات. كما تمت مقارنة النظام ذي التيار المستمر بالنظام العادي ذي التيار المتردد و نظامين هجينة. أظهرت النتائج أنّ نظام التيار المستمر ليس مجدي اقتصاديا في المملكة العربية السعودية في الوضع الحالي نظرا لانخفاض قيمة الوقود مما يجعل النظام الكهربائي

التقليدي أفضل من ناحية اقتصادية. أما بالنسبة لدول الخليج العربي الأخرى فإنّ نظام التيار المستمر يعتبر الأوفر اقتصادياً بسبب ارتفاع قيمة الوقود في هذه الدول.

في النهاية، تمّ اقتراح طريقة لحماية نظام التيار المستمر المقترح بناءً على نموذج رياضي. يمكن لهذا النموذج أن يحدد بشكل سريع وفعال مسافة العطل من خلال قراءة قيمة الحمل الكهربائي بالكيلو واط، تيار المصدر عند حدوث العطل وقيمة مقاومة العطل. تم استخدام ترانزستورات ثنائية القطب كقواطع للتيار المستمر وذلك لعزل المنطقة التي حدث فيها العطل دون التأثير على الأحمال الأخرى.

CHAPTER 1

INTRODUCTION

1.1 Overview and Historical Background

The interest in the DC grid field is increasing over the recent years. The advancements in power electronics and the increasing penetration of DC sources have encouraged the researchers to carry out studies and investigations in this field. In addition, appliances manufacturers have now produced various appliances working directly on DC without any converters. This trend has shown the interest of such manufacturers to utilize the latest technology developments for the purpose of producing efficient and energy saving appliances.

The idea of DC distribution is not new. It takes us back to the 19th century where the electrical power was handled using DC power system configuration. This scheme of using the electrical power founded by Thomas Edison suffered from several difficulties. The main obstacles faced by the electrical power facilities at that time included the low voltage at generation level and the challenge of transmitting the power to consumers far from the generation plant. As a result, the power was generated and consumed locally as there were no means for stepping up or lowering the DC voltage. This necessitated transporting the power plants to the loads area or vice versa.

The AC concept was mainly introduced by George Westinghouse and Nikola Tesla. After the invention of the transformer, all drawbacks present in DC distribution were overcome by replacing the DC networks by AC systems. In the AC networks, the power could be transmitted easily by utilizing the transformer where the voltage could be stepped up or down at any desired level in order to transmit the power via conductors with small diameters. The power was also generated in centralized power plants far from the consumption level area where the voltage level was handled easily using the transformer. After the generation level, the voltage could be stepped up to high values to overcome the problems of power losses that resulted from transmitting the power over long distances. Then, the voltage could be stepped down to be used in the distribution level, and then stepped down finally to the consumption level.

This debate between Edison's DC grid and Westinghouse's with Tesla's AC grid was known as "The War of Currents". Tesla and Westinghouse were considered to be the winners and the power incorporated with the transformers had been used from that time till today. However, with the advancements in power electronics devices and control strategies over the last 60 years, DC could be adopted in small power system networks. More attention has been paid to the DC grid at the excessive use of more DC-based sources such as photovoltaic panels (PV) and fuel cells.

1.2 Dissertation Motivations

1.2.1 Emergence of DC Appliances in the Existing Network

Over the recent decades, the advances in power electronics have resulted in several household appliances powered by DC such as laptops, cell phones, TV's, printers and

many other appliances. With the current AC network, these appliances require converting the input power from AC to DC. This means that rectifiers are needed in each appliance to convert the voltage from $230 V_{AC}$ to the required DC voltage such as $12 V_{DC}$ or $5 V_{DC}$. The rectification process results in some power losses and power quality issues.

1.2.2 Use of Variable Speed Drives Motors in Various Household Appliances

Another point of interest is the excessive use of the conventional induction motors in several household appliances such as air conditioners and refrigerators. The idea of variable speed drives (VSDs) is implemented in the recent years for various motors used in the industry. The VSD is supplied with AC utility power with constant frequency. This is rectified and converted to DC which, in turn, is converted again to AC with variable and controlled frequency. This ensures efficient motor control in such a way smooth speed options can be selected instead of the successive ON/OFF behavior [1]. The main AC source supplying the VSD is simply replaced by a DC source to avoid one conversion stage, leading to more efficiency improvement.

1.2.3 Availability of DC Appliances

One point of interest is the current emergence of completely DC appliances in the market. These appliances are ready manufactured to be directly supplied by a DC source, which is commonly $12, 24$ or $48 V_{DC}$. Some of DC appliances available currently in the market include DC air conditioner, refrigerator, TV, lamp, fan, iron, kettle and washing machine. All these appliances are designed to work directly based on one or more of the DC voltages of $12, 24$ and $48 V_{DC}$. These appliances are not assessed, investigated and modeled by previous research studies. It is of interest in this dissertation to carry out

experimental assessments and simulation models for such appliances, and to compare their characteristics with their AC counterpart.

1.2.4 DC Nature of Renewable Energy Sources

The utilization of renewable sources such as solar energy and fuel cells, which generate DC power in nature, is raising the debate again of the possibility and feasibility of using the DC distribution system instead of the existing AC system. In case of DC microgrid, it is easier to integrate such DC sources in the system for the purpose of directly supplying the DC loads. It is important to develop a model to the DC source which is simple, efficient and easy to implement.

1.2.5 Proper DC Voltage Selection

For more implementation of DC systems, it is essential to select an appropriate DC voltage for DC networks. The DC appliances existing in the market are available at a variety of DC voltages. There is no standard DC voltage available for DC systems. It is of interest to design a complete DC network with a common voltage in order to avoid conversion stages of DC voltages.

1.2.6 Energy Saving Opportunities and Cost Analysis

The DC appliances available in the market are characterized by low energy consumption and high capital costs. For energy assessment and cost analysis, it is important to study and implement a complete DC network that comprises all these appliances and carry out a comparative study with the conventional AC network and hybrid AC-DC systems.

It is interesting to explore, address and investigate the aforementioned points and discuss the idea of the DC grid including DC generation sources as well as DC loads. It is also

important to design, model and analyze a complete DC network and compare its characteristics with a corresponding AC network in terms of different points of view. Several aspects can be investigated including systems modeling, energy saving opportunities and cost analysis.

1.3 Dissertation Objectives

In this dissertation, DC grid area of study is treated and analyzed based on different points of view. This field is extensively adopted in this study to achieve the following objectives:

- Performing a literature review about the state of art of the DC distribution systems and their applications.
- Analyzing the PV source, as one of the major renewable DC sources, by proposing efficient models to predict PV module characteristics under variable weather conditions by the knowledge of data sheet parameters and temperature and irradiance values.
- Proposing a maximum power point tracking (MPPT) algorithm for PV systems using simple mathematical representation methodology.
- Exploring and preparing the modern DC appliances for analysis and study.
- Proposing simulation models for various major AC and DC household appliances using two approaches based on experimental field measurements.
- Integrating the proposed AC and DC appliances models as to represent typical AC and DC houses employed for carrying out systems simulations and studies.

- Designing and implementing a small standalone house with different power system architectures, and carrying out comparative cost analysis and energy assessments.
- Designing an entire network representing AC and DC microgrids and performing extensive energy saving comparisons as well as life cycle costs assessments based on the supply utility perspective.
- Proposing an efficient and simple scheme for system protection and fault detection in DC microgrid.

1.4 Dissertation Organization

The dissertation is divided into 8 chapters as follows:

Chapter 1 introduces the dissertation work along with some introductory overview about the topic. Dissertation motivations and objectives are also addressed in this chapter.

Chapter 2 discusses the recent research works related to the DC grid field.

Chapter 3 proposes a new method to predict the characteristics of PV modules from weather parameters and PV module data sheet specifications without estimating the parameters of the PV equivalent circuit model. The chapter also explains how the proposed models are employed for achieving MPPT for different PV systems. The performance of the proposed models is compared with SIMULINK simulations, some recent research works and I-V curves for some commercial PV modules.

Chapter 4 analyzes various major household AC and DC appliances. Simulation models are built for the appliances under study using two approaches by utilizing field measurements.

Chapter 5 presents the design and implementation of a small scale DC house supplied by distributed generation (DG) sources. Corresponding AC and hybrid AC/DC houses are also designed for assessments and comparisons. The houses are extensively compared in terms of energy consumption and cost analysis.

Chapter 6 designs a complete DC microgrid, as well as similar AC and hybrid microgrid configurations. Systems sizing and DC distribution voltage selection are addressed in this chapter. The chapter also presents the cost analysis and life cycle costs assessments of the proposed configurations based on the supply utility perspective.

Chapter 7 presents a fault detection and identification methodology for the proposed DC microgrid. Rapid faulty feeder identification and isolation using IGBTs breakers are discussed in this chapter.

Chapter 8 presents the conclusions and main findings obtained from this research and points out some directions for possible future work.

CHAPTER 2

LITERATURE REVIEW

2.1 Overview

Research efforts around the world on the DC grid area have increased significantly in last decades. In 2015, the IEEE organized the first international conference on DC microgrids (ICDCM) in the USA [2]. More than 80 papers were published with diverse tracks on DC microgrid areas including monitoring and control, performance analysis and optimization, communication and security analysis and protection and switching techniques. The second ICDCM has been organized in 2017 in Germany [3]. More than 100 research works have concentrated on recent topics in the DC environment. Some selective topics include DC breaker and arc detection, protection and grounding, energy management and DC appliances integration in the microgrid. More extensive research efforts are expected to be presented in the third ICDCM to be held in Japan in 2019.

Although AC power is dominant for a long time, DC power has also been used for some applications. There are several applications of the DC grid employed in various facilities. The research efforts have concentrated more in this area especially during the last decade. This chapter presents some research works that have adopted the DC environment in different applications.

2.2 Research on DC Systems and Existing Applications

DC systems are found in several applications. It is interesting to explore where such DC systems are found and how the idea of DC distribution is adopted. Various studies are carried out in distinct applications for DC networks. DC distribution is commonly adopted in isolated power systems such as telecommunication systems, electric vehicles, ships, as well as in small systems like computer systems. This section describes some of the facilities that adopt the DC distribution system and overviews several research works carried out for each application.

2.2.1 Shipboards

The shipboard distribution system is an example of adopting DC network. Due to the removal of transformers and switchgears in the case of the DC, the system provides several benefits like weight and space savings as well as flexible component arrangement [4].

A DC distribution system for a marine vessel power system was proposed [5]. Furthermore, an end-to-end modeling and simulation methodology was presented in [6] in order to facilitate system-level design, control, analysis and optimization of medium voltage DC (MVDC) ship power system. The computational speed and accuracy of the proposed method have been verified.

A heterogeneous multi-agent system (MAS) framework was proposed for a DC zonal system of an electric ship. The purpose of this framework is to achieve load balancing and dynamic generation. At the same time, all operational constraints are satisfied and

load priorities are considered. The results have shown an efficient performance of this methodology [7].

The benefits of DC-based shipboard and comparison of its performance with the conventional AC solution was explored in [8]. A survey of emerging concepts, design challenges and current initiatives has been performed. Different aspects were considered in this review including safety, power quality, reliability and efficiency. It is concluded from the survey that DC-based ships hold significant potentials.

Extensive efficiency analysis for a shipboard with DC hybrid power system has also been performed [9]. The authors proposed an optimization algorithm for the purpose of minimization of fuel consumption when subjected to load variations. Using MATLAB/SIMULINK, an online optimization methodology for fuel saving is proposed. Furthermore, offshore support vessel simulations were carried out at different operating modes under the online optimization control. It has been concluded that the proposed methodology could achieve about 15% fuel saving with optimally utilized energy storage in the DC system under study.

2.2.2 Data Centers

A data center is a facility employed for housing computer systems and associated components including storage systems. In general, data centers involve backup power supplies, redundant data communications connections, environmental controls such as air conditioning and fire suppression, and several security devices [10].

A DC distribution system has been proposed to replace the existing AC network for a data center [11]. In addition, the efficiencies of 220 V_{AC} and 300 V_{DC} systems feeding a

data center were compared [12]. The study shows that there is 15 % efficiency improvement when using the DC system compared to the AC system.

A study has been presented by Lawrence Berkeley National Laboratory (LBNL) to compare the efficiencies of AC and DC systems for a data center [13]. It concludes that the DC system can improve the efficiency by up to 28 % as compared with the typical AC distribution system [13].

Reference [14] presented the possible power quality disturbances occurring in DC data centers as well as their effects on the performance of the system. In addition, design considerations to overcome these disturbances were discussed. There are various transients that occur in 380 V_{DC} power system networks. These transients include voltage dip, short interruption, electrostatic discharge, electrical fast transient burst, surge voltage, radio frequency disturbances and inrush current. The most common disturbances in DC data centers are voltage sag, DC bus faults and load transients. The opportunity of using energy storage support with its capability to improve the power quality was also presented.

2.2.3 Commercial Facilities

Energy assessments on DC microgrid over the traditional AC networks were carried out [15]. The study assessed the system performance in different locations for various commercial facilities and operating conditions. The results show that the DC microgrid uses PV energy around 6% to 8% more efficiently than the conventional AC systems.

Daniel et al have performed a simulation-based efficiency comparison of AC and DC power distribution networks in commercial buildings. The work has shown that DC distribution system is more efficient [16].

An efficient DC electrical distribution system was analytically demonstrated in [17]. A 48 V_{DC} level was recommended to be used for distribution systems in rural banks. Three distribution systems were presented in this study which are: the conventional solar hybrid power system with battery back-up, hybrid distribution system and the 48 V_{DC} electrical distribution system. The sizes of the system components (primarily solar PV capacity and the battery bank capacity) were calculated for the three distribution systems for comparison purposes. The results show that the DC distribution system is the most efficient system and also has shown savings of 15% over the conventional system.

2.2.4 Telecommunication

Similar to data centers, telecommunication networks are used to transfer substantial amounts of information. Telecommunications systems should be inexpensive, efficient and reliable [18]. The crucial components of a telecommunication system are rectifiers, batteries and a power system controller. Telecommunication systems distribute a DC power obtained from a backup battery that is continually charged by a rectifier/charger from the AC supply.

A new power supply topology was suggested in [19] in order to use multitudes of power supply systems in telecom buildings. Two DC voltage levels are selected; 48 V_{DC} and 380 V_{DC}. The topology is expected to enable to design highly reliable and efficient power supply systems [19].

2.2.5 Lighting Systems

Light emitting diode (LED) lamps are a rapidly developing technology which produces light in a more efficient way. It already outperforms the efficiency and quality of the existing lighting technologies including incandescent and fluorescent lamps. Each LED lamp is equipped with AC/DC and DC/DC converters. The advantage of DC-LED based lighting system is to mitigate the problem of AC/DC conversion using switched mode power supplies (SMPS) for each LED unit.

In the work presented by [20], the authors examined the techno-economical advantages of low voltage DC distribution to a lighting system in a building using PV-based generation system. In the proposed DC scheme, the conventional fluorescent light bulbs are replaced by LED light resulting in efficiency improvement. It is shown that 60% load capacity is reduced and substantial energy saving has been achieved [20].

Substantial energy saving was also achieved by adopting the DC-based LED lamps [21]. A comparison of AC and DC-based LED lights efficiencies has been carried out in [22]. The thermal stability and driver efficiency have been evaluated for both AC and DC lighting systems. The testing results have shown that DC LED lights are more reliable and efficient than AC lights with 5 to 10% better efficiency, 3 to 10 times better reliability and a 20% lower cost [22].

2.3 Analysis of Different Aspects of DC Systems

The DC systems have been analyzed in the previous research in terms of different points of view. This section presents some research studies analyzing some topics including modeling of PV systems, modeling of loads and some DC protection systems.

2.3.1 Modeling and Maximum Power Point Tracking of PV systems

An essential field of study in the PV systems is the tracking of the maximum power produced by the PV at changing environmental conditions. Many algorithms have been proposed in the literature to track this point and improve the PV system efficiency. To achieve this purpose, the parameters at maximum power must be located properly. Several MPPT algorithms are basically dependent on predicting and setting one of the maximum power parameters as a reference value that changes with changing temperature and irradiance. This reference value is compared with the actual value in order to evaluate the error. Based on some algorithm, the duty ratio of a connected DC-DC converter is then adjusted in such a way that the maximum possible power at the specified conditions, can be harvested.

Researchers have usually used three variables as reference parameters for MPPT purposes. These include the maximum power [23-30], voltage at maximum power [31-38] and current at maximum power [39-44]. Without proper prediction of such variables, the MPPT algorithms may lead to inaccurate tracking of the maximum power which results in PV efficiency reduction.

Recently, several new MPPT algorithms are proposed while some are modified in order to meet the requirements of the PV system. The techniques differ in several aspects including tracking speed, complexity, implementation, accuracy and the variety of software and hardware components involved.

The most popular algorithms employed in MPPT purposes include incremental conductance (INC) [45, 46] and perturb and observe (P&O) [47, 48] algorithms. These

algorithms have been widely used. Intelligent techniques such as fuzzy logic (FL) [49], gravitational search algorithm [50], differential evolution (DE) [51], particle swarm optimization (PSO) [52] and artificial neural network (ANN) [53] have been also used in PV systems for MPPT purposes. A hybrid method that integrates PSO with P&O is presented in [54]. Another hybrid technique is used including PSO and FL [55]. Other techniques like Taguchi method [56], flower pollination algorithm [57], and BAT search algorithm [58] have been also presented.

2.3.2 Modeling of Household Appliances

Several research works have analyzed load modeling concept and its applications to different power system networks. The authors of [59] have adopted simple, multiple linear and quadratic regression analyses to predict the energy consumption for a research house on an hourly and daily time bases.

A genetic algorithm (GA) based methodology for modeling the loads in power system has been proposed in [60]. The values of voltage, active power and reactive power are evaluated after a disturbance in the voltage. The GA is then used to calibrate the load model parameters. The validity of the parameters values is tested with some different scenarios.

The work presented by [61] has combined polynomial with the Fourier series models to analyze the power consumption of buildings. The model has used a polynomial for long-term trends and Fourier series for periodic activities in which the data used in the analysis are divided to two parts. The model parameters are evaluated in the first part whereas the number of terms of Fourier series and the polynomial are determined in the second part.

A new method was proposed to model the load characteristics [62]. The method adopted multiple Gaussian functions for analysis. The model performance is compared with two different techniques. Efficient performance is achieved and mean percentage errors are reduced significantly using this model.

Various research works have analyzed load modeling using the widely used exponential model [63-66] and the static polynomial *ZIP* model [67-71]. More extensive research efforts focusing on reviewing the recent research of load modeling and forecasting methodologies can be found in [72-77]. The available-in-market DC appliances with dominant DC voltages of 12 V_{DC} and 48 V_{DC} have not been yet analyzed and modeled.

2.3.3 Protection and Fault Analysis in DC Systems

A protection method against short-circuiting using the assistance of solid state circuit breakers (SSCB) in low voltage DC microgrid was presented [78]. The authors of [79] have used artificial neural network (ANN) for fault detecting and locating in a low voltage DC microgrid system. The faults on DC bus could be detected rapidly and then isolated without de-energizing the entire system, hence achieving a more reliable system.

A protection scheme for DC microgrid against faults has been proposed [80]. The scheme isolates only faulty section from the system. The scheme is based on taking the difference between the sending and receiving end currents. A controller is implemented in order to detect this current difference and then opens the power switches for faulty section isolation.

A protection scheme algorithm for a ring type DC microgrid system was discussed [81]. The algorithm senses the fault using differential current and then current derivative is

taken for segment isolation without isolation the entire system. A fault detection method using fuzzy logic has been proposed [82].

The authors of [83] have proposed a novel DC protection scheme based on the use of the combination of the voltage rate of change and the current rate of change. The methodology was developed for detecting and locating faults with reduced fault current levels within the DC system. The proposed protection scheme was tested on a LVDC distribution network using PSCAD/EMTDC simulation tool.

2.4 DC Grid Research Challenges

Although the concept of DC distribution has been studied by various research works, there are, however, some topics not well explored. Various works performed in this field have opened doors for future research opportunities. This section discusses and presents the topics that are recommended to be explored and the questions that have been raised in previous research. The following are various research gaps that are needed to be discussed, as stated by the indicated reviewed research works:

- Various MPPT algorithms for PV systems have been proposed. These algorithms are usually characterized by the requirement of special software for executing and simulating the algorithms. In addition, some of the techniques require long simulation time since most of these techniques are based on iterative processes and trial and error operations till reaching to the optimal solution [84].
- The feasibility of adopting DC systems is evident, especially with the high penetration of DC sources and loads and the presence of advanced power electronics technologies. More work needs to be done on the topics of voltage

selection, modeling and protection. A complete system design has to be investigated with its practical aspects and impacts [85].

- The most essential problem in low voltage DC systems is that DC voltage values of devices are different from each other and that there is no standardization with regard to DC voltage as in AC system [86].
- One of the barriers of DC distribution systems is lack of DC ready products in the market [87].
- Modeling in DC distribution is constrained by the lack of available DC appliances and their power electronic interface with the mains. It is needed to show how a multiplicity of appliances that require different operating voltages can be interfaced to fixed voltage mains [88].
- Further work is needed to determine a feasible transition pathway to increase the presence of high-efficiency DC appliances in the homes and optimize DC generation technologies such as solar PV. The outcomes and cost-effectiveness are highly uncertain given the lack of previous research [89].
- One of the most promising applications are VSDs and LED lighting. Both of these technologies have proven their ability to generate savings when supplied by DC power, but little is known about their application in the residential sector [89].
- It is interesting to investigate the possibility of decreasing the size of a home's solar array to serve only a base DC demand. This allows the capital cost of the system to be decreased, while optimizing the benefits of DC distribution [89].
- While the use of DC has been studied in the commercial building sector and is being recommended as a key strategy for improved reliability and increased

energy saving, residential applications have received relatively little attention [90].

- A number of studies have examined residential DC systems. The majority of studies are analytical in nature, involving no demonstrations or laboratory measurements [90].
- Though DC distribution has been widely discussed in the literature, only a few research efforts focus on residential buildings, especially single-family houses [91].
- Although there are detailed reviews and analyses considering various aspects of low voltage DC systems, there are still some challenges, such as the simulation and implementation of DC systems because of a lack of object models and simulation skill [92].
- Limited attention is given to costs analysis of DC systems [93].
- Feasibility study of a complete DC distribution system based upon local DC generation is needed. In this case, an appropriate model of the whole system starting from DC generation to the loads can be simulated. Alongside this, the life cycle cost of this system and its components can also be compared with those of a corresponding AC system [94].
- A final decision may be given as to which of the AC and DC systems is better suited for residential power distribution in the modern day when the concepts of DGs and microgrids are gaining interest and power electronic converters have been developed [94].

- It is of interest to validate the device models via experimentation using a sufficient selection of devices. It is essential to implement small mixed AC-DC distribution system test cases and compare the performance with the optimization results [95].
- Quantitative analysis has to be carried out to verify, via laboratory controlled measurements, that DC appliances use less energy than equivalent AC appliances [96].
- With the implementation of the DC home in emerging markets, what size will the new market for DC appliances be? How can this influence or/and convince appliance manufacturers to invest in research and development to produce low powered DC appliances? [96].
- It is interesting to study the protection of DC systems with respect to fault detection and isolation [97]. Several research works analyzing DC systems protection were based on specific conditions such as constant load or constant fault resistance. Thus, not all operating conditions were covered.
- It is required to perform a comparison of AC and DC-based distribution for PV systems. The comparison can be done with the help of simulation or by analyzing identical actual AC and DC systems [98].

In this dissertation, the gaps and challenges stated by previous research will be analyzed and discussed for an attempt to cover and close these gaps. Thus, this dissertation will analyze the following aspects:

- Proposing simple and efficient mathematical models for predicting the I-V curves of PV modules. The models can be executed in very short time without any

iterative processes and trial and error operations. In addition, no special software such as MATLAB or PSCAD is required for models estimation.

- Proposing MPPT methodology by utilizing the proposed mathematical models.
- Modeling of various major AC and DC household appliances based on field experiments.
- Proposing typical AC, DC and hybrid identical houses considered as typical test systems ready for performing different analysis and studies.
- Designing and implementing a complete DC house by utilizing the modern DC appliances while selecting an appropriate DC voltage level for the entire house to minimize the number of the required converters.
- Performing extensive energy assessments and cost analysis for the DC house and compare the performance with different systems including conventional AC house as well as hybrid houses.
- Creating a DC microgrid representing a town and carrying out a feasibility study and economical analysis in the utility company perspective.
- Proposing a simple and efficient mathematical-based protection scheme for the DC microgrid under different operating conditions such as different fault distances, different load and different fault resistance values.

CHAPTER 3

MATHEMATICAL MODELS FOR

PERFORMANCE CHARACTERIZATION OF PV

SYSTEMS

3.1 Introduction

PV generation source is analyzed and discussed in this chapter in terms of different points of view. Two major aspects are given attention in this chapter. The first aspect is to propose a new methodology for predicting the PV module characteristics. The methodology presents general and robust mathematical models for any PV module with the knowledge of only standard test conditions (STC) values given from the PV module data sheet, as well as the temperature and irradiance values. Using these models, several important variables can be estimated under varying weather conditions including maximum power conditions, open circuit voltage and short circuit current. The variables are evaluated without needing to estimate the parameters of the PV equivalent circuit model. The prediction of the variables is useful in different applications such as MPPT and I-V curves generation under variable weather conditions.

In this chapter, all such variables, along with others, are modeled in the first part of the chapter using mathematical relationships without evaluating the PV equivalent circuit model parameters. The models take the STC values and weather parameters as input variables and determine the respective variables as output parameters. The effectiveness of the proposed methodology is assessed by comparing its performance with results obtained from specification sheet of different commercial PV modules, as well as simulations in SIMULINK. The performance is also compared with several recently published research articles. The results obtained from the proposed models are in close agreement with the results obtained using other methods.

The second part of the chapter utilizes the proposed models in order to design a MPPT algorithm. The algorithm is also based on knowledge of STC values and weather variables. The validity of the proposed MPPT methodology is tested by application on two different PV systems. The algorithm performance is also compared with two of the most commonly used MPPT algorithms; INC and P&O algorithms. All mathematical models presented in this chapter are formulated using a commercially available software; EUREQA software [99, 100].

The chapter first gives a brief overview about EUREQA software. Then, the proposed methodology to formulate the mathematical models of PV module characterization is explained in details. This is followed by discussing the proposed MPPT algorithm and its applications to different PV systems.

3.2 EUREQA Software: General Overview [99, 100]

Eureqa is a proprietary artificial intelligence-powered modeling engine originally created by Cornell's artificial intelligence lab and later commercialized by Nutonian, Inc. The software uses evolutionary search for determining mathematical equations that describe sets of measured inputs and outputs in their simplest form. Current modeling techniques require users to choose from a set number of predetermined algorithms (K nearest neighbor, support vector machine, etc.). Eureqa, on the other hand, builds numeric, time series, and classification models from the ground up, generating and updating models automatically [99]. Figure 3.1 shows the block diagram that illustrates the basic function of EUREQA.

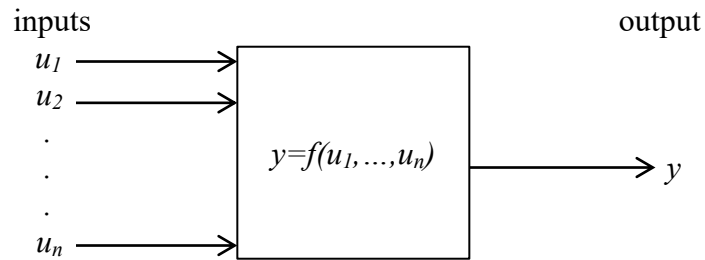


Figure 3.1: Basic function of EUREQA

In this figure, the input parameters (u_1, u_2, \dots, u_n) and the corresponding output parameter (y) are usually measured experimentally, where enough samples are necessary in order to represent all operating conditions of the system. The input and output data points are then transferred to EUREQA software to formulate the mathematical models. The equation representing the output, as a function of input parameters, takes the following form:

$$y = f(u_1, u_2, \dots, u_n) \tag{3.1}$$

In EUREQA, a series of simple and complex models are generated based on various selected mathematical operations such as addition, subtraction, multiplication and trigonometric and logarithmic functions. The user then selects the best model that fits the data with the lowest error. The flow chart shown in Figure 3.2 illustrates the steps followed for mathematical models formulation tasks using EUREQA.

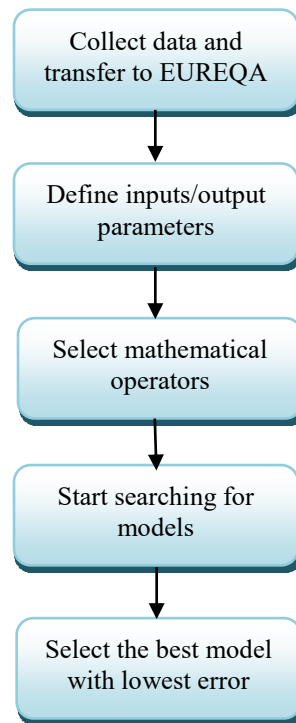


Figure 3.2: Summary of steps followed in EUREQA to build mathematical models

3.3 General Mathematical-Based Models for Characterization of PV Module Performance

This section proposes and discusses in details a methodology for predicting the I-V curves of any PV module at different weather conditions.

3.3.1 Proposed Methodology

3.3.1.1 Identifying key points on the I-V curve

One of the essential topics in PV modeling is the generation of the I-V curves under varying environmental conditions. In this study, ten key points on the I-V curve are predicted and calculated using mathematical models. The predicted points are listed in Table 3.1 and are shown graphically in Figure 3.3.

Table 3.1: Ten key points on I-V curve to be predicted

point	voltage	current
1	0	I_{sc}
2	$0.25*V_{oc}$	I_{25}
3	$0.5*V_{oc}$	I_{50}
4	$0.6*V_{oc}$	I_{60}
5	$0.7*V_{oc}$	I_{70}
6	V_m	I_m
7	$0.8*V_{oc}$	I_{80}
8	$0.9*V_{oc}$	I_{90}
9	$0.95*V_{oc}$	I_{95}
10	V_{oc}	0

Where V_{oc} is the open circuit voltage, I_{sc} is the short circuit current, V_m is the voltage at maximum power, I_m is the current at maximum power, and I_{25} to I_{95} represent current values at voltages between 25% to 95% of the open circuit voltage, respectively. For each of these points, mathematical relationships are formulated using EUREQA software as functions of weather parameters and STC values provided in the datasheet.

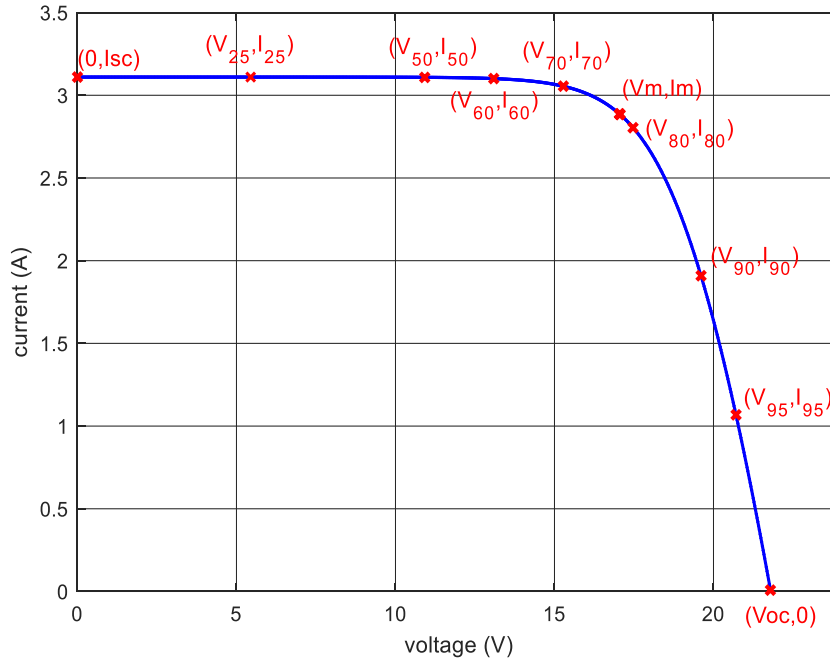


Figure 3.3: The ten key points on the I-V curve

3.3.1.2 Mathematical models formulation process

The proposed formulation starts by adopting the SIMULINK model of the PV module. Various PV modules are selected to carry out the simulations under diverse temperature and irradiance conditions. The selected PV modules represent different manufacturers, power ratings, numbers of cells, and STC parameters. As a first step, each selected PV module is simulated at a representative and uniform range of temperature and irradiance points. The I-V curve is generated for each temperature and irradiance point, and the ten key points are calculated and recorded. Along with these points, the STC parameters of the PV module are also recorded. This process is repeated for all PV modules chosen for the training process. By the end of SIMULINK simulations, the input and output variables are defined as shown in Table 3.2.

Table 3.2: Input and output variables employed in the proposed models

input variables	T
	G
	N
	V_{m_stc}
	I_{m_stc}
	P_{m_stc}
	V_{oc_stc}
	I_{sc_stc}
output variables	P_m
	V_m
	V_{oc}
	I_{sc}
	I_{25}
	I_{50}
	I_{60}
	I_{70}
	I_m
	I_{80}
	I_{90}
	I_{95}

Where T is the temperature in °C, G is the irradiance in W/m², and N is the number of cells. The subscript _{stc} denotes the value of the respective parameter at STC. The STC values play a major role in model formulation since they represent the operating characteristics of the PV modules and are usually given in the module nameplate data. The collected data are then transferred to EUREQA to build a mathematical model for each of the output parameters as a function of one or more of the aforementioned input variables. The mathematical models generally take the following form:

$$Y = f(T, G, N, V_{m_stc}, I_{m_stc}, P_{m_stc}, V_{oc_stc}, I_{sc_stc}) \quad (3.2)$$

Where Y represents any of the output variables listed in Table 3.2.

For certain output variables, it may be necessary to include other modeled output variables as inputs. This occurs in cases where the model is not capable of describing the parameter behavior properly. For example, the mathematical model of open circuit voltage may include the maximum power model as an input variable, along with the other defined basic input variables. This may take the following form:

$$V_{oc_mdl} = f(T, G, N, V_{m_stc}, I_{m_stc}, P_{m_stc}, V_{oc_stc}, I_{sc_stc}, P_{m_mdl}) \quad (3.3)$$

The flowchart shown in Figure 3.4 summarizes all steps needed for the mathematical modeling of all output parameters.

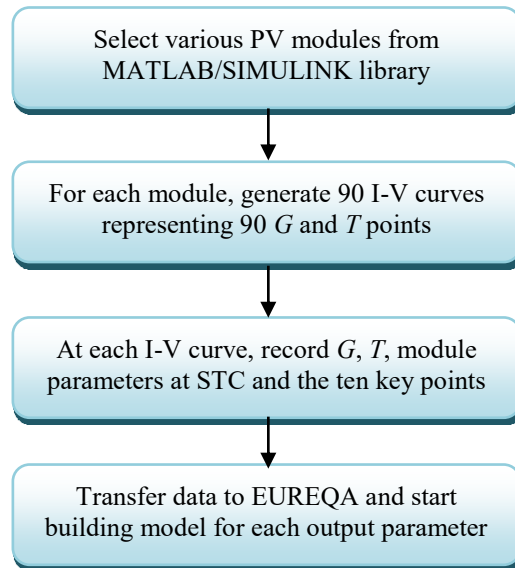


Figure 3.4: Summary of proposed methodology for building the predictive models

3.3.1.3 PV modules selected for training and the resultant generated models

To formulate the parameters models, 20 PV modules are employed to generate the I-V curves and to manipulate all input and output values. It is important to select PV modules with different characteristics in order to represent a uniform range of all possible values.

The specifications of the selected modules are listed in Table 3.3. For example, the first PV module in the table has 63 W maximum power and 22 cells. The parameters values at STC are 11.9 V for the voltage at maximum power, 5.3 A for the current at maximum power, 14.5 V for the open circuit voltage and 5.5 A for the short circuit current.

Table 3.3: Specifications of PV modules selected in training process

N	$V_m (V)$	$I_m (A)$	$P_m (W)$	$V_{oc} (V)$	$I_{sc} (A)$
22	11.9	5.3	63	14.5	5.5
24	13.45	5.65	76	16.2	6.02
60	29.02	7.58	220	36.3	8.3
60	29.6	7.7	228	37.8	8.3
60	29.42	7.99	235	36.96	8.48
72	40	5	200	47.8	5.4
72	39.8	5.4	215	48.3	5.8
72	40.5	5.55	225	48	5.93
72	40.5	5.88	238	48.5	6.25
72	40.5	5.93	240	48.6	6.3
96	54.2	5.45	295	63.3	5.83
96	54.7	5.49	300	64	5.87
96	54.7	5.64	308	64.3	6.02
96	54.7	5.67	310	64.4	6.05
96	54.7	5.76	315	64.6	6.14
96	54.7	5.82	318	64.7	6.2
96	54.7	5.86	320	64.8	6.24
128	72.9	5.35	390	85.3	5.72
128	72.9	5.49	400	85.3	5.87
128	72.9	5.69	415	85.3	6.09

For each PV module, ninety points of temperature and irradiance values are generated. The corresponding I-V curve is plotted at each point, and all the input and output parameters are identified and recorded. To cover a wide range of operating conditions, the irradiance values are varied from 200 to 1000 W/m² in steps of 100 W/m² while the temperature values are changed from 15 to 60 °C in steps of 5 °C. Figure 3.5 shows the

generated temperature and irradiance points used in the training process for each selected PV module.

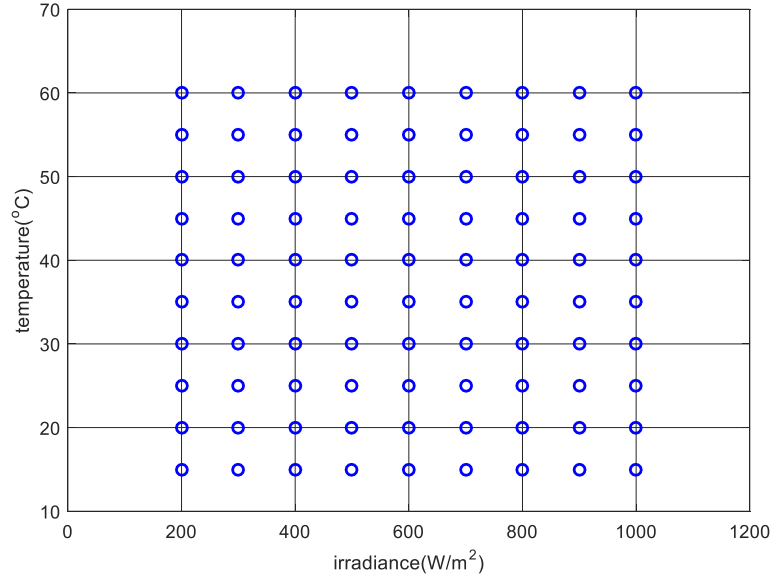


Figure 3.5: Temperature and irradiance points adopted in training process

All simulations have been carried out and the data composed of 20 PV modules \times 90 points (thus 1800 entries) have been collected. In other words, each input and output variable has 1800 entries to be processed by EUREQA for building the mathematical models. Models with different fitting accuracy can be obtained by using EUREQA.

In EUREQA software, mathematical operators that are used to build the models must be selected before starting searching for the models. Different operators are available like addition, division, absolute value, exponential, factorial, square root and many other operators. Initially, the basic mathematical operations are selected to formulate the best model for each parameter. If the model does not fit the data accurately, additional operators are selected and the process is repeated till the most accurate model is

generated. The flowchart shown in Figure 3.6 illustrates the process of models generation.

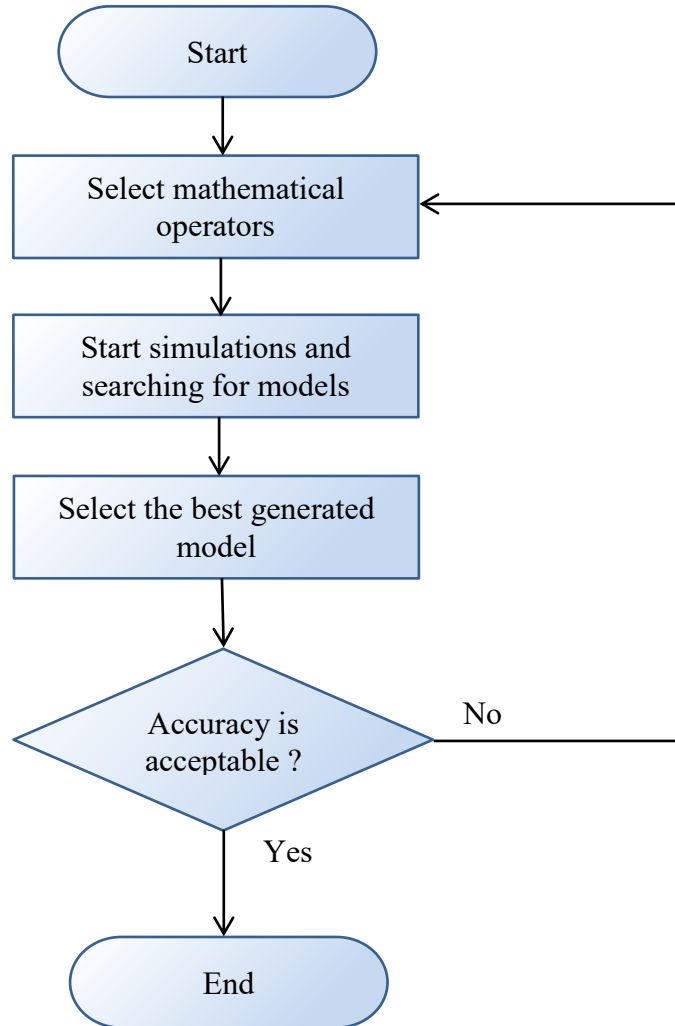


Figure 3.6: Steps of mathematical operators adjustments and selecting the best model

For example, maximum power is basically evaluated by selecting the basic operators including addition, subtraction, multiplication and division. Then, the selection goes further for different combination till the desired level of accuracy is achieved. Table 3.4 summarizes the generated models accuracy with respect to each combination of mathematical operators. Coefficient of determination (R^2) is used as a tool for estimating

the models accuracy. Large number of combinations can be selected. The table shows that the combination of addition, subtraction, multiplication, division, constant, sine and cosine operators gives the best fitting accuracy for maximum power evaluation models. Same process is carried out for all other key points considered in this chapter.

Table 3.4: Impact of changing operators on the accuracy of maximum power models

selected mathematical operators	R ² of the best generated model
+, -, ×, /	0.9392
+, -, ×, /, constant	0.9998
+, -, ×, /, exp, log	0.9531
+, -, ×, /, abs	0.9427
+, -, ×, /, constant, sin, cos	0.9999
+, -, constant, abs, square root, exp, power	0.9886

In summary, the best selected model for each of the output parameters is as follows:

$$P_{m_mdl} = 0.81V_{oc_stc} + 0.001GP_{m_stc} + V_{oc_stc} \sin(1.8 \times 10^{-7} GTV_{m_stc}) - V_{m_stc} - 3.88 \times 10^{-6} GV_{m_stc} V_{oc_stc} - 5.2 \times 10^{-6} GTP_{m_stc} \quad (3.4)$$

$$I_{m_mdl} = 0.009I_{m_stc} + 6.42 \times 10^{-5} G + 0.0008GI_{m_stc} + 0.0002GI_{sc_stc} + \frac{2.73 \times 10^{-6} G - 1.63 \times 10^{-11} GP_{m_stc} T^2}{\cos(N)} - 0.047 \quad (3.5)$$

$$V_{m_mdl} = \frac{P_{m_mdl}}{I_{m_mdl}} \quad (3.6)$$

$$V_{oc_mdl} = 0.056 + 0.153V_{oc_stc} + 0.0008GV_{oc_stc} + 2.95 \times 10^{-7} GV_{oc_stc}^2 + \frac{0.978P_{m_mdl} - 0.243 - 0.0003V_{oc_stc} P_{m_mdl}}{I_{m_mdl}} - 0.001GV_{m_stc} \quad (3.7)$$

$$I_{sc_mdl} = 0.001GI_{sc_stc} + 4.44 \times 10^{-7} GTI_{sc_stc} - \frac{1.25 \times 10^{-7} GT}{\sin(4.12 + N)} \quad (3.8)$$

$$I_{50_mdl} = 0.0006I_{sc_stc} + 0.0005GI_{m_stc} + 6.34 \times 10^{-7} GTI_{sc_stc} - 3.25 \times 10^{-8} GT^2 \cos(V_{m_stc} + 0.0006I_{sc_stc})^2 + 0.0005GI_{sc_stc} \quad (3.9)$$

$$I_{25_mdl} = 0.5I_{sc_stc} + 0.5I_{50_mdl} \quad (3.10)$$

$$I_{60_mdl} = 0.0007G + 0.0008GI_{m_stc} + 2.67 \times 10^{-6} GT + 1.88 \times 10^{-5} GI_{sc_stc}^2 + 1.57 \times 10^{-8} GT^2 \cos(0.72N) \quad (3.11)$$

$$I_{70_mdl} = 0.009I_{sc_stc} + 0.0009GI_{m_stc} + 0.0002GI_{sc_stc} + 3.58 \times 10^{-8} GTN - 0.052 - 8.45 \times 10^{-9} GN^2 \quad (3.12)$$

$$I_{80_mdl} = 0.013 + 0.001GI_{m_stc} + 3.51 \times 10^{-9} TG^2 \cos(0.192N) - 4.37 \times 10^{-16} TG^3 I_{m_stc}^5 \quad (3.13)$$

$$I_{90_mdl} = 1.7I_{60_mdl} + 0.0006T + \frac{4.03P_{m_mdl} - 0.341}{V_{oc_mdl}} - 0.0008V_{oc_mdl} - 0.329I_{sc_mdl} - 3.97I_{m_mdl} \quad (3.14)$$

$$I_{95_mdl} = 2.41I_{70_mdl} + 1.87I_{90_mdl} + 0.101I_{80_mdl}^2 - 0.004 - 3.75I_{80_mdl} + 0.333I_{90_mdl} \cos(I_{80_mdl} - I_{50_mdl}) - 0.121I_{60_mdl} I_{90_mdl} \quad (3.15)$$

These models represent the ten key points that are required for generating the I-V curves for any PV module. The validity and effectiveness of the models are assessed in the next subsection.

3.3.2 Simulation Results and Models Assessment

The validity of the models is assessed using alternative PV modules with their respective STC parameters and new temperature and irradiance values. Three comparative assessment cases are considered. In the first case, ten random PV modules are selected from the SIMULINK library. The I-V curves generated from SIMULINK simulations are then benchmarked with the proposed models at three random temperature and irradiance points. In the second case, three commercially available PV modules are selected. The chosen PV modules have experimental data provided through manufacturer's data sheet. The proposed mathematical models are subsequently compared with the module I-V curves from data sheet, as well as SIMULINK simulations. In the third case, the proposed models are used to evaluate variables analyzed in three recent research publications based on different algorithms.

3.3.2.1 Comparison with different PV modules in SIMULINK library

The performance of the proposed models is evaluated by considering alternative PV modules selected from the SIMULINK library. Ten different PV modules are chosen which represent different manufacturers and STC values. The specifications of the selected modules are shown in Table 3.5.

Table 3.5: PV modules specifications selected for models assessments

	manufacturer	N	$V_m (V)$	$I_m (A)$	$P_m (W)$	$V_{oc} (V)$	$I_{sc} (A)$
PV ₁	AU Optronics	72	37.58	8.21	308.53	44.57	8.77
PV ₂	China Sunergy	60	31	8.55	265.05	38.2	8.98
PV ₃	Colored Solar	80	42	8.09	339.78	51.1	9.12
PV ₄	DJ Solar	66	33.07	7.75	256.29	39.86	8.32
PV ₅	Fire Energy	48	23.6	7.62	179.83	29.4	8.2
PV ₆	GCL-Poly	54	27.79	7.93	220.37	33.69	8.54
PV ₇	Grape Solar	96	50.32	8.15	410.11	61.06	8.77
PV ₈	Hengji PV-Tech	36	18.52	5.13	95.01	22.56	5.54
PV ₉	SunPower	128	72.9	6.04	440.32	86.5	6.5
PV ₁₀	Tainergy Tech	36	17.32	7.52	130.25	21.8	8.06

For each PV module, three random points of temperature and irradiance are generated. The I-V curves are then plotted using SIMULINK simulations and the proposed mathematical models represented by equations (3.4)-(3.15). Figure 3.7 to Figure 3.16 show the I-V curves for all selected PV modules. The comparison shows that the proposed models fit the simulated I-V curves characteristics. This verifies the effectiveness of the proposed models to predict the I-V curves of any PV module, at any weather condition, by utilizing only the information provided in the data sheet at STC, in addition to temperature and irradiance values.

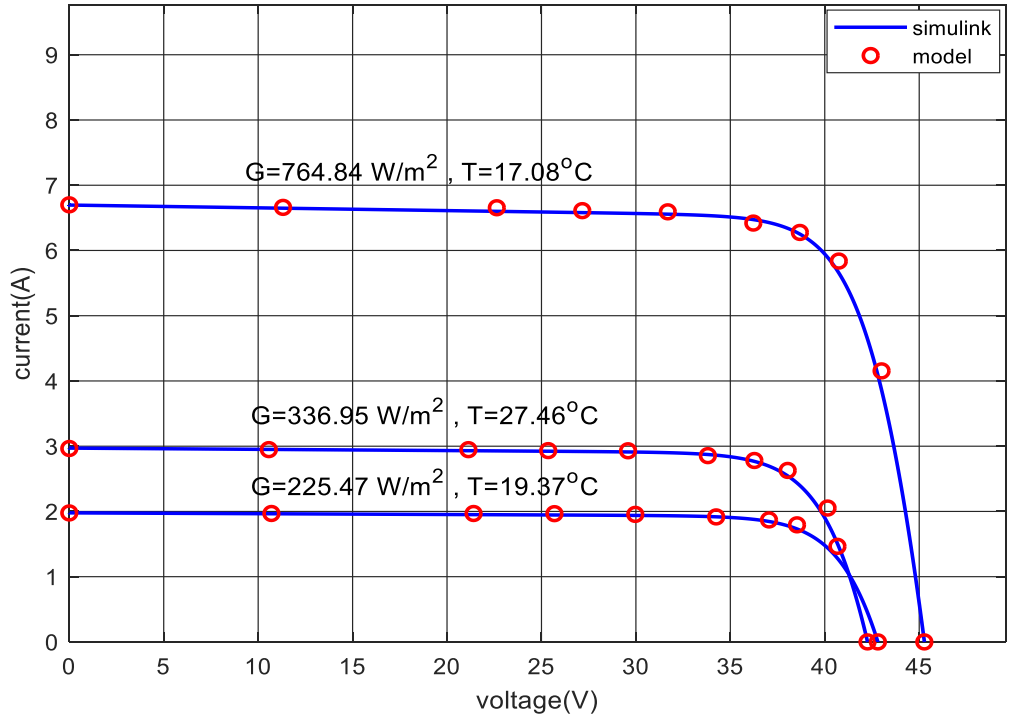


Figure 3.7: I-V curves of PV module # 1 at the indicated weather conditions

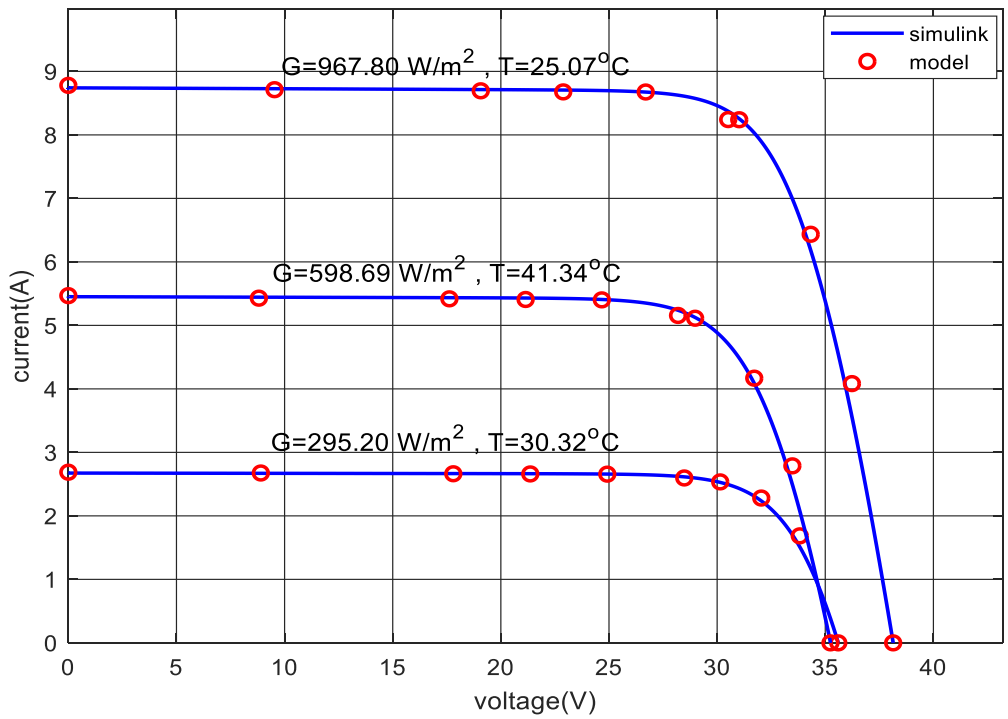


Figure 3.8: I-V curves of PV module # 2 at the indicated weather conditions

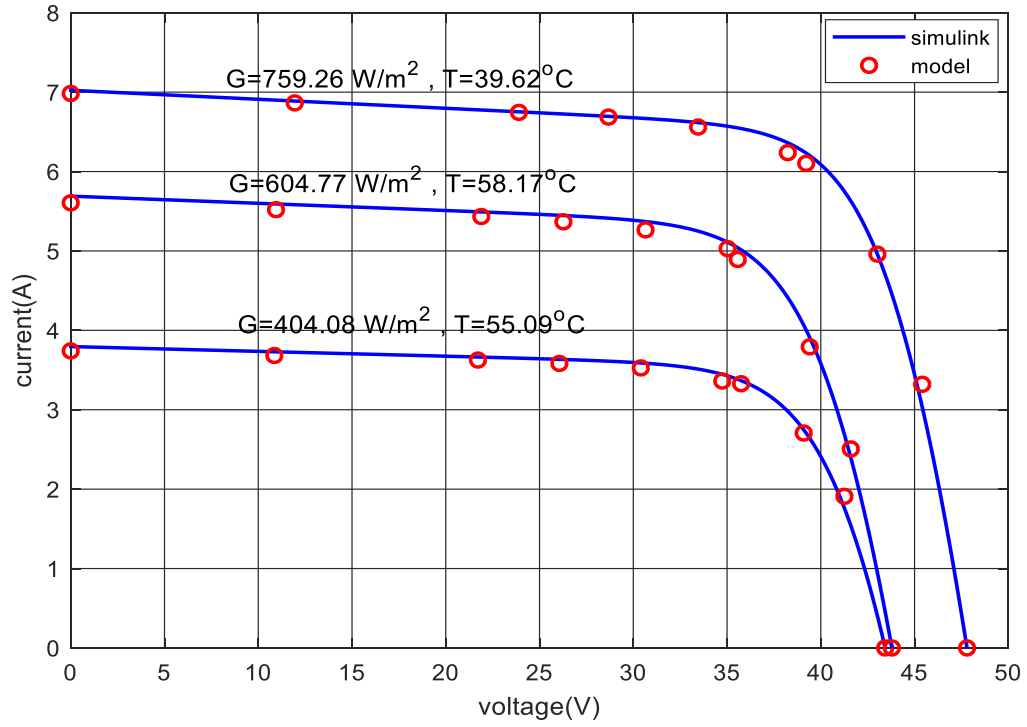


Figure 3.9: I-V curves of PV module # 3 at the indicated weather conditions

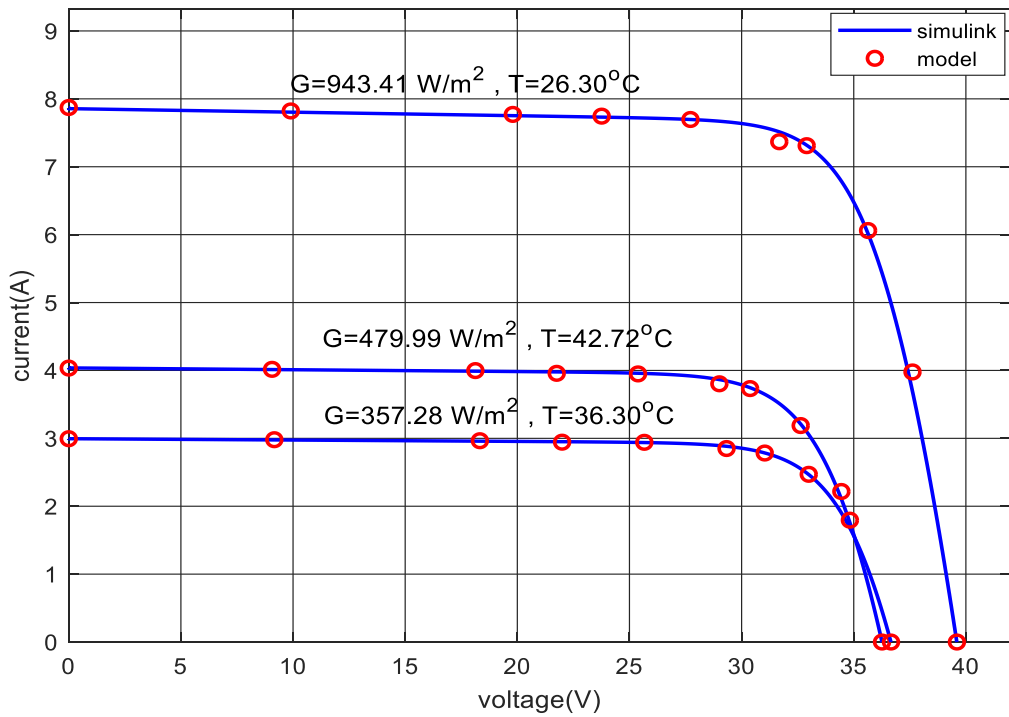


Figure 3.10: I-V curves of PV module # 4 at the indicated weather conditions

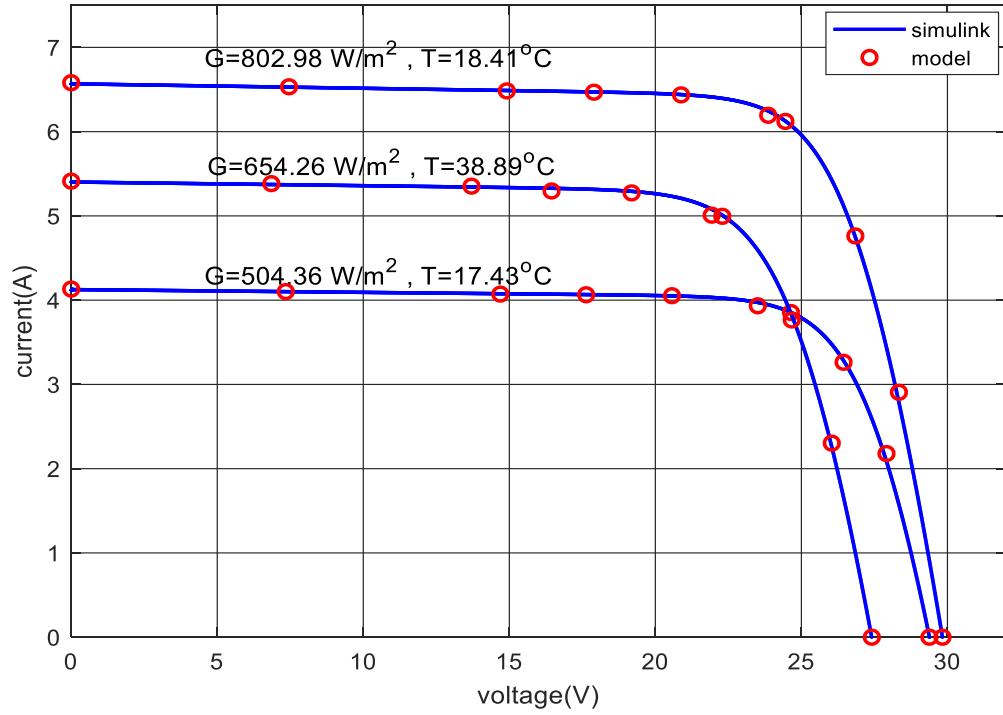


Figure 3.11: I-V curves of PV module # 5 at the indicated weather conditions

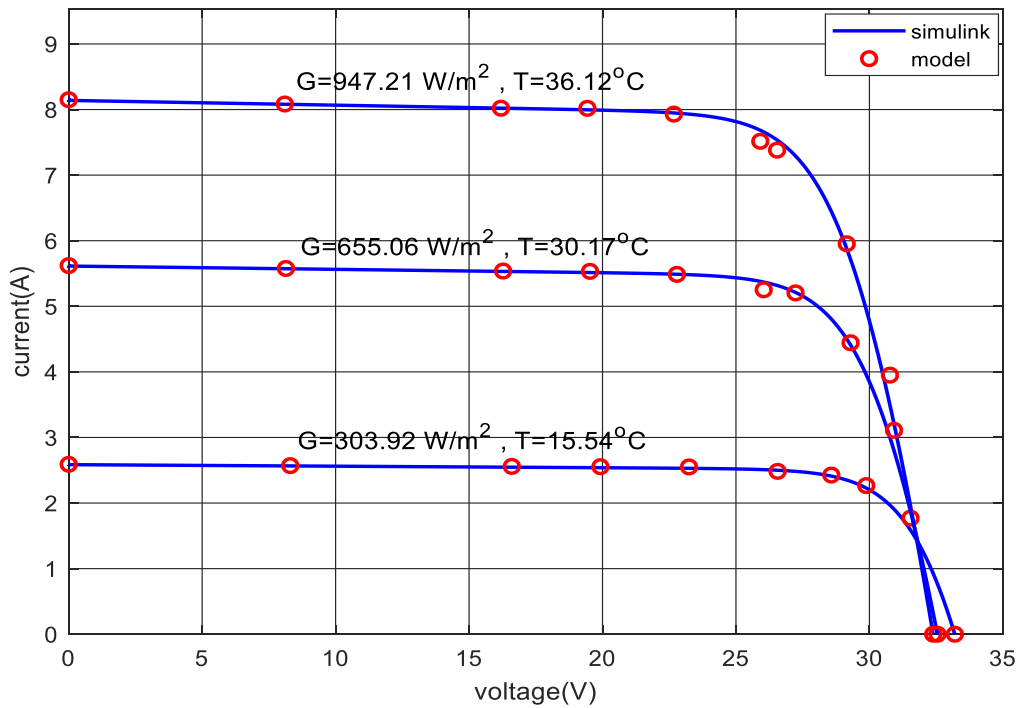


Figure 3.12: I-V curves of PV module # 6 at the indicated weather conditions

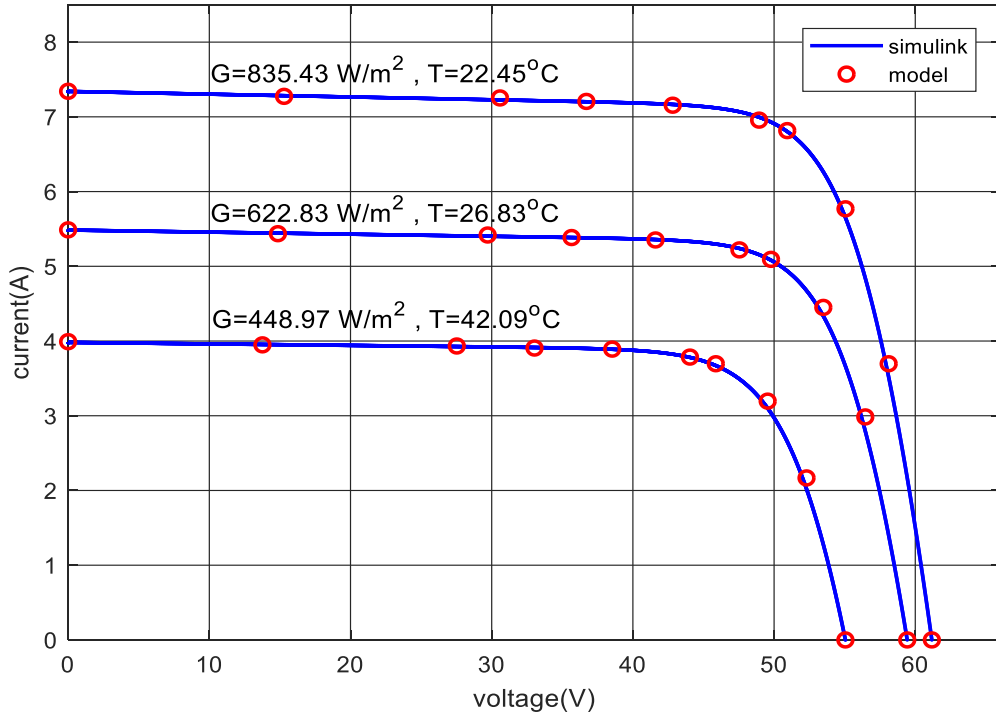


Figure 3.13: I-V curves of PV module # 7 at the indicated weather conditions

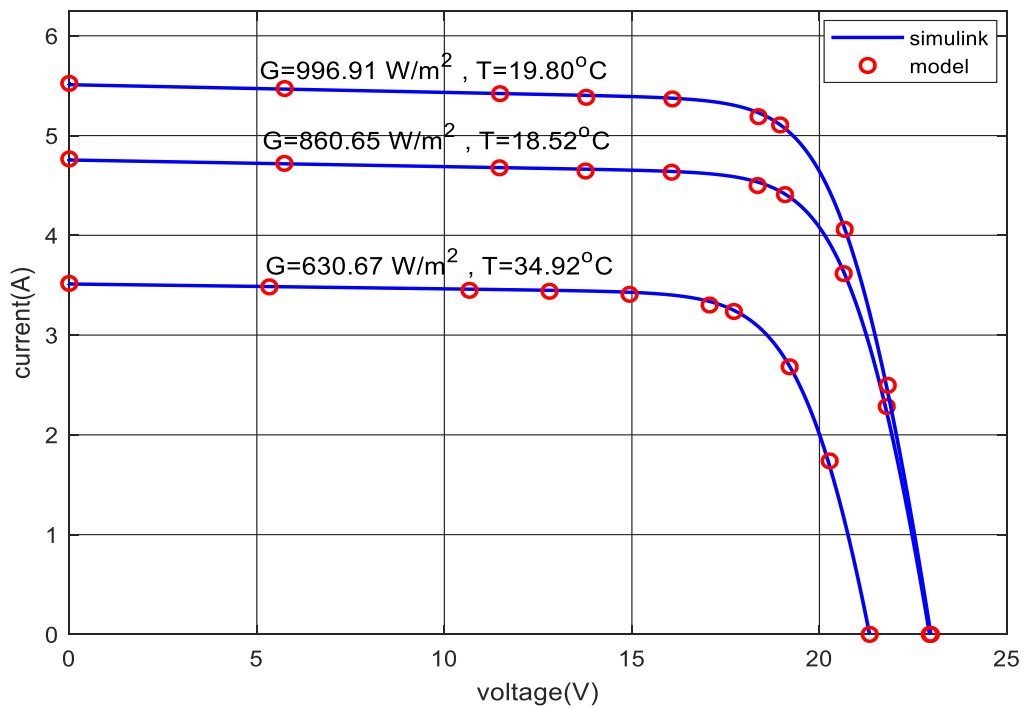


Figure 3.14: I-V curves of PV module # 8 at the indicated weather conditions

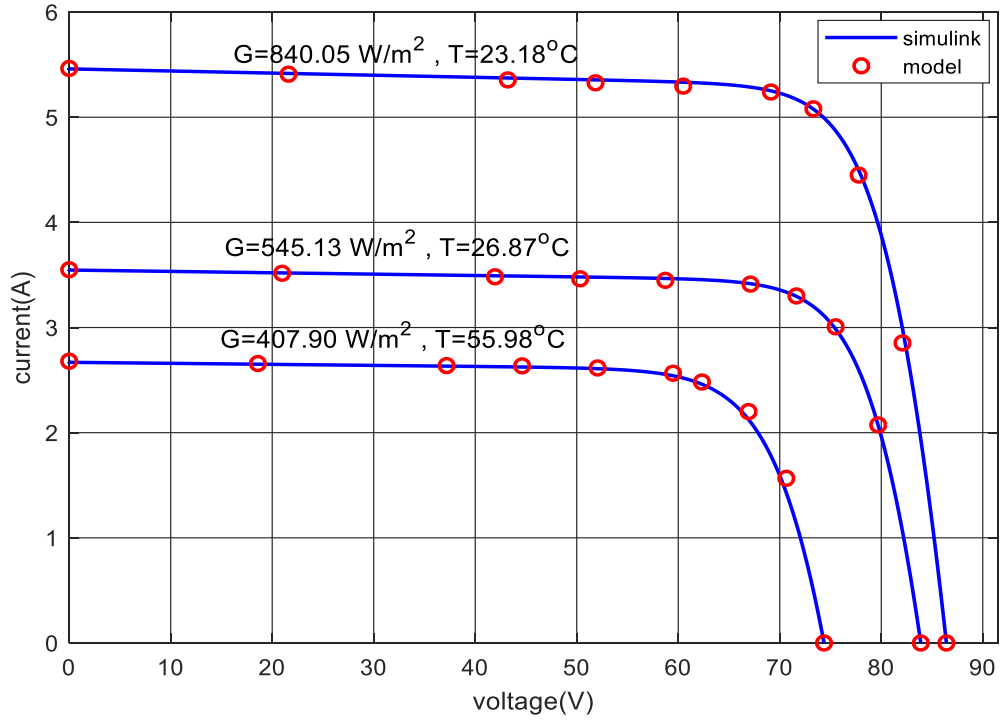


Figure 3.15: I-V curves of PV module # 9 at the indicated weather conditions

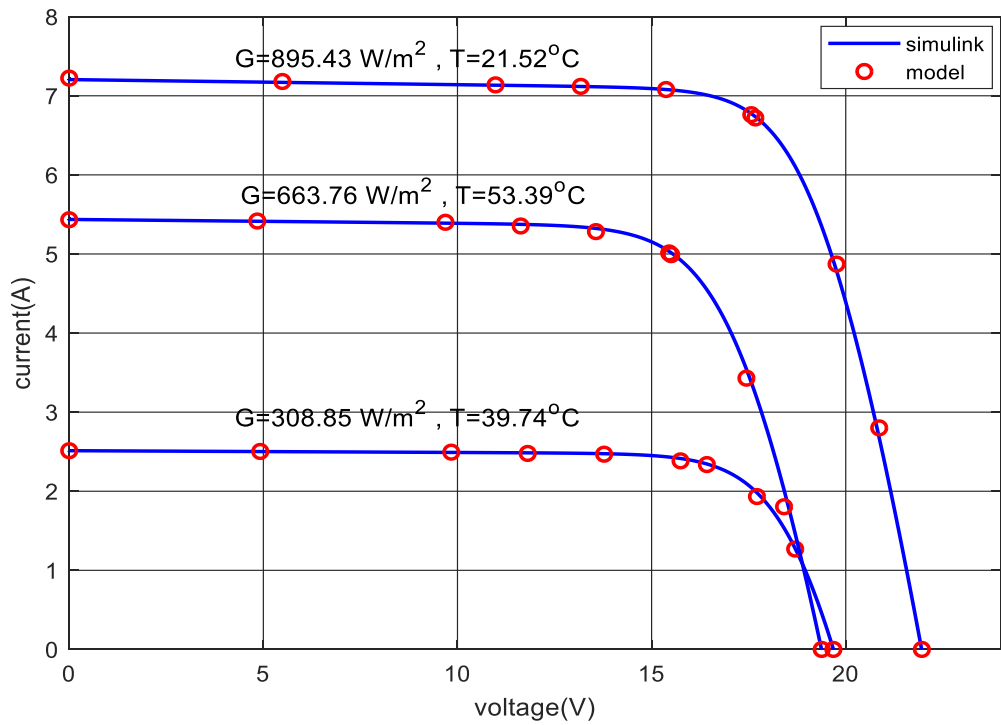


Figure 3.16: I-V curves of PV module # 10 at the indicated weather conditions

3.3.2.2 Comparison with parameters extracted from commercial PV module datasheet

For this assessment, three commercially available modules are selected. The technical specifications are listed in Table 3.6. The specifications data sheet including the I-V curves for the three modules are shown in the appendix. The points on the I-V curves are extracted using Digitizelt software [101]. Figure 3.17 to Figure 3.19 compare the I-V curves of the selected modules derived via SIMULINK simulations, the proposed models, and the extracted points. The effectiveness of the models performance is verified by the similarity of the depicted I-V curves for all modules at different weather conditions.

Table 3.6: Selected commercial PV modules employed in models assessment

	manufacturer	N	$V_m (V)$	$I_m (A)$	$P_m (W)$	$V_{oc} (V)$	$I_{sc} (A)$
PV ₁	S-Energy	60	30.4	8.08	245.63	37.4	8.63
PV ₂	SunPower	96	54.7	5.58	305.23	64.2	5.96
PV ₃	SunPower	128	72.9	5.83	425.01	85.6	6.18

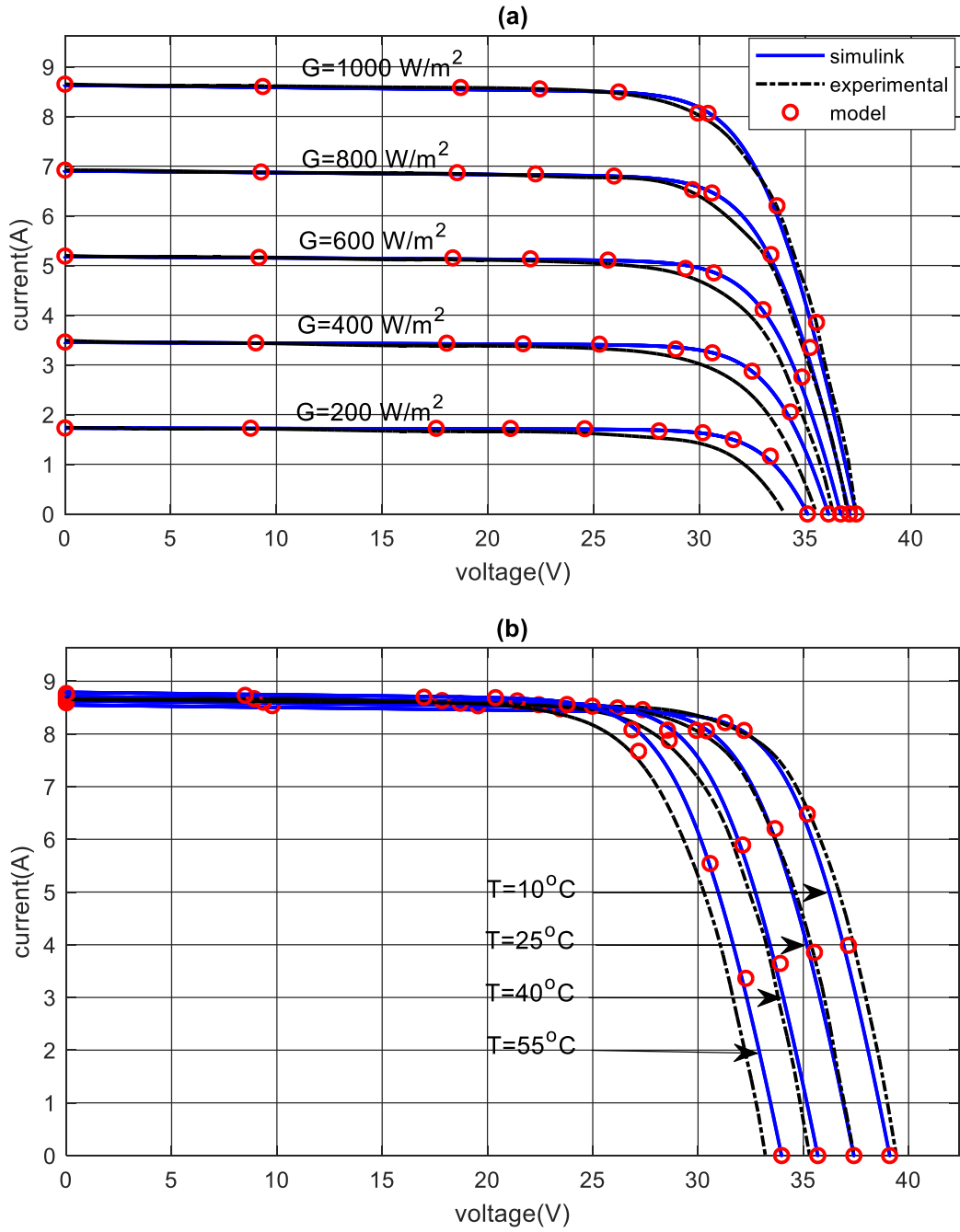


Figure 3.17: I-V curves of 245 W S-energy module:(a) $T=25^{\circ}\text{C}$ and different G (b) $G=1000\text{ W/m}^2$ and different T

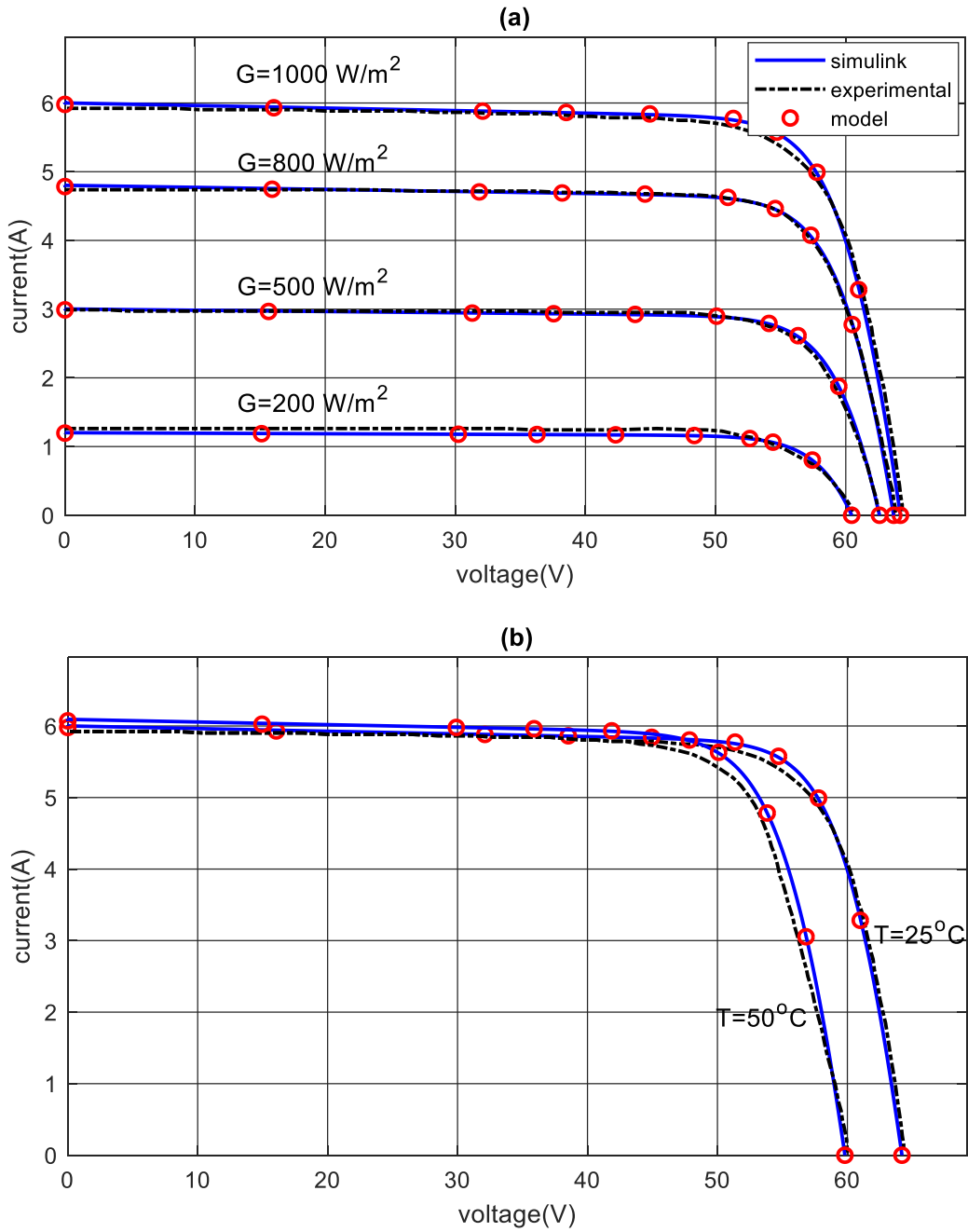


Figure 3.18: I-V curves of 305 W SunPower module:(a) $T=25^{\circ}\text{C}$ and different G (b) $G=1000\text{ W/m}^2$ and different T

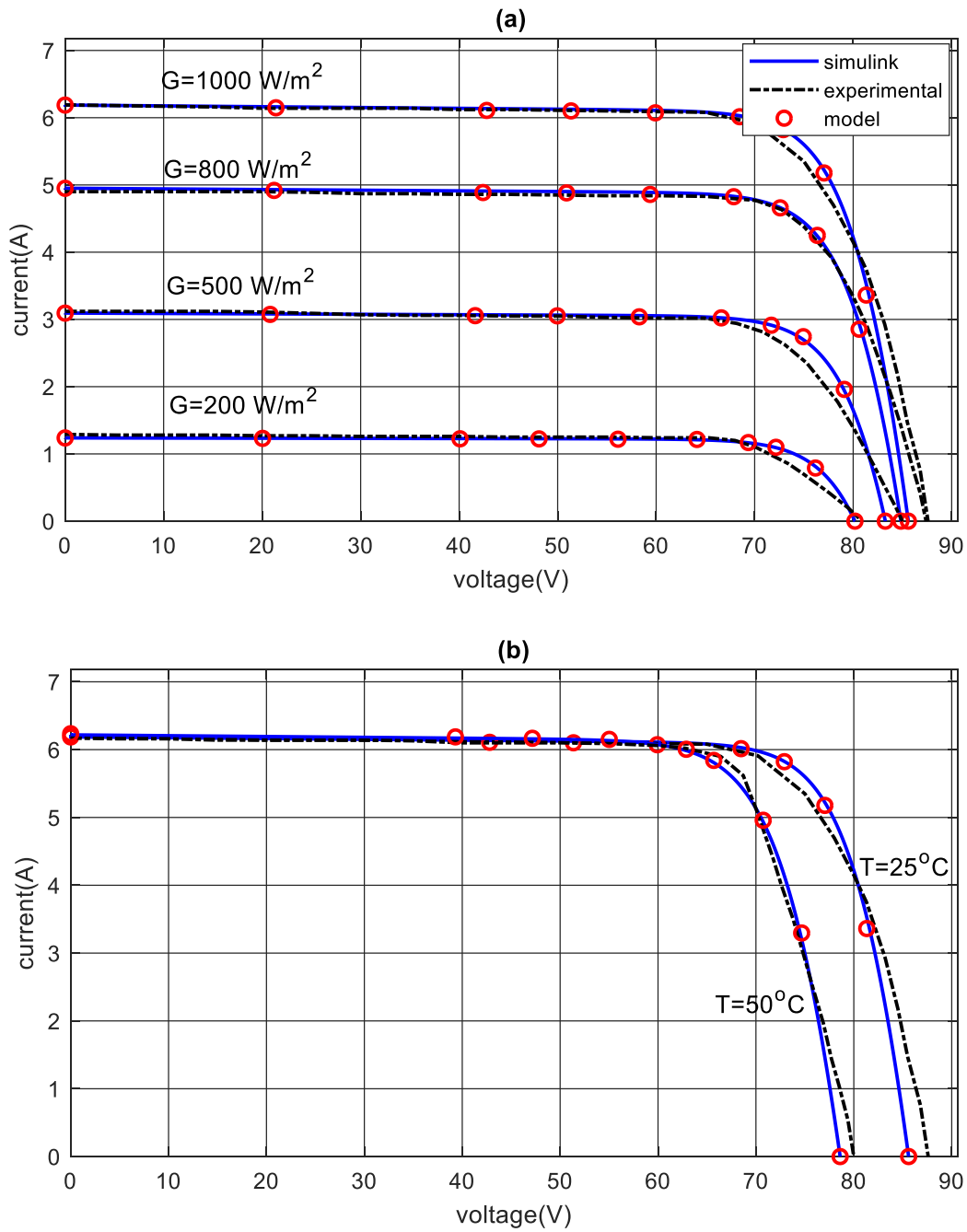


Figure 3.19: I-V curves of 425 W SunPower module:(a) $T=25^{\circ}\text{C}$ and different G (b) $G=1000\text{ W/m}^2$ and different T

3.3.2.3 Comparison with previously published research

In the final assessment, the proposed models are applied to various PV modeling scenarios presented in the literature. For each of the cases presented, the parameters of the PV equivalent circuit are extracted using some optimization algorithms. The I-V curves are then generated based on the estimated parameters at different weather conditions. Three recent research articles are adopted in this analysis.

The work presented in [102] has proposed an algorithm to estimate the I-V curves of PV modules based on the Levenberg–Marquardt (LM) method. The performance of this method is then compared with six alternative methods including genetic algorithm (GA), pattern search algorithm (PS), mean value theorem (MVT), Saloux model, non-linear least square (NLS) method and Gauss-Seidel (GS). These methods are applied to a 250 W PV module for estimating the maximum power at different weather conditions. The specifications of the selected module are listed in Table 3.7.

Table 3.7: PV module specifications at STC used in [102] for methods assessments

N	$V_m (V)$	$I_m (A)$	$P_m (W)$	$V_{oc} (V)$	$I_{sc} (A)$
60	30.3	8.25	250	37.3	8.76

The model proposed in this chapter to estimate the maximum power is applied to this PV module as well. The aforementioned methods are compared with experimental data provided by [102] at different weather conditions. The models are estimated at a temperature of 25 °C and irradiance values between 300 and 700 W/m². The experimental results for evaluating the maximum power are listed in Table 3.8. The simulation results

of all seven models presented in [102], as well as the proposed model in this chapter are shown in Table 3.9.

Table 3.8: Measured maximum power data at different conditins [102]

$G (W/m^2)$	$P_{m_{exp}}(W)$
300	74.2
500	125.70
700	176.8

Table 3.9: Maximum power evaluation using the proposed model and [102]

method	$G (W/m^2)$	$P_{m_{est}}(W)$	error (%)
GA [102]	300	70.89	4.46
	500	123.17	2.01
	700	173.21	2.03
PS [102]	300	71.44	3.71
	500	123.06	2.1
	700	173.85	1.66
MVT [102]	300	70.76	4.63
	500	121.11	3.65
	700	172.63	2.35
Saloux model [102]	300	78.08	5.22
	500	129.9	3.34
	700	182.82	3.4
NLS [102]	300	72.71	2
	500	123.46	1.78
	700	174.27	1.43
GS [102]	300	71.92	3.07
	500	122.24	2.75
	700	174.27	1.43
LM [102]	300	73.18	1.37
	500	124.16	1.22
	700	175.07	0.97
Proposed	300	75.14	1.27
	500	125.48	0.18
	700	175.81	0.56

The results indicate that the proposed model for estimating the maximum power has superior accuracy over the seven other reported methods. In the proposed methodology,

the maximum power model only requires one equation that can be evaluated without any iteration process or sophisticated operations. This has resulted in fast execution and estimation of the maximum power value.

The authors in [103], have adopted the same 250 W module to build a complete 100 kW PV array. The array is composed of 10 modules connected in series to form a string. 40 strings are connected in parallel to form a 10×40 PV array. The LM method is also employed by the authors for maximum power estimation. The performance of this method is evaluated at 25° C temperature and irradiances of 300, 500, 700, and 900 W/m². The experimental results are listed in Table 3.10. The results of maximum power evaluation using the LM method and the proposed model are summarized in Table 3.11. The proposed model has again outperformed the method proposed by [103] in terms of both execution time and estimation accuracy.

Table 3.10: Measured maximum power values at different conditions [103]

$G (W/m^2)$	$P_{m_exp}(W)$
300	29.93
500	50.38
700	70.75
900	90.43

Table 3.11: Maximum power evaluation using the proposed model and [103]

Method	$G (W/m^2)$	$P_{m_act}(kW)$	$P_{m_est}(kW)$	error (%)
LM [103]	300	29.93	29.16	2.57
	500	50.38	49.52	1.7
	700	70.75	69.81	1.32
	900	90.43	89.88	0.6
Proposed	300	29.93	30.06	0.42
	500	50.38	50.19	0.38
	700	70.75	70.33	0.60
	900	90.43	90.46	0.03

In the work presented in [104], the crucial points at the I-V curve have been evaluated using three approaches including the Sandia model, software simulations, and adaptive neuro-fuzzy inference systems (ANFIS). A 70 W PV module is selected with specifications listed in Table 3.12.

Table 3.12: PV module specifications at STC used in [104] for methods assessments

N	$V_m (V)$	$I_m (A)$	$P_m (W)$	$V_{oc} (V)$	$I_{sc} (A)$
36	16.5	4.24	70	21.4	4.7

The predicted parameters by [104] are open circuit voltage, short circuit current, maximum power voltage, and maximum power current. Simulation results comparing all techniques at temperature of 25 °C and different irradiance values are listed in Table 3.13. The results show that the results of the models proposed in this study are similar to what were obtained by the estimation approaches presented in [104]. For example, at 600 W/m², the results have shown an error of 0.35 % in estimating the short circuit current using the proposed model with respect to Sandia model.

Table 3.13: Parameters evaluation using the proposed model and [104]

method	$G (W/m^2)$	$V_{oc\ est} (V)$	$I_{sc\ est} (A)$	$V_m\ est (V)$	$I_m\ est (A)$
Sandia model [104]	1000	21.4	4.7	16.5	4.24
	800	21.17	3.76	16.56	3.42
	600	20.85	2.82	16.55	2.57
	400	20.29	1.87	16.35	1.72
	200	19.49	0.94	15.87	0.87
simulation results [104]	1000	21.37	4.68	16.37	4.25
	800	21.1	3.75	16.43	3.39
	600	20.74	2.81	16.41	2.53
	400	20.23	1.87	16.24	1.66
	200	19.32	0.93	15.66	0.79
ANFIS-based results [104]	1000	21.38	4.68	16.33	4.27
	800	21.11	3.75	16.43	3.41
	600	20.77	2.81	16.45	2.54
	400	20.28	1.87	16.33	1.67
	200	19.42	0.93	15.82	0.80
proposed	1000	21.53	4.71	16.68	4.26
	800	21.15	3.77	16.73	3.41
	600	20.78	2.83	16.80	2.55
	400	20.46	1.88	16.95	1.70
	200	20.33	0.94	17.39	0.85

The previous analyses have verified the effectiveness of all proposed models by comparison with recently reported research publications. The proposed models have effectively evaluated all parameters discussed in the presented publications.

3.4 Application of the Proposed Models for MPPT of PV Systems

MPPT concept is a crucial area of study in the field of optimization and control of the power obtained from PV systems. Employing MPPT algorithms in PV systems can significantly help to harvest the maximum power under varying environmental conditions. The change of temperature and irradiance values leads to a change in the

output PV power. Efficient MPPT control is thus essential for tracking the maximum power at any change in such environmental conditions.

This section discusses the application of the proposed mathematical models to track the MPP of PV systems. The performance of the MPPT control is assessed by application to two different grid-connected PV systems. The methodology is also compared with two commonly used MPPT algorithms; INC and P&O algorithms. .

3.4.1 Proposed MPPT Methodology

The proposed MPPT methodology utilizes the mathematical models presented in the previous section. By considering the model proposed for the voltage at maximum power, and assuming that a DC-DC boost converter is connected to the PV array, the optimal duty cycle can be determined as follows:

$$D_{opt} = \frac{V_{dc} - V_{m_mdl}}{V_{dc}} \quad (3.16)$$

Where D_{opt} is the optimal duty cycle and V_{dc} is the output fixed voltage of the boost converter.

Utilizing equation (3.16) and the model previously proposed for maximum power voltage, MPPT methodology can be designed as shown in Figure 3.20.

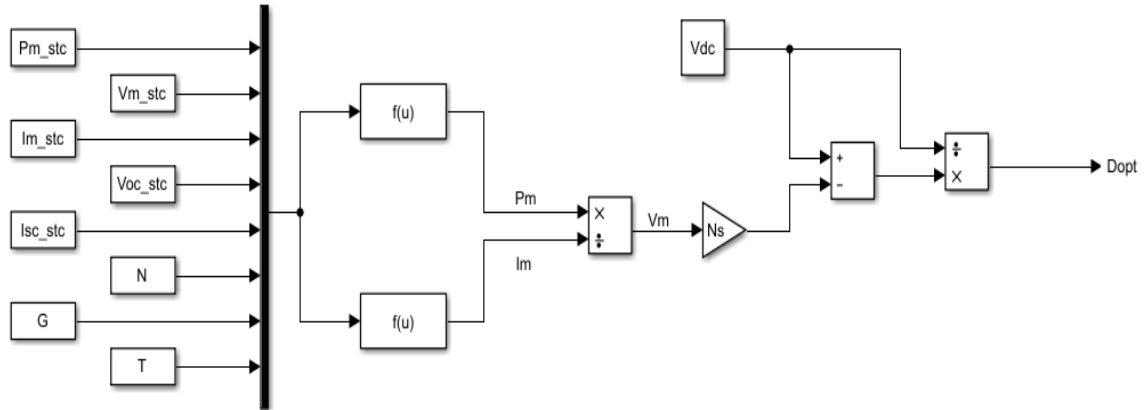


Figure 3.20: Proposed MPPT algorithm

In this scheme, the voltage at maximum power is determined using its respective model which is defined in (3.6) as the ratio of the modeled maximum power over the modeled current at maximum power. In large PV systems, this value is multiplied by the number of series connected PV modules, N_s . The optimal duty cycle is then computed using equation (3.15). The effectiveness of the proposed MPPT control is verified by application to two different grid-connected PV systems.

3.4.2 Study Case#1: Application to 100 kW Grid-Connected PV system [105]

3.4.2.1 System description

This system consists of a 100 kW PV array, DC-DC boost converter and inverter [105]. The complete system has been built using MATLAB/SIMULINK. The PV array is composed of 66 strings of 5 series-connected, SunPower 305 W modules connected in parallel. The total power is found as $66 \times 5 \times 305.2 = 100.72$ kW. The DC-DC converter output is connected to a common 500 V_{DC} bus. The layout of this scheme is depicted in Figure 3.21.

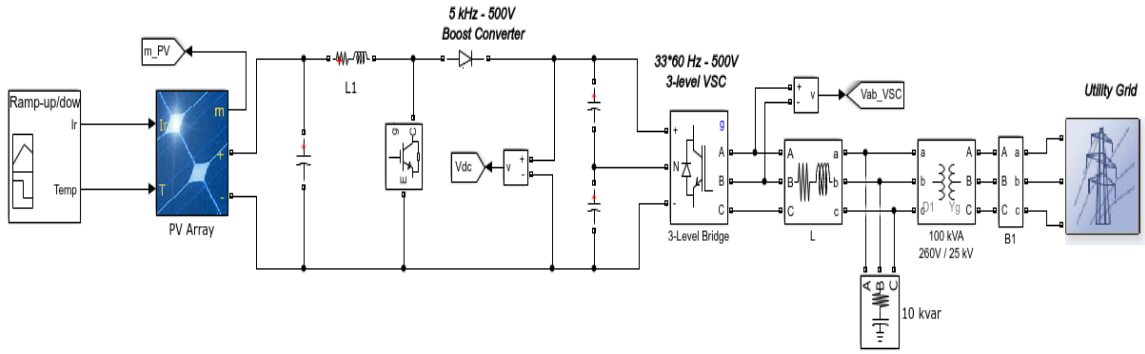


Figure 3.21: Scheme of the 100 kW grid-connected PV system

3.4.2.2 Results and analysis

The system is simulated for 3 seconds under varying temperature and irradiance profiles as shown in Figure 3.22. The simulations are carried out using the INC-based MPPT algorithm as well as the proposed methodology. Performance comparisons of the two approaches are shown in Figure 3.23 for the extracted power comparison. The maximum power extracted using both approaches are identical. The extracted interval shows that the behavior of the power using the proposed approach is steady while it is oscillating using the INC algorithm.

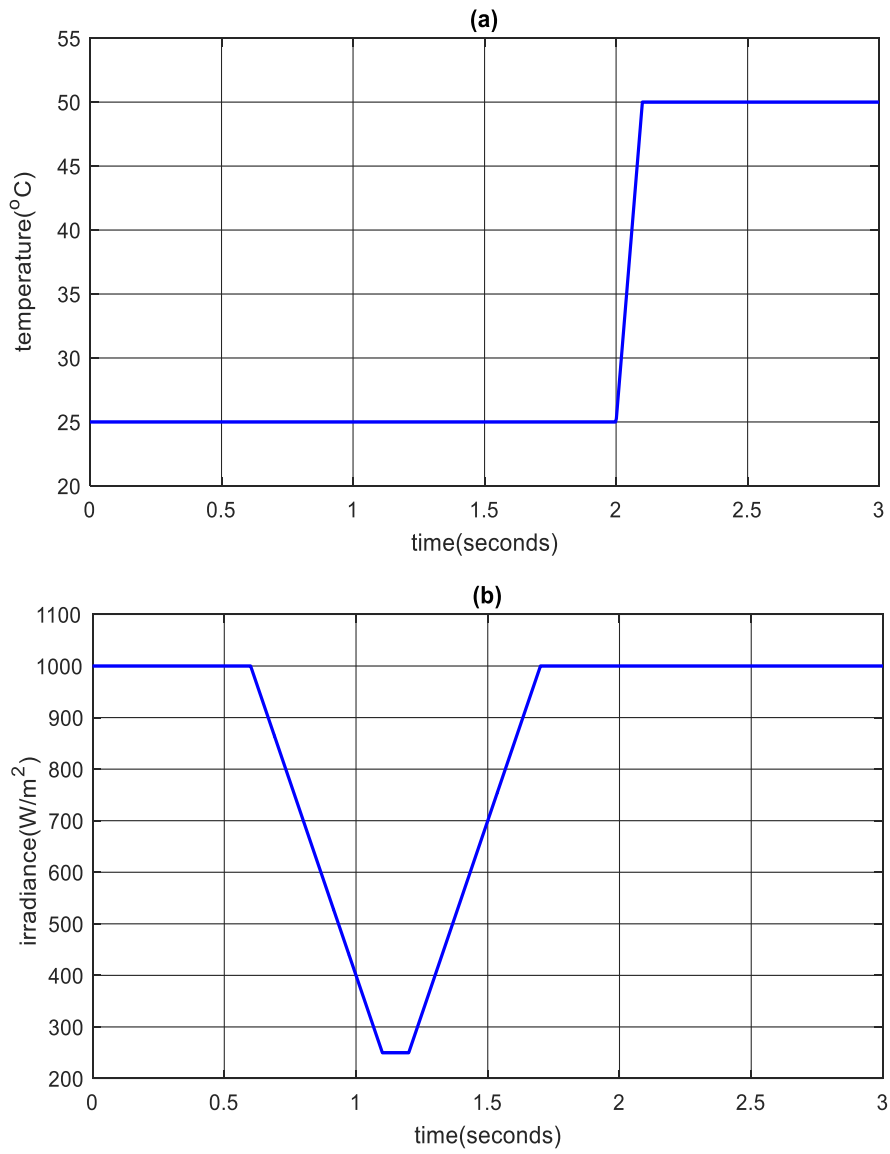


Figure 3.22: Temperature and irradiance profiles applied to the 100 kW system

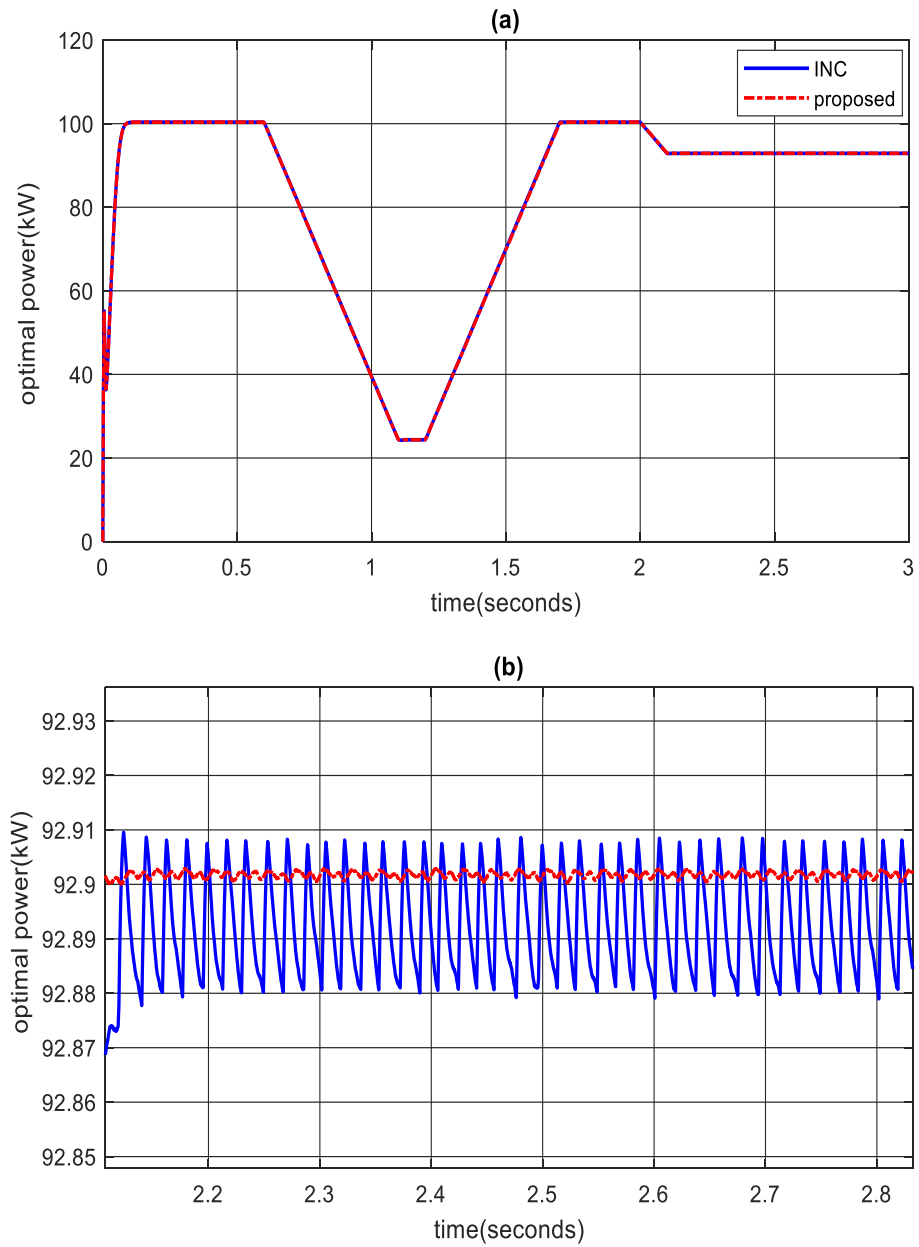


Figure 3.23: proposed model and INC: (a) complete profiles (b) extracted period

3.4.3 Study Case#2: Application to 400 kW Grid-Connected PV system [105]

3.4.3.1 System description

This system consists of four PV arrays each delivering 100 kW at STC [105]. A single PV array block consists of 64 parallel strings where each string has 5 SunPower SPR-315E modules connected in series. Each PV array is connected to a DC/DC converter, and subjected to different weather conditions. The outputs of the boost converters are connected to a common DC bus of 500 V_{DC}. Each converter is controlled by an individual MPPT. The configuration of this system is shown in Figure 3.24.

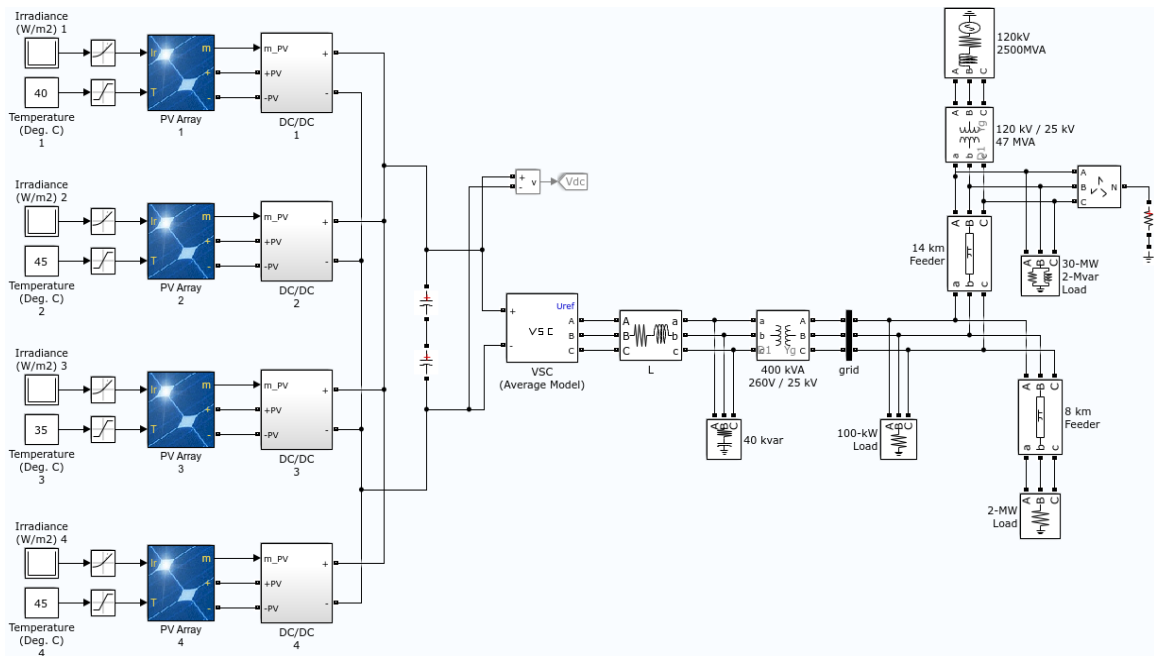


Figure 3.24: Scheme of the 400 kW grid-connected PV system

3.4.3.2 Results and analysis

The system is simulated for three seconds at different weather conditions. Each PV array is subjected to temperature and irradiance profiles different than the other arrays. The

proposed temperature and irradiance profiles are depicted in Figure 3.25. Under these weather profiles, the duty cycle for each DC-DC converter has been adjusted based on the implemented MPPT algorithm. The proposed MPPT control is compared with the MPPT control using P&O algorithm. The extracted maximum power profiles are shown in Figure 3.26 and Figure 3.27 for the individual PV arrays and the complete system, respectively. Efficient performance capability of the proposed methodology has been achieved.

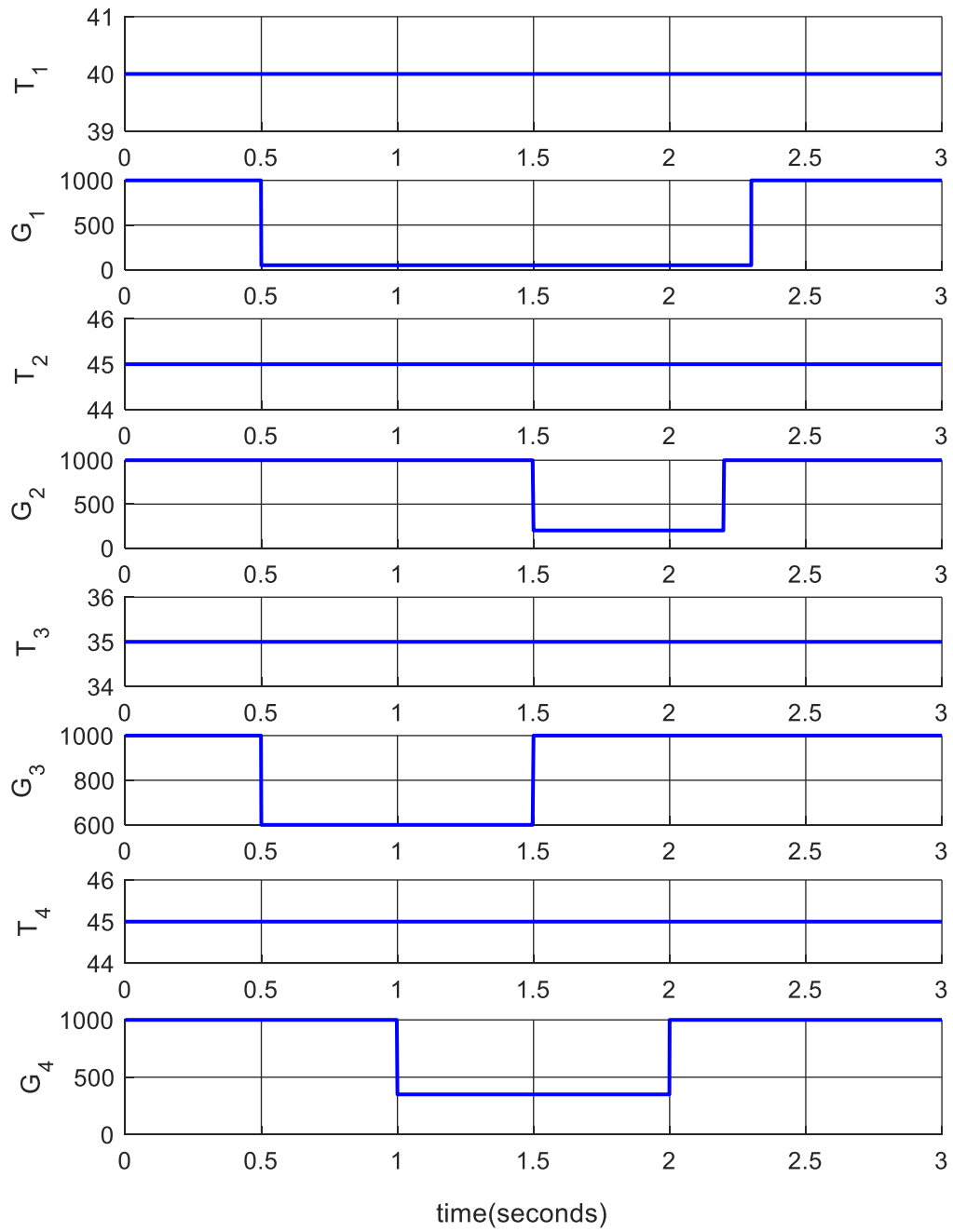


Figure 3.25: Temperature and irradiance profiles for each PV array

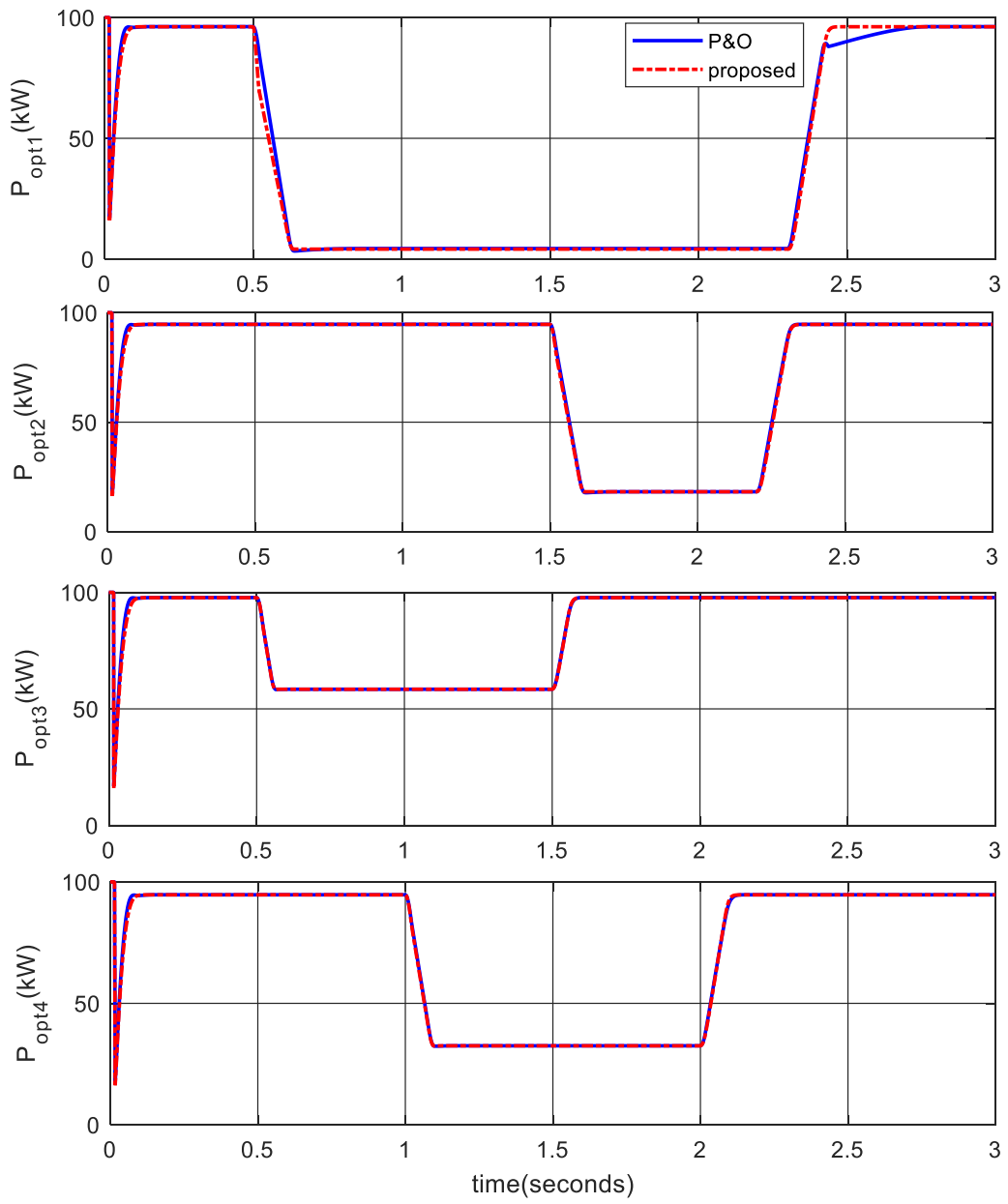


Figure 3.26: Extracted maximum power profiles for each PV array

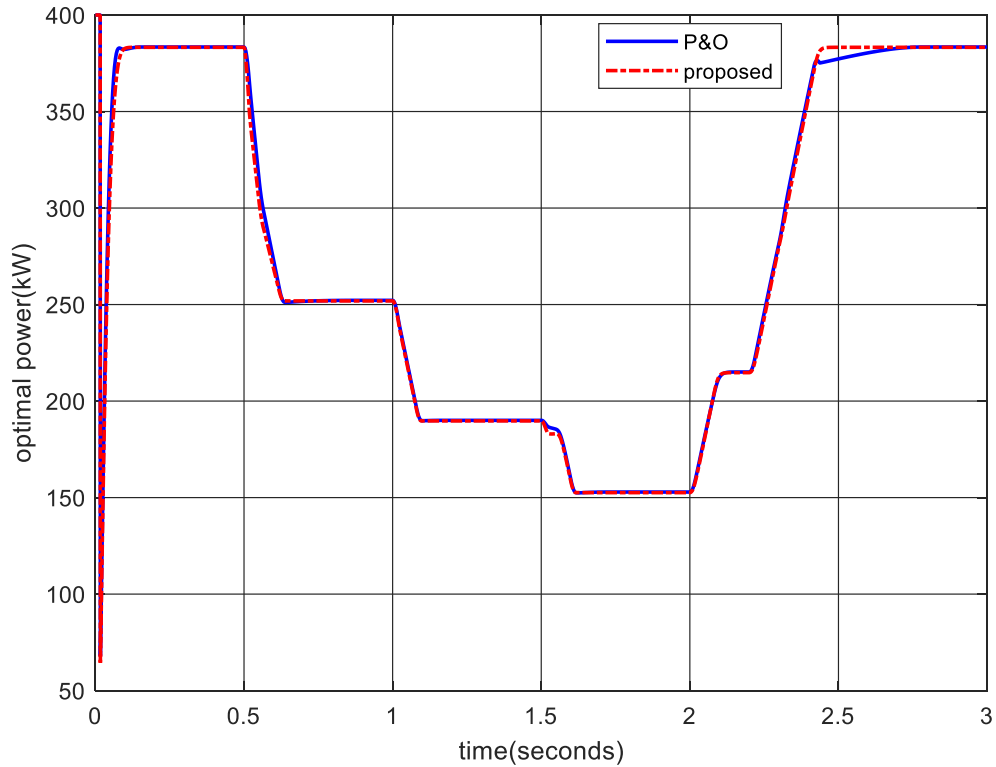


Figure 3.27: Extracted maximum power for the entire system:

3.5 Summary and Conclusions of the Chapter

The main points addressed in this chapter include the following:

- General predictive models for generating the I-V curves of a PV module have been proposed.
- The models can appropriately evaluate ten key points on the I-V curve with just knowledge about the temperature and irradiance values, as well as the STC values.
- The performance of the proposed models is compared with SIMULINK simulations data and commercial modules I-V curves for different selected PV modules.

- The models are also assessed by comparisons with other recent published research.
- The models assessments have shown efficient modeling capability of all proposed models under all performance assessments.
- The proposed models are then employed to implement a MPPT algorithm.
- The proposed MPPT algorithm is applied to two different grid-connected PV-systems and compared with the most commonly used MPPT algorithms; INC and P&O algorithms.
- The simulations results have shown identical results to what have been achieved using the INC and P&O algorithms.
- The main advantages of the proposed MPPT methodology are its robustness since it can be used for any PV system and its effectiveness since it tracks the MPP efficiently.
- Unlike most of the other techniques, the predictive models can be easily evaluated using any tool. No special software is required to apply the proposed methodology for I-V curve prediction.
- Having modeled the DC source, it is important to develop models for household appliances. This will be discussed next chapter.

CHAPTER 4

DEVELOPMENT OF MODELS FOR MAJOR AC AND DC HOUSEHOLD APPLIANCES

4.1 Introduction

Load modeling is an important component of electrical power system. Proper representation of loads can effectively help to study the loads characteristics in both steady and transient states under different operating conditions. The models can be incorporated into any power system software. The integration of such models helps to carry out detailed system analysis.

Moreover, efficient load forecasting and demand side management can be achieved by building accurate models. The models may represent entire network load, a small residential substation, a house or, more specifically, a single appliance. In addition, several parameters and characteristics of loads can be investigated using detailed models. This includes modeling and studying the problem in terms of various aspects such as power consumption, power quality issues and harmonics.

The scope of this chapter is to build simulation models for some selected major AC and DC household appliances. The appliances models can be further incorporated into an

entire network to represent AC, DC or hybrid systems in order to carry out various studies in electric power systems. The work presented in this chapter is characterized by:

- Building models for individual appliances for both AC and DC versions using two approaches utilizing actual field measurements.
- All electrical parameters can be obtained from the proposed models including active power, current and power factor.
- The data gathered from field measurements are taken each second in order to properly track the exact behavior of the appliances under study.
- The modeling analysis includes the DC appliances available in the market working at the commonly used DC voltages of $12 V_{DC}$ and $48 V_{DC}$.

The chapter focuses on building models for various major AC and DC home appliances. All models are analyzed based on actual measurements and implementation. For all AC appliances, the power source is the conventional $230 V_{AC}$ supply. The DC appliances are supplied by a DC source of appropriate DC voltage level including $12 V_{DC}$ and $48 V_{DC}$.

4.2 Methodology

The research method followed in this chapter is to measure and collect the electrical parameters data using actual field measurements for selected major AC and DC home appliances. The collected data represents the electrical specifications of appliances under study. Using the collected data, two approaches are proposed in order to build a representative model for each appliance. The purpose of the appliance model is to be

used as a representative block that comprises the electrical specifications of the appliance under a fixed supply voltage. The research method is summarized as follows:

- Step # 1: each appliance is operated for some predefined time that can insure that all operating conditions are covered.
- Step # 2: various electrical parameters are measured and recorded each second using an efficient measuring device.
- Step # 3: the collected data are employed for building representative models for each of the selected appliances using two approaches.
- Step # 4: after the models are formulated, they are validated and compared with the actual measured data to assess and evaluate the effectiveness of such models.

4.3 Experimental Set-up and Measurements Process

4.3.1 AC and DC Appliances under Study

Various major home appliances are adopted in this analysis. The selected appliances are an air conditioner, a refrigerator, a TV, a lamp and a fan. Such appliances are considered as crucial and major appliances in any average family house. Each selected appliance has both AC and DC versions in which the required task is achieved, irrespective of their electrical specifications. This includes, for example, same intensity levels for both AC and DC lamps and same size for the AC and DC TVs. The specifications of each appliance are listed in Table 4.1.

Table 4.1: Specifications of the appliances under study

	AC		DC	
	input voltage	rated power	input voltage	rated power
4100 lumens lamps	230 V _{AC}	45 W	12 V _{DC}	49 W
32 inch TV	230 V _{AC}	35 W	12 V _{DC}	20 W
fan	230 V _{AC}	50 W	12 V _{DC}	15 W
98 L refrigerator	230 V _{AC}	95 W	12 V _{DC}	75 W
18,000 Btu air conditioner	230 V _{AC}	~ 1500 W	48 V _{DC}	~ 1500 W

One of the DC systems issues is the breaking of the DC current due to the absence of zero crossing point. In the experiments performed in this study, as long as we are in low voltage DC network, the normal AC breaker can be used successfully in such DC systems. In this study, a 40 A conventional AC circuit breaker is implemented in all experiments including the AC and DC appliances measurements.

4.3.2 Measured Electrical Parameters

Three major electrical parameters are given attention in the measurements and modeling. These parameters are the voltage, current and active power, in addition to the power factor that can be calculated from the measured current and power values. Once these parameters are measured and recorded, the other parameters such as apparent power and reactive power can be estimated. For the purpose of this chapter, apparent and reactive powers are not considered in modeling.

4.3.3 Instrument used in Measurements

The device used in the measurements is the single phase power quality analyzer (PQA), CA 8230 model, which can measure and store most electrical parameters such as active power, reactive power, voltage, current and power factor. It has an efficient measuring

capability and large data saving memory by reading and storing the measured parameters each second for several continuous operating hours [106].

4.3.4 Process of Measurements

All selected appliances are operated for some time that is sufficient to collect a representative data for building the models. Based on the power characteristics of each appliance, the behavior and performance of the TV, lamp and fan are not affected by any other factors such as ambient temperature, room area and occupancy level. In case of refrigerator, as long as the refrigerator door is closed most of the time, and the set temperature is not changed, the ambient temperature factor has a minor or negligible impact. Moreover, as stated in the study presented in [107], the refrigerator door openings have small impact in altering refrigerator performance characteristics. This leads to a conclusion of having the flexibility in measurements time, duration and environmental conditions as such parameters have negligible impact on the performance of the aforementioned appliances, including the refrigerator.

The desired temperature and the initial room temperature are main two driving factors that affect the power consumption behavior of the air conditioner. For measuring the AC and DC air conditioners performances, all operating conditions have to be identical for both AC and DC cases. These include same set temperature, same initial room temperature and same room to be cooled.

Table 4.2 summarizes the duration for carrying out the measurements and collecting the data for all appliances in their both AC and DC versions.

Table 4.2: Measurements duration of the appliances under study

appliance	measurement duration (hours)
air conditioner	4
refrigerator	24
TV	1
lamp	1
fan	1

4.4 Proposed Modeling Approaches

In this section, each appliance is modeled using data gathered from real measurements. The parameters considered in the proposed models include the current, active power and power factor. Two approaches are proposed in this modeling analysis. The first approach is based on building mathematical relationships between the input and output parameters that characterize the operation behavior of the appliance. The second approach is based on physical representation of electric circuit elements. Each appliance in this approach is modeled by a combination of resistor, inductor and capacitor. Each approach is discussed in details in the following subsections.

4.4.1 Modeling using Mathematical Representation

The main idea followed in this approach is to build mathematical models of the output parameters as functions of the input parameters that characterize the appliance performance. The mathematical relationships are formulated using EUREQA software.

Based on the measured data, an output parameter, Y can be formulated as a function of an input parameter, X . This formulation takes the following form:

$$Y = f(X) \tag{4.1}$$

Where Y represents any of the output parameters including power and current. X represents any input parameter such as supply voltage and time. For all selected appliances, the proposed models are formulated for the following parameters:

- Active power
- Current

The input variables depend on the operation characteristics of the modeled appliances. At constant supply voltage, most of the appliances are not affected by any other factors such as temperature or other environmental conditions. The operation in this case is mainly dependent on manual switching by the user. These appliances may be represented by constant values. In addition, time variable is included in the appliances in which their operation is based on pulsating and periodic behavior. The appliances are classified and modeled based on their operation characteristics.

After the models are formulated, they are incorporated into MATLAB software for the purpose of representing each appliance by a MATLAB code that includes all mathematical relationships representing the selected appliance characteristics.

4.4.2 Modeling using Circuit Representation

In this approach, electric circuit elements are utilized to represent the behavior of the appliances. Data field measurements adopted in the previous approach are used here as well. Each appliance is then modeled as a parallel combination of resistor, inductor and capacitor. The values of the elements for each appliance can be computed by applying the electric circuits laws utilizing the measured parameters.

The modeling starts by assuming that any appliance can be represented by a parallel combination of resistor, R , inductor, L and capacitor, C , as shown in Figure 4.1.

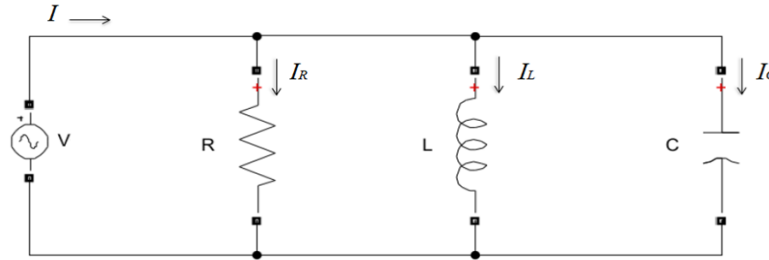


Figure 4.1: Parallel RLC circuit used for appliances models

The values of R , L and C can be determined using the equations of parallel RLC circuits by employing the values of the measured parameters.

4.4.2.1 Resistor estimation

To estimate the value of the resistor, R , the following equation is used:

$$R = \frac{V^2}{P} \quad (4.2)$$

Where V is the supply voltage and P is the active power found from the measurements.

4.4.2.2 Inductor and capacitor estimation

To evaluate the inductor and capacitor values, the equation of the power factor of parallel RLC circuit as a function of inductor and capacitor is first formulated. The power factor for any circuit is found by taking the ratio of the total impedance real part over the impedance magnitude as follows:

$$pf = \frac{\Re\{Z\}}{|Z|} \quad (4.3)$$

Where $|Z|$ is the magnitude of the total impedance.

Using circuit theorem, it can be shown that the power factor of parallel RLC circuits is:

$$pf = \frac{1}{\sqrt{(1 + R^2(\omega C - \frac{1}{\omega L})^2)}} \quad (4.4)$$

The inductor and capacitor values are evaluated using APMonitor optimization toolbox in MATLAB [108]. The objective function is formulated as follows:

$$\text{minimize } (pf_1 - pf_2)^2 \quad (4.5)$$

Subject to:

$$1 \times 10^{-3} \leq L \leq 100 \times 10^{-3} \quad (4.6)$$

$$1 \times 10^{-6} \leq C \leq 100 \times 10^{-6} \quad (4.7)$$

Where pf_1 is the measured (actual) power factor and pf_2 is the estimated power factor from equation (4.4), using the selected inductor and capacitor values.

At this stage, the calculated values of R , L and C are inserted into the parallel RLC circuit shown in Figure 4.1. This circuit ultimately represents the electrical parameters of each appliance. The models with evaluated elements are then incorporated into SIMULINK software for the purpose of representing each appliance by a SIMULINK model. Next

section presents the application of the proposed approaches to the major home appliances under study.

4.5 AC and DC Appliances Models Building

This section discusses in details the application of the proposed modeling approaches to the selected AC and DC appliances. The section builds the mathematical models formulated to the considered appliances and evaluates the values of the parallel *RLC* circuit elements for each appliance. As the operating characteristics are similar for the TV, lamp and fan, such appliances are modeled by the same concept. These appliances are categorized in one category in which their working performance follows steady and constant behavior under fixed input voltage. The second category includes the refrigerator and the air conditioner in which the operating behavior of these appliances is time-dependent and follows pulsating ON/OFF cycles. Each category is analyzed individually in the following subsections.

4.5.1 Category I: Appliances with Constant Operating Characteristics

The operation duration for these appliances is controlled completely by the user. As long as the supply voltage is not changed, the power consumption behavior, as well as other electrical quantities are steady and not affected by any other operating conditions. After the appliance performs its intended job, it is switched OFF manually by the user. Different types of loads belong to this group. The TV, lamp and fan are categorized to this type of appliances. The current and power profiles of these appliances are simply modeled as constant values. Table 4.3 summarizes the current and active power values for category I appliances.

Table 4.3: Power and current values for mathematical models of category I appliances

appliance	input voltage	active power (W)	current (A)
AC TV	230 V _{AC}	32.5	0.32
AC lamp	230 V _{AC}	9.3	0.08
AC fan	230 V _{AC}	46.5	0.21
DC TV	12 V _{DC}	24.4	2
DC lamp	12 V _{DC}	7.1	0.59
DC fan	12 V _{DC}	14	1.16

These constant values are stored in a MATLAB M-file or in SIMULINK for representing the active power and current of each appliance, and then can be simulated for controlled simulation intervals.

For the circuit representation approach, the measured active power and current are used to evaluate the resistor, inductor and capacitor values of the *RLC* circuit as discussed in the previous section. In this case, the measured active power and current of the AC TV during the operation interval are required. At 230 V_{AC} input voltage, the averaged measured active power is 32.58 W, current is 0.32 A and the calculated power factor is 0.45. This gives the values of the resistor, inductor and capacitor of the parallel *RLC* circuit as 1623.54 Ω, 84.72 mH and 79.78 μF, respectively.

The evaluated elements values are inserted now into the SIMULINK *RLC* circuit with 230 V_{AC} supply voltage as shown in Figure 4.2. This circuit represents the final AC TV model considered in this chapter.

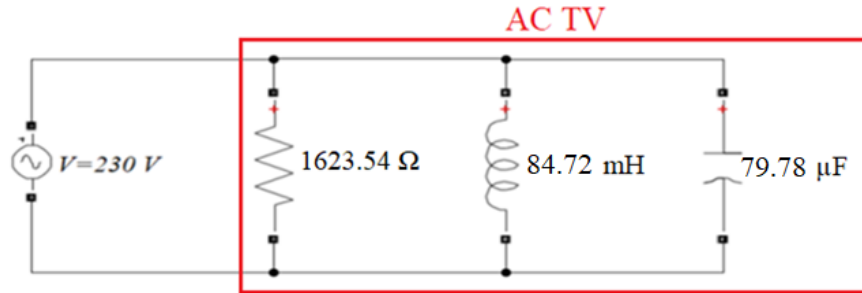


Figure 4.2: Evaluated circuit elements for the AC TV

Table 4.4 lists the determined resistor, inductor and capacitor values of all appliances under this category. The DC appliances are simply modeled using resistors due to the absence of reactive power in DC circuits. The resistors values are evaluated by dividing the 12 V_{DC} supply voltage by the averaged measured DC current.

Table 4.4: Circuit elements values for appliances under category I

	input voltage	R (Ω)	L (mH)	C (μ F)
AC TV	230 V _{AC}	1623.54	84.72	79.78
AC lamp	230 V _{AC}	5667.69	71.37	99.42
AC fan	230 V _{AC}	1137.74	84.48	82.63
DC TV	12 V _{DC}	5.91	-	-
DC lamp	12 V _{DC}	20.16	-	-
DC fan	12 V _{DC}	10.35	-	-

Each appliance is now modeled using circuit representation. The models are implemented using SIMULINK in which each appliance has its own parallel *RLC* circuit model that represents its electrical characteristics.

4.5.2 Category II: Appliances with Pulsating Operating Characteristics

The AC air conditioner and the refrigerators adopted in this study are all of ON/OFF compressor-type. On the other hand, the DC air conditioner selected in this chapter has a variable speed compressor. The power consumption profiles of these devices are depicted

in Figure 4.3 for a sample interval of two hours. The pulsating behavior is clear in case of the AC air conditioner, as well as the AC and DC refrigerators. The same modeling procedure is followed for modeling such appliances. The DC air conditioner first works at its rated power. Once the set temperature is achieved, it starts to decrease and stabilize its power till the end of operation, at an assumption of there is no further change of the weather conditions inside the room. The modeling approach of the DC air conditioner is slightly different.

For the devices with pulsating behavior, it is not possible to model such behavior as constant values. As the pulsating behavior in this case is time-dependent, the electrical parameters are now modeled as functions of time for the mathematical modeling approach. The AC air conditioner model is discussed in details where the other appliances in this category follow the same approach.

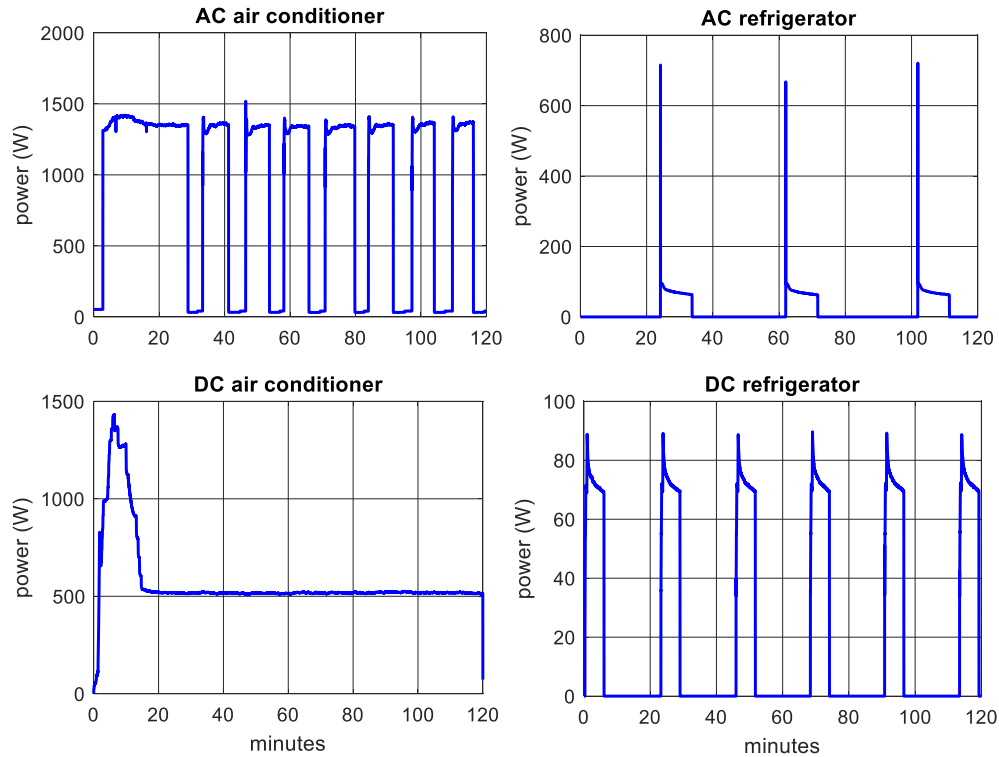


Figure 4.3: Power profiles for the air conditioners and refrigerators

The desired temperature and the initial room temperature are the main two driving factors that affect the power consumption behavior of the air conditioner. The modeling analysis starts by operating the AC air conditioner for a typical period of time and measuring and recording the electrical parameters as well as initial and current room temperature values each second. The modeling analysis is based on some specified operating conditions. The following are the operating conditions considered in this analysis:

- initial room temperature is 30 °C.
- desired temperature is 23 °C.

The figure shows that the AC air conditioner starts and continues in operation for a long ON cycle for some time before it fluctuates between almost symmetric ON/OFF positions. The first long ON cycle depends mainly on the initial room temperature and

the set temperature that specify the ability of the air conditioner to cool the room. Based on a 30 °C initial temperature and a 23 °C set temperature, it is found that the first long ON interval stays for around 35 minutes. This is followed by approximately symmetric periods of ON/OFF cycles with around 5 minutes for the OFF cycle duration and about 7 minutes for the ON cycle duration.

For the mathematical representation approach, the complete model is divided to three equations as functions of time. The first equation represents the power value of the first long ON interval whereas the other two equations represent the power values of the OFF and ON intervals, respectively. The models of the power and current are proposed using mathematical representation as functions of time. The following equations represent the power consumption performance of the AC air conditioner used in this study under the specified operating conditions.

$$P_{AC_air\ conditioner} = \begin{cases} 1291 + 0.084t + 129.9 \sin(0.004t) - 0.096t \sin(0.0046t), \\ \quad 1 < t < 1561 \\ 444.1 + 4.72 \times 10^{-8} t^3 + 3.4 \times 10^{-6} t^2 \cos(0.045t) - 0.38t - 9 \cos(0.045t), \\ \quad 1562 + 744n < t < 1869 + 744n, \text{ where } n = 1, 2, \dots, 11 \\ 1408.4 \sin(0.0007t) + 0.078t \sin(0.046t) - 55.67 - 174.27 \sin(0.046t), \\ \quad elsewhere \end{cases} \quad (4.8)$$

Same approach is followed to model the current which has the following model:

$$I_{AC_air\ conditioner} = \begin{cases} 5.68 + 0.0004t + 0.57 \sin(0.004t) - 0.0004t \sin(0.005t), \\ \quad 1 < t < 1561 \\ 3.85 + 0.038 \times 10^{-8} t^3 + 0.03 \times 10^{-6} t^2 \cos(0.045t) - 0.003t - 0.078 \cos(0.045t), \\ \quad 1562 + 744n < t < 1869 + 744n, \text{ where } n = 1, 2, \dots, 11 \\ 6.28 \sin(0.0007t) + 0.0003t \sin(0.046t) - 0.25 - 0.778 \sin(0.046t), \\ \quad elsewhere \end{cases} \quad (4.9)$$

Where t represents the time in seconds and n is the number of periods. Each period has one complete ON/OFF cycle.

The first equation represents the first long ON interval for the AC air conditioner where the other two equations represent the OFF and ON cycles, respectively.

The DC air conditioner selected in this study has a variable speed motor that changes its speed based on the cooling requirements with no successive ON/OFF cycles. Unlike the AC air conditioner, the performance of the DC air conditioner follows steady behavior at its rated power at the starting of operation. Once the set temperature has been reached, the power gradually decays to a value corresponding to the adjusted temperature. The following equation represents the power characteristics of the DC air conditioner at the specified operating conditions:

$$P_{DC_air\ conditioner} = \begin{cases} 20 + 1.2t + 7 \cos(-0.002t^2) - \frac{0.069}{\cos(2.4 + 20t)} - 1.6 \cos(5.5 + 0.4t), & 1 \leq t \leq 80 \\ 5.49t + 1.75 \times 10^{-11}t^5 - 12.32 - 8.15 \times 10^{-21}t^8 - 1.55 \times 10^{-5}t^3, & 81 \leq t \leq 882 \\ 516.58, elsewhere \end{cases} \quad (4.10)$$

The current is found by dividing this equation by the input DC voltage, which is 48 V_{DC} in this case.

The AC refrigerator follows the same modeling procedure performed for the AC air conditioner. The behavior in this case is pulsating over the entire operation interval with symmetric ON and OFF cycles. When the compressor is OFF, the power value is zero. Therefore, one representative ON cycle can be modeled. The remaining cycles are just

repetitions of this cycle. For the ON cycle, the active power and current are represented by the following equations:

$$P_{AC_refrigerator} = 72.2 + \frac{997}{t} - \frac{7736}{21.2+t^2} + 0.02t \sin\left(\frac{-8785}{t^2}\right) - \frac{76497}{8708+t^3-407t} - 0.02t \quad (4.11)$$

$$I_{AC_refrigerator} = 0.54 + 4.15 \times 10^{-6} t^2 + 5.8 \times 10^{-12} t^4 + \frac{35.81}{9.3+0.27t^6} - 0.001t - 8.1 \times 10^{-9} t^3 \quad (4.12)$$

The range of the time variable is from 1 to 600 seconds which is the duration of each ON cycle. The above equations are evaluated for the time values from 1 to 600 seconds. The OFF cycle lasts for 1600 seconds. This ON/OFF cycle is now representing a complete period comprising the first ON cycle followed by the first OFF cycle. This period is then just repeated till the end of operation. This formulation can be implemented easily using SIMULINK blocks or an M-file code using *for* loop and *if* statements in MATLAB.

Following exactly the same approach, the power consumption of the DC refrigerator is formulated as follows:

$$P_{DC_refrigerator} = 57.6 - \frac{149.2}{t} + \frac{106.6}{t^2} + 10.6 \sin\left(\frac{77.7}{t}\right) * \sin\left(\sin\left(\frac{77.7}{t}\right)\right) + 6.3 \sin\left(\frac{-251}{t^2} + \frac{5.4}{t^2 \sin\left(\frac{77.7}{t}\right)}\right) + \frac{57.6 + 10.6 \sin\left(\frac{77.7}{t}\right) \sin\left(\sin\left(\frac{77.7}{t}\right)\right)}{t} \quad (4.13)$$

The ON and OFF cycles duration in this case are 300 seconds and 1000 seconds, respectively. The DC refrigerator current can be calculated by dividing the modeled power equation above by the supply DC voltage value, which is 12 V_{DC}.

In case of circuit representation approach, the ON cycle for the AC air conditioner is averaged as an active power of 1350 W and current of 6 A. The elements values are then estimated based on these values. This gives constant performance over the entire operation interval. To represent the pulsating behavior, this constant profile is controlled by a pulse generator waveform that has a peak value of one and pulses widths of 35 minutes to represent the first long ON cycle, 5 minutes to represent the OFF cycle and 7 minutes to represent the ON cycle. The circuit diagram of the AC air conditioner model is shown in Figure 4.4. Other appliances in this category follow the same approach. Table 4.5 and Table 4.6 list respectively the circuit elements values for all AC and DC appliances under this category.

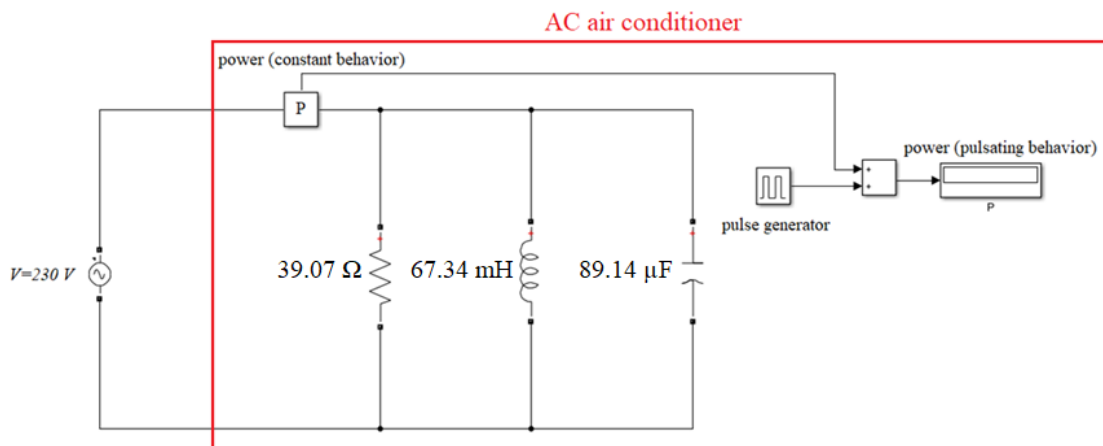


Figure 4.4: AC air conditioner SIMULINK model using circuit representation

Table 4.5: Circuit elements values for category II AC appliances

	R (Ω)	L (mH)	C (μ F)
AC air conditioner	39.07	99.70	85.92
AC refrigerator	755.71	87.50	84.07

Table 4.6: Circuit elements values for category II DC appliances

	R (Ω)	L (mH)	C (μ F)
DC air conditioner	4.46	-	-
DC refrigerator	2.06	-	-

4.6 AC and DC Appliances Models Validation and Assessments

In this section, the proposed models are simulated and compared with the experimental data. The mathematical models are coded in MATLAB using M-file scripts whereas the circuit-based models are implemented in SIMULINK. For both approaches, the models are simulated for some predefined time and the evaluated electrical parameters profiles are compared with the measured data. As sample results for models assessments, power consumption profiles for some selected appliances are demonstrated in this analysis. The appliances considered here are the AC fan, AC air conditioner and DC air conditioner. The measurements duration in assessment process are two hours for the AC fan, around three hours for the AC and DC air conditioners. The power values are captured each second. Figure 4.5 to Figure 4.7 respectively show the power consumption profiles for these appliances at the defined operation intervals. The figures compare the profiles obtained using the proposed models with the measured data. The proposed models profiles are in good agreement with the measured data.

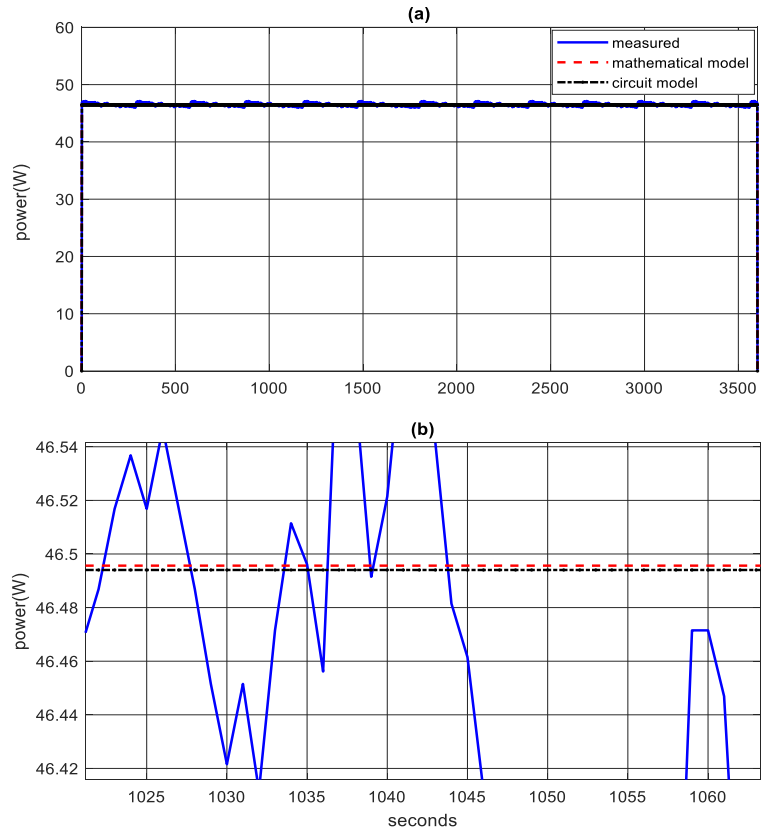


Figure 4.5: AC fan power: (a) complete power profile (b) extracted interval

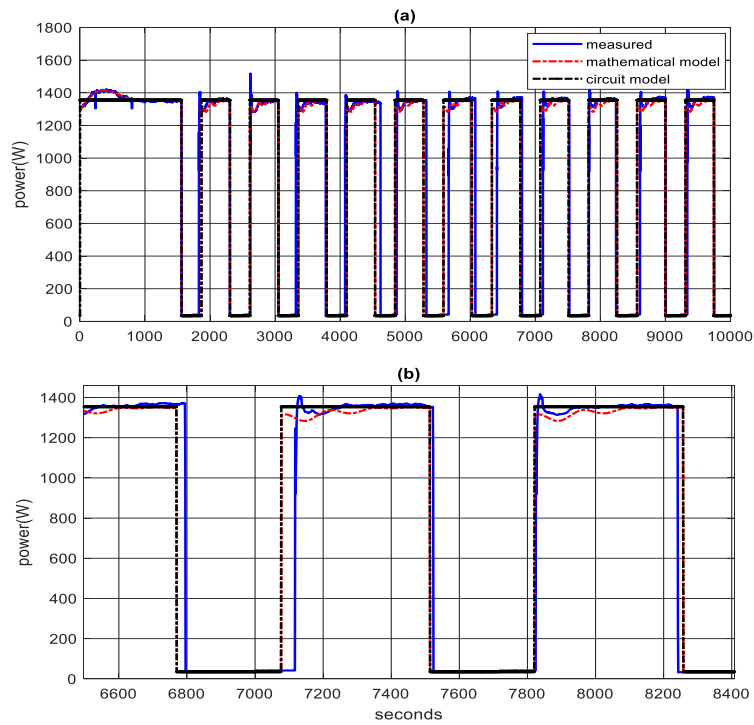


Figure 4.6: AC air conditioner power: (a) complete power profile (b) extracted period

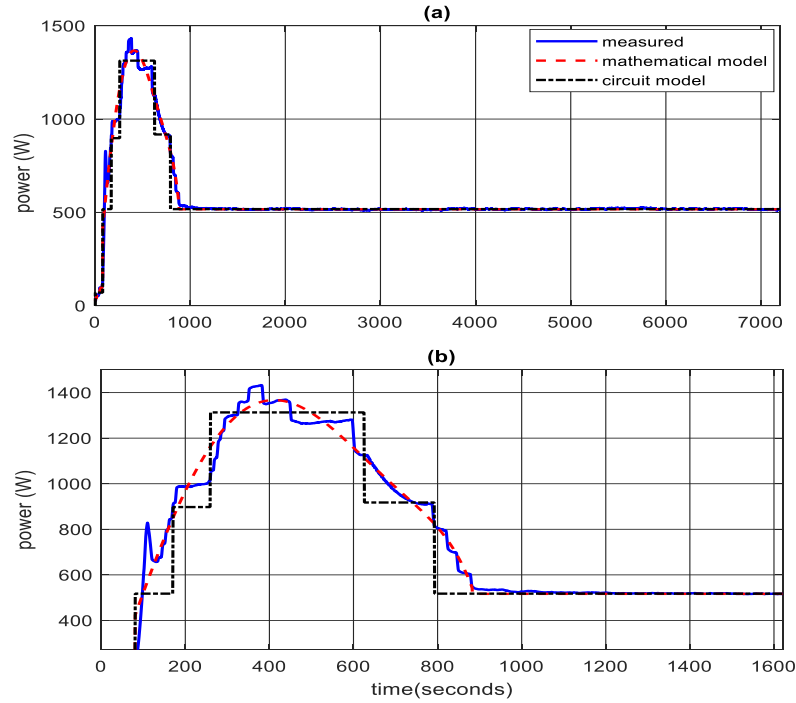


Figure 4.7: DC air conditioner: (a) complete power profile (b) extracted interval

To summarize the testing and assessments of the models, the mean absolute percentage error (MAPE) is adopted to evaluate the accuracy of all proposed models. Table 4.7 summarizes the MAPE values of the proposed models of category I as compared with the measured data. For the AC appliances, the parameters considered in comparisons are the power consumption, current and power factor whereas the power consumption and current are considered for the DC appliances.

Table 4.7: Proposed models performance compared to the measurements (category I)

	MAPE (%)					
	mathematical model			circuit model		
	P	I	pf	P	I	pf
AC lamp	0.204	0.184	0.054	0.205	1.757	1.727
AC fan	0.543	0.526	0.040	0.543	0.552	0.207
AC TV	0.242	0.710	0.886	0.240	0.879	1.037
DC lamp	0.002	0.002	-	0.0001	0.0001	-
DC fan	0.0003	0.0003	-	0.0004	0.0004	-
DC TV	0.406	0.406	-	0.405	0.405	-

For the pulsating-behavior appliances, along with the DC air conditioner, the error calculation is applied here for the total energy consumed over the entire time of operation, rather than the instantaneous power consumption because an error in one second of predicting a point in the ON cycle instead of the OFF cycle results in considerable error. The power profiles for the measured data and proposed models are identical as seen from the figures. Table 4.8 compares the total energy consumed using both approaches for the AC and DC air conditioners and refrigerators. The table shows that the total energy consumed using the proposed models are in well agreement with the ones obtained from the measured data.

Table 4.8: Air conditioners and refrigerators energy comparisons to measurements

	total energy consumed (kWh)			absolute error (%)	
	measured	mathematical	circuit	mathematical	circuit
AC air conditioner	2.418	2.40	2.430	0.707	0.534
DC air conditioner	1.637	1.638	1.646	0.098	0.611
AC refrigerator	0.056	0.057	0.057	0.378	0.310
DC refrigerator	0.023	0.023	0.024	1.494	2.797

4.7 Summary and Conclusions of the Chapter

In this chapter, the following points have been addressed and analyzed:

- Models for various AC and DC home appliances have been proposed.
- Two modeling approaches are proposed. First approach is based on representing the electrical parameters of each appliance by mathematical representation. Second approach represents each appliance by its representative parallel *RLC* circuit. The modeling also includes the new DC appliances available in the market.

- The results of models verification prove the effectiveness of all models proposed for all appliances, in which low comparison percentage error is obtained.
- All models of all appliances can be integrated into a complete system to represent actual AC house, DC house or hybrid house. The main advantage of building such models is the possibility of connecting the appliances models as to represent actual AC or DC house in order to study these systems at different points of view.
- In addition, AC and DC houses models can be built using MATLAB/SIMULINK and extensive comparisons can be performed in terms of cost analysis and energy assessments by utilizing the proposed models. Further analysis on such systems can be carried out such as load flow, protection, load profiles comparisons and fault analysis.
- In case of circuit representation models, the models are implemented in SIMULINK. In general, connection of several physical models in SIMULINK needs long simulation time. Incorporating of all models in one SIMULINK file to represent a complete house requires long simulation time. This issue can be solved by carrying out the simulations in PC's with high speed processors and sufficient memory.
- The mathematical models can be simulated in MATLAB M-files with fast computational time.
- Even though the proposed models have been built for some selected and specific appliances, the same modeling concepts can be applied to other appliances.
- The house that incorporates such selected appliances can be treated as a typical test system comprising major AC and DC appliances, in which the AC and DC

houses are performing the same required task, irrespective of the power consumption behavior for each house.

- In addition, the proposed models for the new available-in-market DC appliances can help to study and simulate the characteristics of these new and efficient energy saving devices

CHAPTER 5

AC AND DC DISTRIBUTION ARCHITECTURES

FOR A STANDALONE HOUSE

5.1 Introduction

This chapter discusses the design and analysis of different low voltage AC and DC networks. The analysis is presented for a small standalone house, in which several distribution schemes are proposed and analyzed. The proposed layouts present preliminary supplying AC appliances from AC source. Another configuration discusses designing a complete DC network consisting of DC sources and loads. Hybrid systems are also proposed in which combinations of different AC and DC sources and loads are incorporated into the same network. The proposed configurations are studied and evaluated extensively in terms of energy consumption, systems sizing, required components and detailed economical analysis. Comparative analysis between all proposed schemes is then carried out. In all cost analysis presented in this chapter, all components required by each of the proposed configurations are prepared and purchased by the consumer. These include appliances, converters, diesel generators, PV modules and batteries.

5.2 Design and Architectures of the Standalone House

This section discusses in details the design and analysis of supplying the power to a small standalone house. Several major household appliances are incorporated into the proposed house, in which both AC and DC versions are available for the selected appliances. A proper DC supply voltage level is first selected based on the dominant DC voltage levels available currently in the market. In this analysis, a diesel generator is considered as the main AC supply whereas solar PV panels and batteries represent the main DC source.

The appliances considered represent the major home appliances essential for a small house in Saudi Arabia. The appliances are air conditioner, refrigerator, lamps, TV, fan, laptop, phone charger and internet router. For the first five appliances, both AC and DC versions are available. On the other hand, the laptop, phone charger and internet router are working internally based on DC due to the internal electronic components integrated into the structure of these appliances. In the conventional AC network, these electronic appliances are usually equipped with external AC/DC converters for the purpose of converting the utility $230 V_{AC}$ voltage to the appropriate DC voltage level. The analysis in this section starts by designing the standalone house, which is followed by networks analysis and comparison.

5.2.1 Layout of the Proposed Standalone House

The proposed standalone house is composed of one room, a kitchen and a bathroom. The arrangements of the appliances locations are listed in Table 5.1.

Table 5.1: Appliances locations in the proposed standalone house

appliance	location
air conditioner	room
refrigerator	kitchen
lamps	room, kitchen, bathroom, outdoor
TV	room
table fan	portable
internet router	portable
laptop	portable
phone charger	portable

The first step is to select the appropriate operating voltages for all AC and DC appliances. All selected AC appliances are based on 230 V_{AC}. The DC appliances voltage selection depends on the available-in-market appropriate operating DC voltages for each appliance.

5.2.2 DC Appliances Voltage Selection and Specifications

A challenging task in dealing with DC distribution systems is the selection of the appropriate DC voltage [85]. As concluded from an extensive search in the market, DC home appliances are available with wide range of voltages 12, 24 and 48 V_{DC}. Other DC voltages are also available such as 36 and 72 V_{DC} but these levels are not commonly used.

Table 5.2 summarizes the availability of the selected DC appliances at each DC voltage level, where “1” means “commonly available” and “0” means “unavailable” or “rarely available”.

Table 5.2: Appliances common DC voltage levels available in the market

	DC voltage				
	5	12	20	24	48
air conditioner	0	0	0	0	1
refrigerator	0	1	0	1	0
fan	0	1	0	1	0
LED lamp	0	1	0	1	1
TV	0	1	0	0	0
laptop	0	0	1	0	0
phone charger	1	0	0	0	0
internet router	0	1	0	0	0

48 V_{DC} air conditioner is selected in this study whereas all other appliances are based on 12 V_{DC}. The DC voltage selection depends on limiting the steady state current to be below than 100 A as shown in in Table 5.3. [109].

Table 5.3: System DC voltages based on 100 A maximum current [109]

rated power	system DC voltage
< 1200 W	12 V _{DC}
1200 - 2400 W	24 V _{DC}
2400 - 4800 W	48 V _{DC}

Another reason for selecting all other appliances at 12 V_{DC} is to avoid several DC voltage conversion stages in case of selecting the appliances at different voltages. Same AC circuit breaker adopted in the experiments carried out in chapter 4 is used here as well.

In summary, Table 5.4 lists all AC and DC appliances used in this study along with their specifications and electrical power ratings. The main issue addressed in appliances selection is to choose an appliance in which the required job is similar for its both AC and DC versions, irrespective of their electrical parameters and specifications. This

includes, for instance, the same size for AC and DC TV's, same lumens levels for both AC and DC lamps and same size for the AC and DC refrigerators.

Table 5.4: Specifications of the selected appliances

	AC		DC	
	input voltage	rated power	input voltage	rated power
~4100 lumens lamps	230 V _{AC}	45 W	12 V _{DC}	49 W
32 inch TV	230 V _{AC}	35 W	12 V _{DC}	20 W
fan	230 V _{AC}	50 W	12 V _{DC}	15 W
98 L refrigerator	230 V _{AC}	95 W	12 V _{DC}	75 W
18,000 Btu air conditioner	230 V _{AC}	~ 1500 W	48 V _{DC}	~ 1500 W
19 inch laptop	-	-	20 V _{DC}	45 W
phone charger	-	-	5 V _{DC}	13 W
internet router	-	-	12 V _{DC}	13 W

5.2.3 Proposed Power System Configurations for the Standalone House

Different configurations for powering the proposed standalone house are suggested. These configurations represent AC system, DC system and hybrid AC-DC systems. Each configuration is analyzed and investigated separately in terms of several factors including energy consumption, required components and cost. The systems are implemented experimentally in order to study the electrical behavior under proposed load profile. In the measurements, the AC supply is represented by the 230 VAC utility supply whereas the DC supply is represented by batteries.

5.2.3.1 Architecture I: diesel generator supplying AC appliances

In this architecture, a standalone AC source, represented by a diesel generator, is used to power the conventional AC appliances. AC/DC converters are used for all appliances that work on DC voltage. Other appliances are connected directly to the main AC feeder. Figure 5.1 depicts the schematic of this architecture.

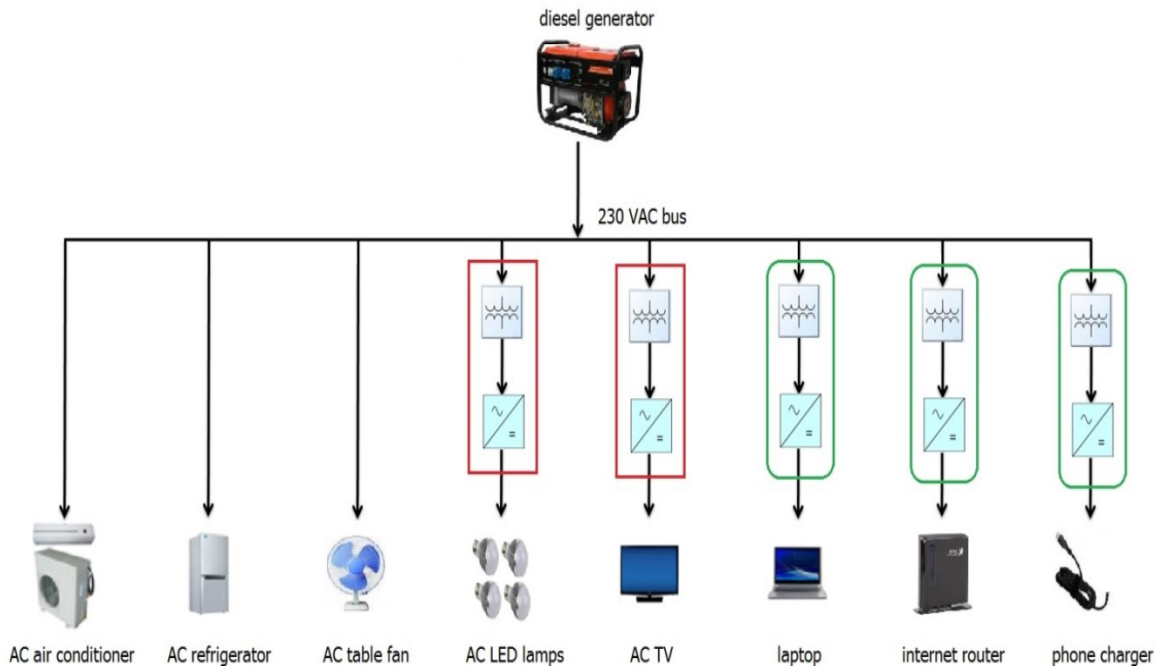


Figure 5.1: Standalone house AC appliances supplied by AC source

5.2.3.2 Architecture II: diesel generator supplying DC appliances

This architecture deals with powering DC appliances by AC supply. A 230 V_{AC}/48 V_{DC} converter is needed to supply the 48 V_{DC} air conditioner. The 12 V_{DC} appliances are connected to the main feeder via central 230 V_{AC}/12 V_{DC} converter. Other electronic devices are connected via their respective converters to the main 230 V_{AC} bus. The schematic of this configuration is demonstrated in Figure 5.2. Figure 5.3 shows sample measurements set up for supplying the 48 V_{DC} DC air conditioner by the main 230 V_{AC} supply via 230 V_{AC}/48 V_{DC} converter.

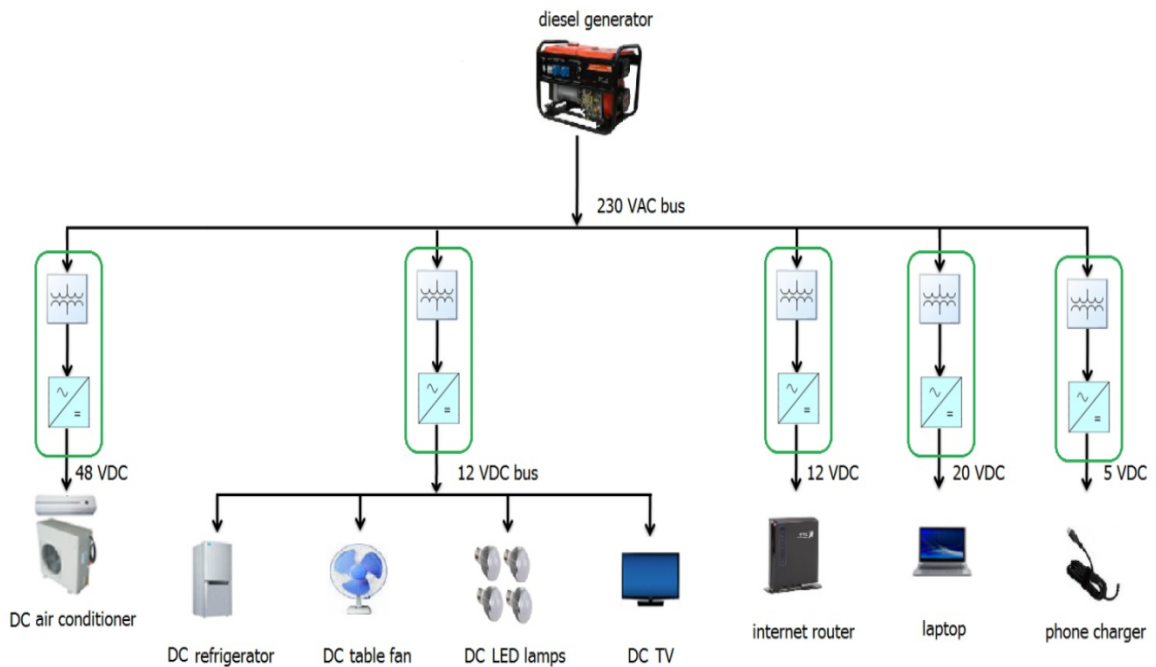


Figure 5.2: Standalone house DC appliances supplied by AC source

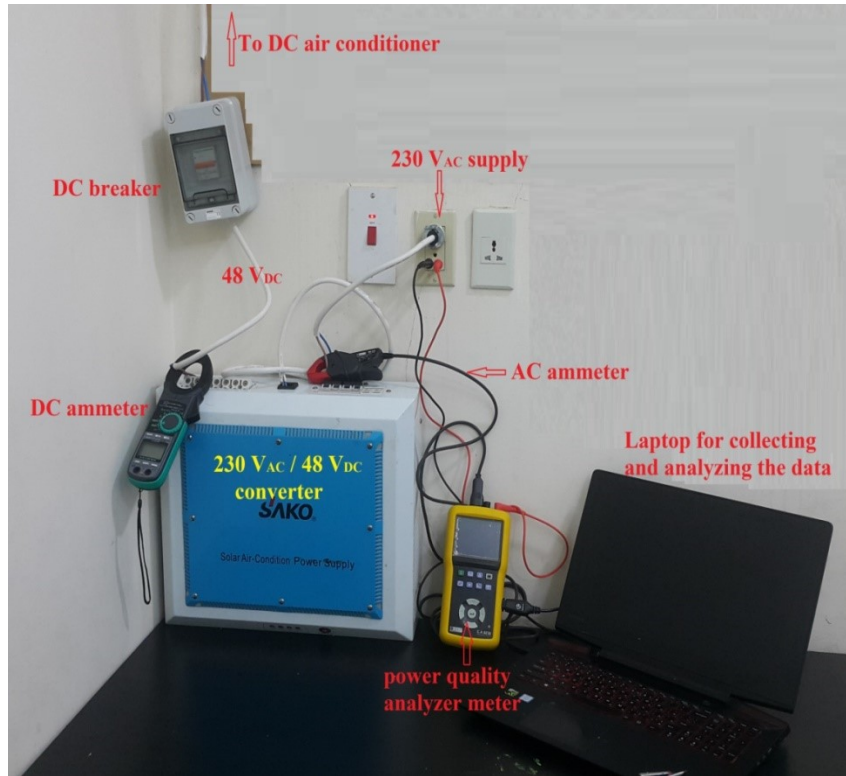


Figure 5.3: Experimental set up for AC-DC configuration (DC air conditioner case)

5.2.3.3 Architecture III: PV panels and batteries supplying AC appliances

In this configuration, PV panels and batteries are used as power sources of the system. DC/AC converter is required to convert the produced DC power to AC at a voltage level of 230 V_{AC}. Figure 5.4 shows the arrangements of this configuration.

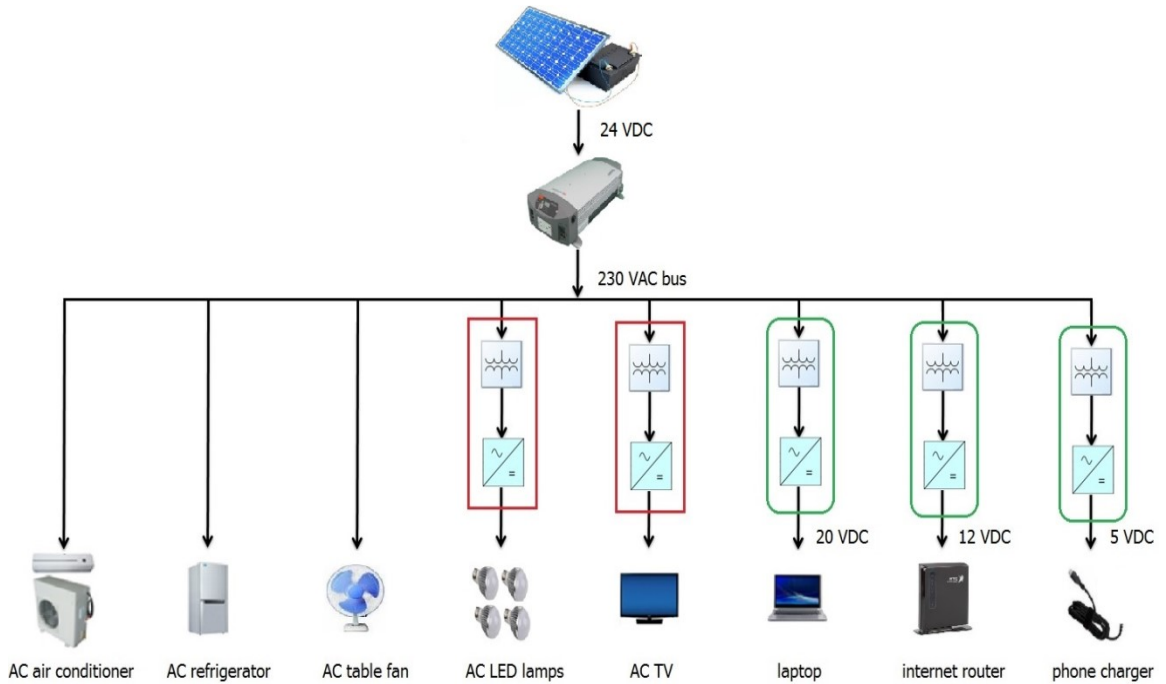


Figure 5.4: Standalone house AC appliances supplied by DC source

5.2.3.4 Architecture IV: PV panels and batteries supplying DC appliances

Completely DC network is proposed in this architecture. Since the DC air conditioner is working solely on 48 V_{DC}, it is supplied by a separate 48 V_{DC} source. Figure 5.5 shows the proposed architecture. Figure 5.6 shows sample measurements set up for supplying the 12 V_{DC} appliances by a 12 V_{DC} battery.

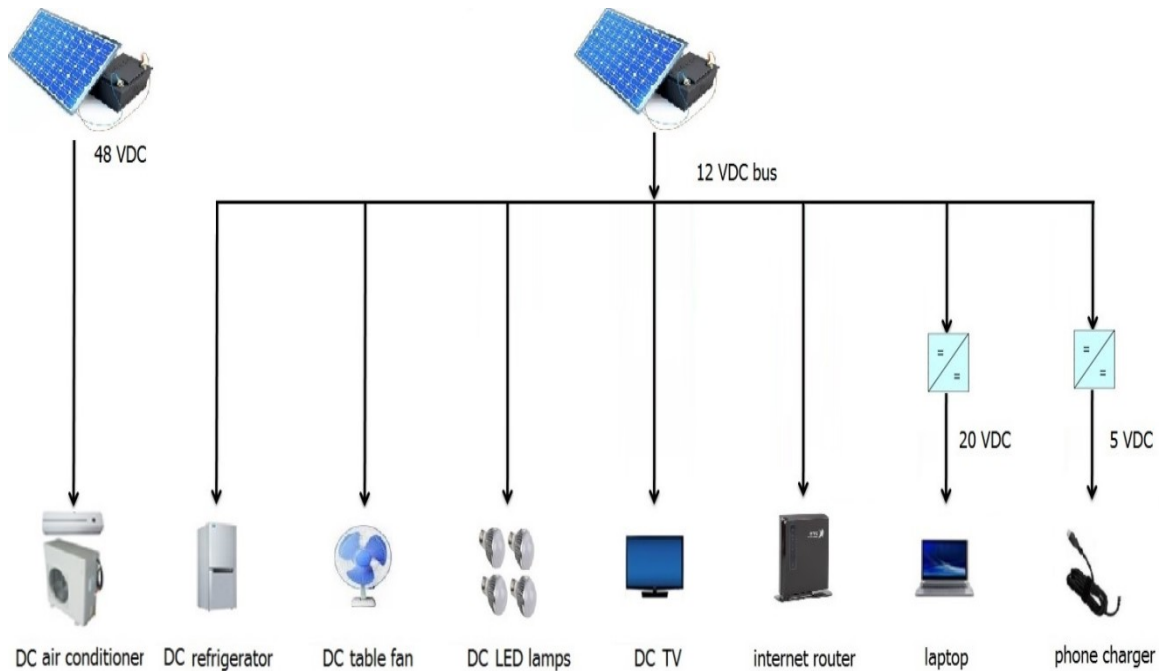


Figure 5.5: Standalone house DC appliances supplied by DC source



Figure 5.6: Experimental set up for DC-DC configuration (12 V_{DC} appliances case)

5.3 AC and DC Sources Sizing

This section discusses the approach followed to size the proposed architectures. This includes estimating the power rating of the diesel generator, rating and number of PV modules, and the required capacity and number of batteries. The sizing is based on a common load profile applied to all proposed configurations. The required components along with their costs are presented and discussed for each architecture.

5.3.1 Diesel Generator Sizing

It is important to select the suitable generator that satisfies the power needed by the supplied appliances. The type and number of the connected appliances are the main two parameters that affect the sizing of the generator. [110]

To properly size the generator, two categories of appliances are available. The first category represents the appliances that have constant running power over the entire operation interval. This includes lamps, fan, laptop, phone charger, internet router and TV. The other category includes the appliances that follow periodic ON/OFF cycles, in which high power is consumed at the beginning of each ON cycle. The appliances belonging to this category are the air conditioner and refrigerator. The operation of such appliances follows cyclic and repetitive ON/OFF behavior. At the beginning of each ON cycle, the starting current may reach 2 to 3 times the running current.

The first step followed in generator sizing is to list all appliances included in the network along with their running power rating values. Then, considering the worst case by assuming that all appliances are working simultaneously, all power values are added up, which simply gives the minimum required generator size. For future additional loads and considering a safety factor, the estimated total power can be increased by around 10-15 % which gives the ultimate generator size. [111]

To avoid shortening the lifetime of the generator, it is recommended to avoid operating it at its maximum power for more than 30 minutes [112]. In this study, to get proper generator sizing, all appliances rated power as well as surge power values are measured experimentally rather than reading their values from their nameplate data. Once a generator that meets the minimum running power is selected, it should be able to supply the required surge power for a designated time. By surveying the specifications of several commercial diesel generators, some generators have the ability to supply more than 50 % of their rated power for short intervals such as 10 or 20 seconds.

5.3.2 PV and Batteries Sizing Approach

To successfully design a solar PV system, the daily energy consumed by the loads has to be estimated accurately. Moreover, the worst case scenarios are taken into consideration including accounting system losses, days of autonomy and different components efficiencies. Several research works and articles have presented different sizing techniques for solar PV system [113-121]. Sizing approach for each component in the PV system is discussed below.

5.3.2.1 Total energy consumption evaluation

As a first step in PV system sizing, the total energy consumed by the loads is calculated. Accurate evaluation of the daily total energy consumption is necessary. To get an accurate estimation in this study, the total energy consumption for each configuration is calculated based on actual practical measurements.

5.3.2.2 PV array sizing

To evaluate the required PV array power, the total energy consumption is divided by the value of the peak sun hours. This value depends on the location of where PV solar system is installed. The resultant value has to be further adjusted based on the efficiencies of all system components. Typically, the inverter and battery round trip efficiencies are around 85-90 % for each [122]. Moreover, a temperature correction factor is included based on the maximum cell temperature. Based on [123], this value is 0.8 at a cell temperature of 60°C. The total power required by the PV array is calculated as follows [122]:

$$\text{required PV array power} = \frac{E}{H \times TCF \times \eta_{inv} \times \eta_{bat}} \quad (5.1)$$

Where E is the total daily energy consumed by the appliances, η_{inv} is the inverter efficiency, η_{bat} is the battery round trip efficiency, H is the peak sun hours for the selected location and TCF is the temperature correction factor.

5.3.2.3 Battery bank sizing

The battery bank should be sufficiently sized in order to supply the required back up power in the cases where no sunlight is available. Three factors are essentially accounted for battery sizing calculations which are the depth of discharge (DoD), system DC voltage and days of autonomy. The total required battery bank size in Ah is estimated as follows [122]:

$$\text{total Ah required} = \frac{E \times d}{DoD \times \eta_{inv} \times \eta_{bat} \times V_{DC}} \quad (5.2)$$

Where d is the value of the days of autonomy and V_{DC} is the system DC voltage.

5.3.2.4 Inverter sizing

The inverter size for the case of AC load is specified by the same way of generator sizing discussed previously. The inverter input DC voltage must be consistent with the DC voltage of PV modules and batteries. The running power ratings and surge power of all appliances are also considered to specify the appropriate required inverter size.

5.3.2.5 Charge controller sizing

The charge controller is a vital component of any solar PV system. Its role is to regulate the power produced by PV array and to protect the battery from overcharging. In this study, MPPT controller is employed in the proposed layouts that incorporate PV systems.

The current rating for the charge controller is simply estimated by evaluating the array short circuit current, which is found as follows: [124]

$$\text{charge controller size} = \frac{\text{total PV array power}}{\text{system DC voltage}} \quad (5.3)$$

The sources employed in all configurations are sized based on the discussed sizing approaches for both AC and DC sources.

5.4 Peak Sun Hours in Dhahran City

All measurements presented in this study were carried out in Dhahran, a city in the Eastern province of Saudi Arabia. Especially in the summer season, this city is characterized by substantial amount of solar radiation, as indicated in Figure 5.7 which shows the monthly variation of peak sun hours in Dhahran. [125]

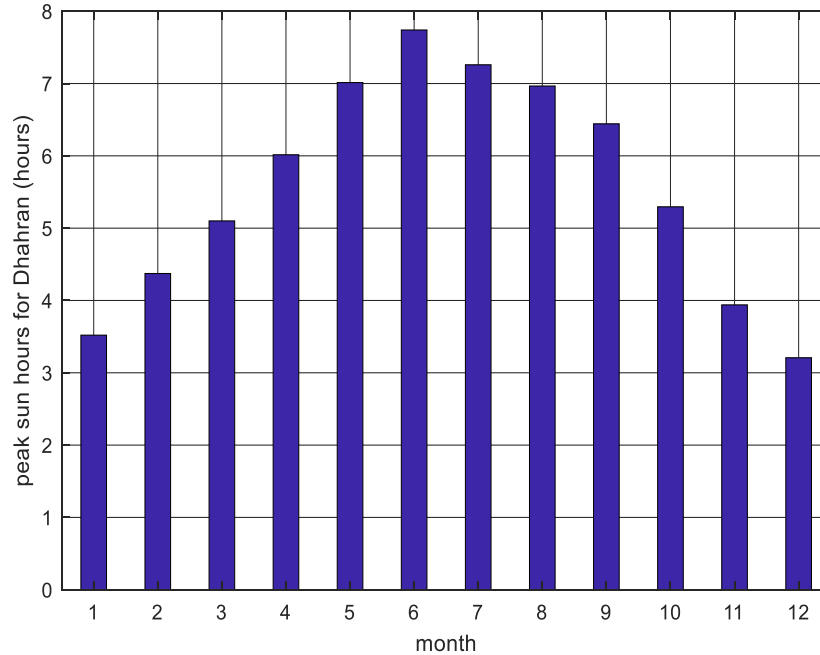


Figure 5.7: Peak sun hours variation per month for Dhahran [125]

The average value of the peak sun hours in summer months (April to September) is 6.906 hours. This high value coincides with the peak demand required by the connected loads due to the frequent use of air conditioners during this period.

5.5 Required Components Preparation and Architectures Sizing

The components needed for each configuration are specified based on the energy required to be supplied to the connected appliances. The total energy consumption for each configuration is first determined based on a common load profile. Accordingly, diesel generator, PV array and batteries are sized.

A common load profile is suggested for all architectures of the standalone house. This profile represents a common behavior for a standalone house in Saudi Arabia. A typical summer day is used to represent the power consumption activities by residents. Table 5.5

demonstrates the working intervals for all appliances considered in the proposed standalone house.

Table 5.5: Common daily load profile for all configurations

appliance	working interval
air conditioner	12.00 – 16.00
refrigerator	24 hours
fan	6.00 – 12.00 , 17.00 – 21.00
LED lamps (room)	20.00 – 00.00
LED lamps (kitchen)	20.00 – 00.00
LED lamps (bathroom)	00.00 – 4.00, 20.00 – 00.00
LED lamps (outdoor)	20.00 – 4.00
TV	12.00 – 13.00 , 19.00 – 22.00
internet router	6.00 – 00.00
laptop	10.00 – 12.00 , 16.00 – 18.00
phone charger	17.00 – 18.00

The total daily energy consumption for each architecture is evaluated based on this load profile, in addition to the power ratings of the appliances incorporated into each configuration.

The total energy consumption is calculated based on the measured secondly-basis power consumption profiles. This can give more accurate results rather than reading the rated power values from the appliances nameplate data. This step is important for accurately estimating the surge power for air conditioner and refrigerator at the starting of each ON cycle. The actual measured running and surge power values for all AC and DC appliances are recorded. Each configuration is treated separately in which total energy consumption and detailed analysis of the required components are presented.

5.5.1 Sizing, Required Components and Costs of Architecture I

Table 5.6 summarizes all resulting power and energy characteristics of all appliances incorporated into this architecture.

Table 5.6: Power and energy characteristics of all appliances for architecture I

	$P_{run} (W)$	$P_{surge} (W)$	$S_{run} (VA)$	$E (Wh)$
5 LED lamps	47	0	93	261
fan	46	0	47	465
TV	33	0	71	130
laptop	47	0	108	187
phone charger	15	0	30	15
internet router	15	0	30	270
refrigerator	95	675	120	448
air conditioner	1420	1518	1471	3227
SUM	1720	2200	1970	5000

The minimum generator rated power shouldn't go below the summation of the running power values for all appliances which is found as 1720 W for this configuration, with a power factor of around 0.87. The total energy consumed by this system is calculated as 5000 Wh , where the surge powers summation for the air conditioner and refrigerator is 2200 W .

To meet such requirements and allowing 1.1 safety factor, a 2 kW , diesel generator is selected. The detailed generator specifications are listed in Table 5.7. Table 5.8 summarizes the capital costs of all components required to implement this architecture. The capital cost of the laptop, internet router and phone charger in all proposed architectures is assumed to be \$ 270. The total cost of this configuration is \$ 1,510.

Table 5.7: Diesel generator specifications selected for configuration I

brand name	Sealine
output type	AC single phase
rated power	2 kW
maximum power	2.2 kW
fuel tank capacity	12.5 L

Table 5.8: Costs of all components required for architecture I

component	cost (\$)
diesel generator	255
AC air conditioner	666
AC refrigerator	160
AC fan	31
5 AC LED lamps	13
AC TV	120
other 3 appliances (common for all systems)	270
total capital cost	1,510

5.5.2 Sizing, Required Components and Costs of Architecture II

A diesel generator is used in this layout to supply DC appliances via several AC/DC converters. For power profiles measurements, it is important to state that the measured power is the AC power as seen from the 230 V_{AC} source side.

For both DC air conditioner and refrigerator, the absence of surge power can significantly reduce the generator size. However, power quality issues caused by AC/DC converters result in larger required generator size. All power and energy summary for this scheme are listed in Table 5.9.

Table 5.9: Power and energy characteristics of all appliances for architecture II

	$P_{run} (W)$	$P_{surge} (W)$	$S_{run} (VA)$	$E (Wh)$
7 LED lamps	62	0	137	318
fan	19	0	45	195
TV	28	0	62	111
laptop	47	0	108	187
phone charger	15	0	30	15
internet router	15	0	30	270
refrigerator	88	0	176	416
air conditioner	1500	0	2550	2052
SUM	1770	0	3150	3560

The evaluated total energy consumed for this configuration is 3560 *Wh* and the total running power of all appliances has an active power of 1770 *W* and apparent power of 3140 *VA* with around 0.57 power factor. This low power factor is expected due to the several power conversion devices incorporated with this system which reduce the power factor significantly and have a negative impact on the overall system power quality. The chosen generator has to be oversized in order to account for such low power factor resulting from the AC/DC converters.

A 3 kW generator with specifications listed in Table 5.10 is selected for this purpose. AC/DC converters should be sized appropriately based on the rated power of the connected load. Converters with specifications listed in Table 5.11 are selected for this configuration. In summary, Table 5.12 lists all components specifications required for this configuration.

Table 5.10: Diesel generator specifications selected for configuration II

brand name	JLT POWER
output type	AC single phase
rated power	3 kW
maximum power	3.3 kW
fuel tank capacity	12.5 L

Table 5.11: AC/DC converters specifications selected for configuration II

	230 V _{AC} /48 V _{DC} converter	230 V _{DC} /12 V _{DC} converter
brand	Leyu	MEILILE
rated power	1536 W	350 W
input AC voltage	200 V-260 V	230 V
output DC voltage	48 V	12 V

Table 5.12: Costs of all components required for architecture II

component	cost (\$)
diesel generator	285
230 V _{AC} /48 V _{DC} rectifier	225
230 V _{AC} /12 V _{DC} rectifier	21
DC air conditioner	1383
DC refrigerator	258
DC fan	40
7 DC LED lamps	22
DC TV	270
other 3 appliances (common for all systems)	270
total capital cost	2,770

5.5.3 Sizing, Required Components and Costs of Architecture III

Same AC appliances employed in the first configuration are also used here. Instead of powering these appliances by a diesel generator, they are supplied in this scheme by PV modules and batteries integrated with a central inverter to convert the produced DC power to AC in order to be compatible with the connected 230 V_{AC} appliances. This configuration is commonly used in off-grid systems. The same energy consumption of architecture I is considered. The running and surge powers are used for sizing the inverter, whereas the total energy consumed is used to size the PV array and batteries.

The inverter is sized by the same approach of generator sizing. To limit the steady state current to be below than 100 A, the selected input DC voltage for this inverter is 24 V_{DC}. This inverter is also integrated with built-in MPPT charge controller. The inverter specifications are summarized in Table 5.13.

Table 5.13: Selected inverter specifications for configuration III

type	MPPT, pure sin waveform
rated power	2 kW
peak power	6 kW
inverter DC input	20 V – 32 V
MPPT input voltage from PV	30 V – 200 V
maximum output current	15 A

For PV modules and batteries sizing, the steps described by equations (5.1)-(5.3) are followed. Accordingly, the total required PV array power is 1120 W while the total Ah capacity needed by the battery bank considering one day of autonomy is 430 Ah. To meet such requirements, a combination of four 290 W PV modules is selected, in which two strings are connected in parallel with two series modules in each string. Also, four 12 V_{DC}, 220 Ah lead acid batteries are chosen for battery bank storage. To get 24 V_{DC} and 440 Ah, two batteries are connected in series, which are connected in parallel with the other two series batteries. The specifications of the selected PV module and battery are listed in Table 5.14. The details and number of all components needed for this system are listed in Table 5.15.

Table 5.14: Specifications of the selected PV module and battery for architecture III

PV module specifications	
type	polycrystalline
brand name	Osda Solar
open circuit voltage	44.32 V
short circuit current	8.37 A
maximum power	290 W
voltage at maximum power	37.08 V
current at maximum power	7.83 A
module efficiency	14.95 %
battery specifications	
type	deep cycle solar battery
brand name	JYC battery
nominal voltage	12 V
nominal capacity	220 Ah

Table 5.15: Costs of all components required for architecture III

component	cost (\$)
PV modules	4×110=440
batteries	4×198= 792
inverter with MPPT charge controller	322
AC air conditioner	666
AC refrigerator	160
AC fan	31
5 AC LED lamps	13
AC TV	120
other 3 appliances (common for all systems)	270
total capital cost	2,810

5.5.4 Sizing, Required Components and Costs of Architecture IV

All DC appliances considered in architecture II are integrated into this network, but are supplied here by PV modules and batteries. The DC air conditioner is supplied by separate PV and battery bank of a voltage of 48 V_{DC}, while all other appliances are supplied by another combination of PV and batteries of 12 V_{DC}. The total energy consumed as well as power data for the DC air conditioner and the remaining DC appliances are summarized in Table 5.16.

Table 5.16: Power and energy characteristics of all appliances for architecture IV

	$P_{run} (W)$	$P_{surge} (W)$	$S_{run} (VA)$	$E (Wh)$
7 LED lamps	48	0	0	245
fan	14	0	0	139
TV	20	0	0	80
laptop	43	0	0	172
phone charger	13	0	0	13
internet router	13	0	0	234
refrigerator	75	0	0	363
SUM	226	0	0	1247
air conditioner	1500	0	0	2000

For the DC air conditioner, the required PV array power is 400 W while the needed battery bank capacity is 75 Ah, considering one day of autonomy. A combination of two 230 W PV modules connected in series is adopted. In addition, four series 12 V, 100 Ah batteries are chosen for power storage giving a total voltage of 48 V_{DC}. The specifications of the selected PV module and battery are listed in Table 5.17.

Table 5.17: Selected PV module and battery data for architecture IV (48 V_{DC} system)

PV module specifications	
type	monocrystalline
brand name	BAWOEI
open circuit voltage	57.8 V
short circuit current	5.24 A
maximum power	230 W
voltage at maximum power	48.33 V
current at maximum power	4.76 A
module efficiency	14.7 %
battery specifications	
type	deep cycle solar battery
brand name	ESG
nominal voltage	12 V
nominal capacity	100 Ah

This system requires MPPT charge controller to regulate the DC voltage at 48 V_{DC}. The controller specifications must comply with the PV and batteries characteristics. The PV array maximum power voltage must lie within the range of MPPT charge controller working interval. Also, the system voltage has to be lower than the PV array voltage. To meet these requirements, MPPT charge controller is selected with specifications listed in Table 5.18. This charge controller is clearly compatible with all PV array and battery bank ratings of this system.

Table 5.18: Selected charge controller data for configuration IV (48 V_{DC} system)

type	MPPT
maximum current	40 A
V _{oc} from PV	72 V-160 V
maximum PV input voltage	190 V
max PV input power	1700 W

For the other 12 V_{DC} appliances, the computed required PV array power is 250 W while the needed battery bank capacity is 190 Ah by considering one day of autonomy. A single 280 W PV module and a single 12 V, 200 Ah battery are selected. Table 5.19 lists the selected PV module and battery specifications.

Table 5.19: Selected PV module and battery data for architecture IV (12 V_{DC} system)

PV module specifications	
type	polycrystalline
brand name	JINSHI
open circuit voltage	38.62 V
short circuit current	9.28 A
maximum power	280 W
voltage at maximum power	31.63 V
current at maximum power	8.85 A
module efficiency	17.11 %
battery specifications	
type	deep cycle solar battery
brand name	Ouyad
nominal voltage	12 V
nominal capacity	200 Ah

This system requires 12 V_{DC} MPPT charge controller, 12 V_{DC}/20 V_{DC} converter and 12 V_{DC}/5 V_{DC} converter. The charge controller and DC-DC converters specifications are shown in Table 5.20 and Table 5.21, respectively. The details and number of all components needed for this entire DC system are listed in Table 5.22.

Table 5.20: Selected charge controller data for configuration IV (12 V_{DC} system)

type	MPPT
maximum current	30 A
V _{oc} from PV	20 V-80 V
maximum PV input voltage	190 V
max PV input power	360 W

Table 5.21: DC-DC converters required for configuration IV (12 V_{DC} system)

	12 V _{DC} /20 V _{DC} converter	12 V _{DC} /5 V _{DC} converter
type	boost	buck
rated power	60 W	15 W
input voltage	10 V-20 V	12/24 V
output voltage	20 V	5 V
application	laptop	phone charger

Table 5.22: Costs of all components required for architecture IV

component	cost (\$)
PV modules (12 V _{DC} system)	1×92=92
PV modules (48 V _{DC} system)	2×85=170
batteries (12 V _{DC} system)	1×180=180
batteries (48 V _{DC} system)	4×75=300
MPPT charge controller (12 V _{DC} system)	72
MPPT charge controller (48 V _{DC} system)	84
DC air conditioner	1383
DC refrigerator	258
DC fan	40
7 DC LED lamps	22
DC TV	270
other 3 appliances (common for all systems)	270
12 V _{DC} /20 V _{DC} converter	18
12 V _{DC} /5 V _{DC} converter	2
total capital cost	3,155

5.6 Energy Saving Opportunities and Capital Cost Analysis

The total energy consumption and load profile are the main affecting parameters on sources sizing. High energy consumption leads to larger sizes of diesel generator, PV array and battery bank storage. The selection of energy efficient appliances can help to reduce the system size significantly. However, these new appliances are expensive resulting in higher capital cost. As analyzed in the previous section, the total energy consumed by each configuration is calculated based on the suggested load profile. It is interesting to compare these configurations in terms of the energy consumption and capital costs of all incorporated components. Table 5.23 and Figure 5.8 summarize the total energy consumption, as well as the total capital costs of all configurations.

Table 5.23: Total energy consumption and capital cost summary of all configurations

architecture		total energy consumed	capital cost
I	AC source → AC appliances	5000 Wh	\$ 1,510
II	AC source → DC appliances	3560 Wh	\$ 2,770
III	DC source → AC appliances	5000 Wh	\$ 2,810
IV	DC source → DC appliances	3240 Wh	\$ 3,155

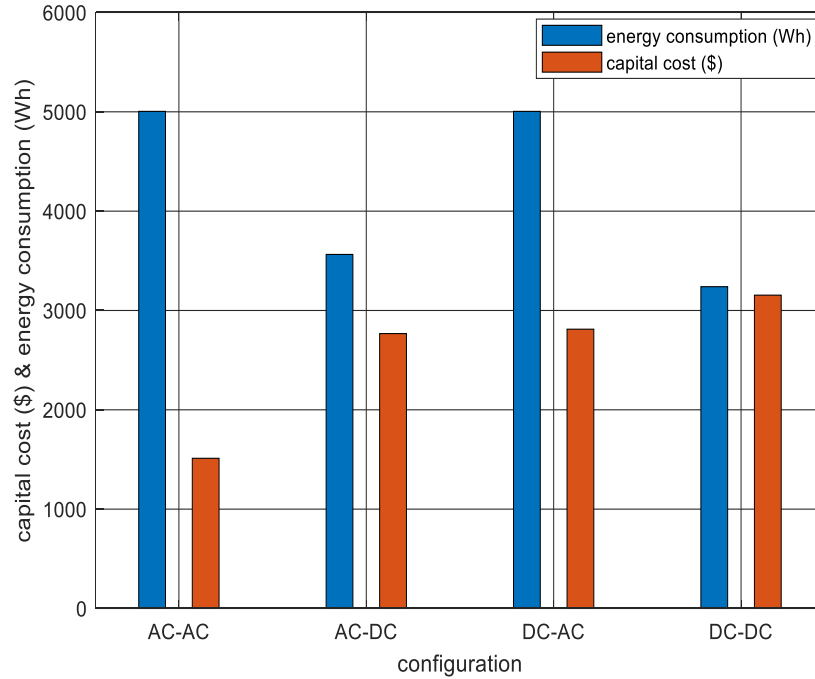


Figure 5.8: Energy and capital cost comparison of all architectures

The first configuration has the lowest capital cost as compared with other systems. This is due to the low cost of the diesel generator as well as the conventional AC appliances, regardless of their relatively higher energy consumption. In addition to its high capital cost due to incorporating of DC appliances, the architecture with the diesel generator supplying DC appliances is difficult to consider due to the low system power factor that leads to several technical problems.

The most widely used scheme in off-grid renewable energy applications is the PVs and batteries system that supply the AC appliances via a central inverter. It is the highest energy consuming system due to the integration of high power consumption conventional AC appliances, in addition to the central inverter that causes some power losses. This system has also high capital cost mainly because of the incorporation of the costly PV modules and batteries.

The complete DC system has the lowest energy consumption. This configuration is characterized by a unified DC voltage for sources and loads which helps in minimizing the losses resulting from power conversion devices. Only two DC/DC converters are required to convert the main bus DC voltage to the required DC voltage by laptop and phone charger. Moreover, induction motor is usually used to drive the compressor of the conventional AC air conditioner and AC refrigerator. The motor type used in DC air conditioner and DC refrigerator is brushless DC motor (BLDC). The employed BLDC compressors are more efficient, free of surge power and compatible with the input DC power.

The negative impact of this configuration is the high cost of the DC appliances. The DC appliances contribute to about 70 % of the total capital cost. Within the DC appliances, the DC air conditioner is the most expensive appliance which contributes to more than 61 % of the total DC appliances cost. Figure 5.9 demonstrates the contribution of each parameter in the total capital cost of the DC-DC system.

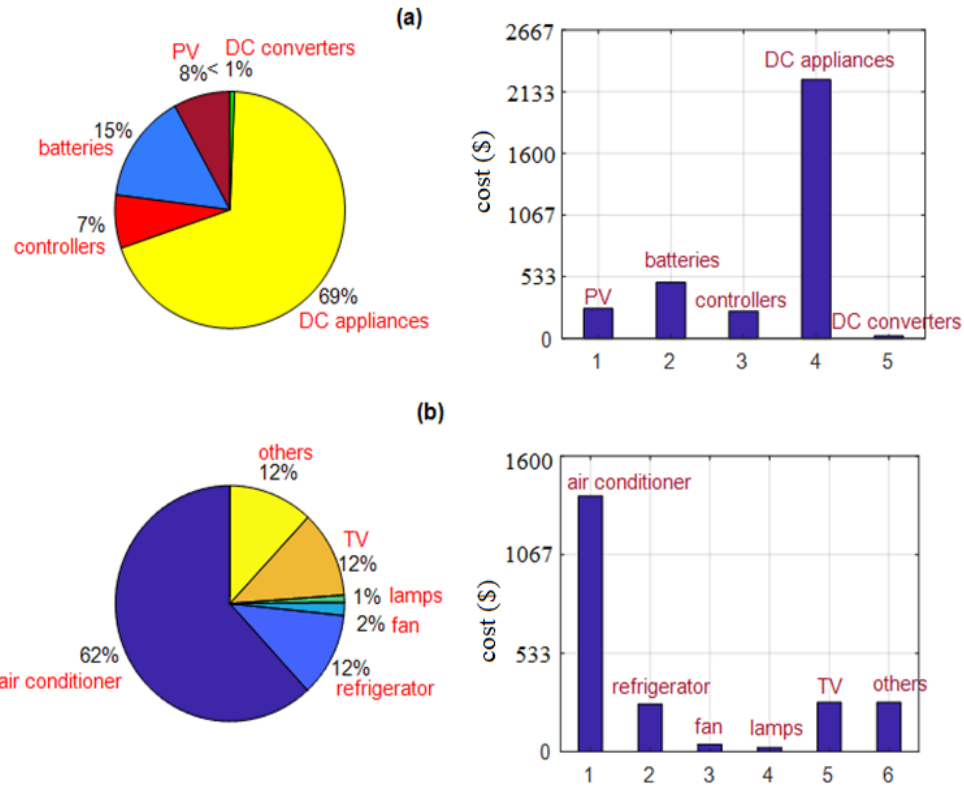


Figure 5.9: Components cost summary of the DC system: (a) components contribution (b) appliances contribution in total appliances cost

The DC air conditioner is the main component responsible for such high capital cost of the DC system. Possible future reduction in DC appliances prices may lead to reducing the capital cost of this system.

5.7 Economic Analysis over the Entire Life Cycle

For a selection of the appropriate power system network, it is essential to carry out extensive cost analysis over the entire life cycle of all configurations. This means that many additional costs can be included in the analysis. Based on these costs, the total cost over the system life cycle can be evaluated. Some parameters included for total cost estimation are capital cost, replacement cost, operation and maintenance (O&M) costs

and fuel cost. Each of these parameters is discussed in which the equations employed in calculations are presented.

5.7.1 Life Cycle Cost of the PV-Batteries Systems

To evaluate the total cost of the PV-batteries systems, the following equation is used [122]:

$$C_{T_PV} = C_{i_PV} + C_{install} + C_{om_PV_pw} + C_{batt_pw} \quad (5.4)$$

Where C_{T_PV} is the total cost, C_{i_PV} is the initial cost of the complete system, $C_{install}$ is the installation cost, $C_{om_PV_pw}$ is the present worth of O&M and C_{batt_pw} is the present worth of the batteries after first replacement. Usually, the life cycle of the PV systems is approximately 20 years. In this study, 20 years is considered as the total life cycle of all proposed configurations.

The installation cost of the PV system can be estimated as 10 % of the initial cost [122]. Moreover, the annual O&M cost is considered as 1 % of the initial cost and it is scaled over the 20 years by present worth calculations [126]. Therefore:

$$C_{install} = 0.1 \times C_{i_PV} \quad (5.5)$$

$$C_{om_PV_pw} = \sum_{n=1}^{20} \frac{0.01 \times C_{i_PV} (1+k)^{n-1}}{(1+i)^n} \quad (5.6)$$

Where n is the year number, k is the annual inflation rate and i is the interest rate. The annual inflation rate and interest rate are 5 % and 6 %, respectively. [127]

To evaluate the present worth of batteries, the old batteries are assumed to be replaced by new batteries every 7 years with a rebate of 7 % [113]. Two replacements are considered for batteries over the life cycle of the PV system. This cost is evaluated as follows:

$$C_{batt_pw} = \sum_{n=7,14} \frac{0.93 \times C_{bat} (1+k)^{n-1}}{(1+i)^n} \quad (5.7)$$

5.7.2 Life Cycle Cost of the Diesel Generator Systems

Unlike the PV system, the most important cost parameter in diesel generator system is the fuel cost. Also, the generator needs to be replaced each several years based on its lifespan interval. The total cost of the diesel generator systems can be evaluated as follows:

$$C_{T_dg} = C_{i_dg} + C_{rep_pw} + C_{om_dg_pw} + C_{fuel_pw} \quad (5.8)$$

Where C_{T_dg} is the total cost of the diesel generator system, C_{i_dg} is the initial cost of the complete system, C_{rep_pw} is the present worth of generator replacements, $C_{om_dg_pw}$ is the present worth of generator O&M and C_{fuel_pw} is the present worth of fuel consumption over the 20-year life cycle.

Usually, manufacturers of low power generators do not provide various generator details such as generator lifespan and fuel consumption at different loading conditions [128]. In the study presented in [129], a 2 kW diesel generator is selected for a hybrid system to supply power to an off-grid area. It is stated that the lifespan of this generator is about 15,000 hours [129]. Generally, the lifespan of small generators operating continuously is around two years [130]. Accordingly, the diesel generator considered in this study is

assumed to be replaced every two years. The present worth of diesel generator replacements can be estimated as follows:

$$C_{rep_pw} = \sum_{n=2,4,6,\dots,18} \frac{C_{dg}(1+k)^{n-1}}{(1+i)^n} \quad (5.9)$$

In addition, the annual O&M and oil changing are considered as 5 % of the cost of the diesel generator [122]. The present worth is calculated as follows:

$$C_{om_dg_pw} = \sum_{n=1}^{20} \frac{0.05 * C_{dg} (1+k)^{n-1}}{(1+i)^n} \quad (5.10)$$

And the following equation evaluates the present worth of fuel consumption:

$$C_{fuel_pw} = \sum_{n=1}^{20} \frac{A \times (1+k)^{n-1}}{(1+i)^n} \quad (5.11)$$

Where A here represents the fuel cost of the first year which is estimated as follows:

$$A = \text{fuel consumption in liters per day} \times \text{fuel price per liter} \times 365 \quad (5.12)$$

The fuel consumption information in liters per hours at different loading conditions are not provided in the data sheets of the selected 2 kW and 3 kW diesel generators. Table 5.24 lists the fuel consumption data for both generators as received from the suppliers. Figure 5.10 and Figure 5.11, respectively show the trend of fuel consumption in liters per hour with the percent loading conditions for the selected 2 kW and 3 kW generators, respectively.

Table 5.24: Fuel consumption in liters per hour at different loading conditions

percent loading (%)	2 kW generator	3 kW generator
25	0.22 L/h	0.347 L/h
50	0.44 L/h	0.694 L/h
75	0.66 L/h	1.042 L/h
100	0.87 L/h	1.389 L/h

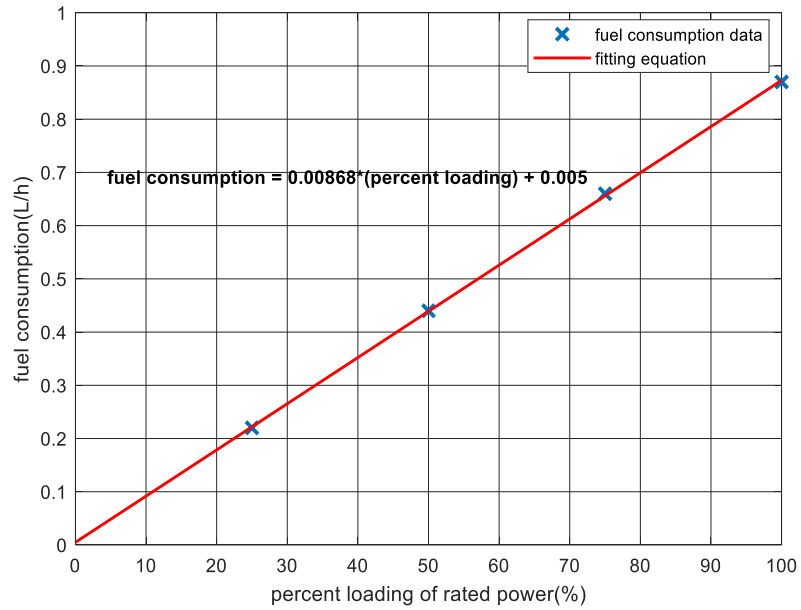


Figure 5.10: Fuel consumption trend for the 2 kW generator

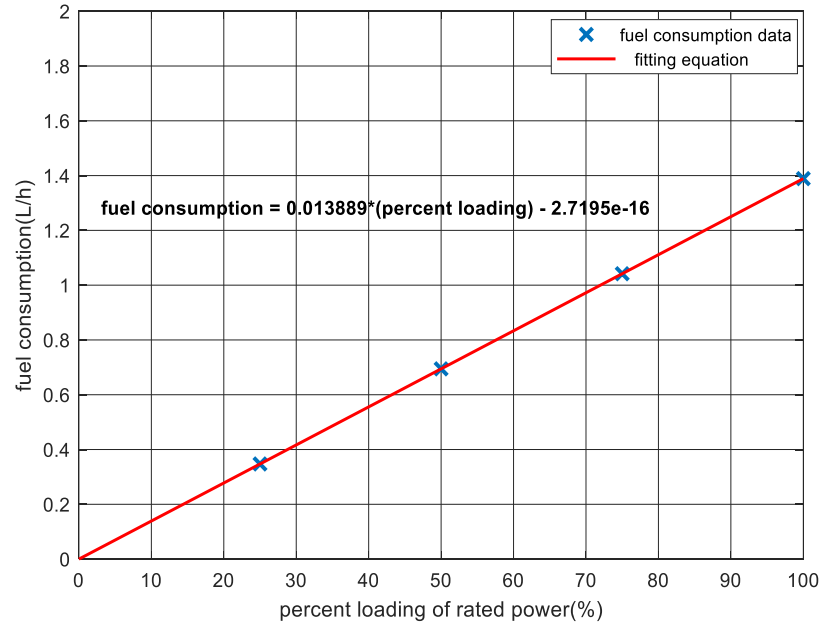


Figure 5.11: Fuel consumption trend for the 3 kW generator

As shown, linear equation is fitted to the data in order to estimate the fuel consumption at any loading conditions for both generators.

All presented equations for PV and generator systems costs are evaluated and the results are used for systems costs comparisons over the entire life cycle, as will be described in next section.

5.8 Systems Comparisons Based on Total Life Cycle Cost

In this section, the total life cycle cost for each configuration is calculated. First, all values of parameters incorporated into the calculations are identified as listed in Table 5.25. Then, the total life cycle costs of all configurations are evaluated and the results are listed in Table 5.26 and shown graphically in Figure 5.12.

Table 5.25: Parameters values used in total cost calculations

systems life cycle	20 years
inflation rate	5 %
interest rate	6 %
fuel price per liter in Saudi Arabia	\$ 0.125 per liter
days of autonomy for PV-batteries systems	1 day
batteries lifespan	7 years
diesel generator lifespan	2 years

Table 5.26: Life cycle costs of all configurations

architecture		total life cycle cost (\$)
I	AC source → AC appliances	5,530
II	AC source → DC appliances	6,540
III	DC source → AC appliances	4,340
IV	DC source → DC appliances	4,080

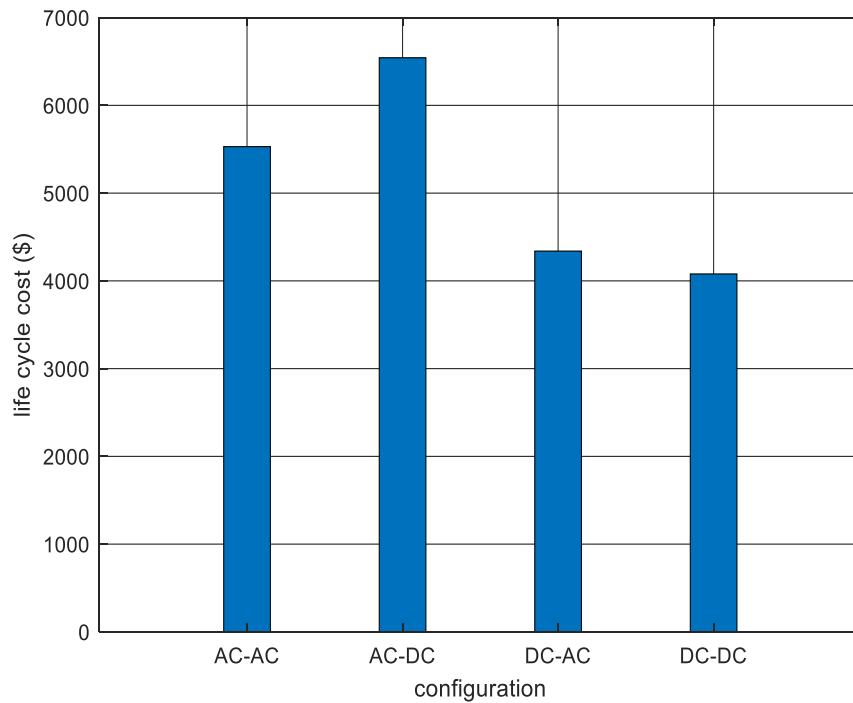


Figure 5.12: Life cycle costs comparisons for all configurations

Based on the assumptions stated, it is clear that the DC system has the lowest life cycle cost over the 20 year period. The major affecting parameters in diesel generator systems costs are the future costs including generator replacement, O&M and fuel costs. On the other hand, PV systems are characterized by high capital cost, but no fuel is required for operation. These factors have resulted in such higher life cycle cost of the AC-AC system as compared with both PV systems configurations. Figure 5.13 shows the comparison of capital and future costs for each configuration and Figure 5.14 demonstrates the percent contribution for each.

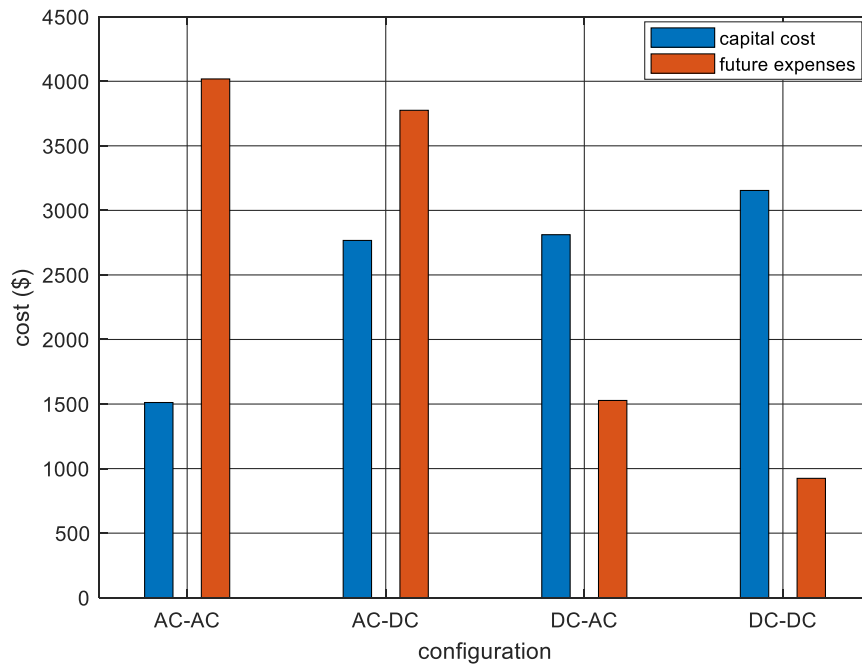


Figure 5.13: Capital and future expenses comparison

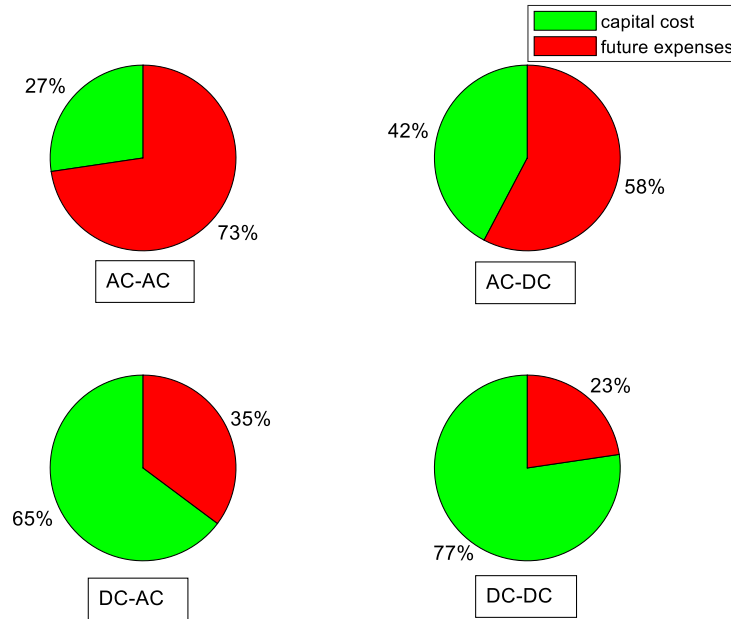


Figure 5.14: Contribution of capital and future expenses in total life cycle cost

In general, as a comparison between all systems in terms of total life cycle costs, the DC-AC and DC-DC configurations have relatively similar life cycle cost. In case of AC-DC scheme, the total life cycle cost is much higher. Moreover, technical problems may be present due to the low power factor resulting from integrating various converters. It is recommended to avoid implementing this system. The most commonly implemented off-grid schemes are the AC-AC and DC-AC systems. The AC appliances are available easily in the market and they are compatible with the output AC power from the inverter.

For the complete DC system, it is interesting to consider this system due to its lowest life cycle cost overall other proposed systems. The expected reduction in DC appliances prices can reduce the total cost more. It is interesting to raise the awareness of consumers to implement such complete DC systems. Except for the DC air conditioner and DC refrigerator, all other appliances are available in the local market in Saudi Arabia, as of

2018. It is also advised for commercial sector and manufacturers to make the DC air conditioner and DC refrigerator available in the local market.

5.9 Sensitivity Analysis

This section discusses some different scenarios and presents the impact on total life cycle costs of all configurations. The analysis carried out before is considered as a base case.

The systems are then re-evaluated based on changing the following factors:

- reduction in DC appliances prices.
- increasing days of autonomy for PV-batteries systems.
- increasing diesel generator lifespan.

Based on the base case situation, each factor is varied in which the response on life cycle cost is noticed.

5.9.1 Reduction in DC Appliances Prices

In this study, the total AC and DC appliances prices are \$ 1,260 and \$ 2,240, respectively. The total life cycle costs of all systems are re-calculated in this subsection considering a reduction of DC appliances prices. By future emergence of such appliances in the market, it is expected that their costs will be reduced. The analysis presented here assumes fixed existing AC appliances prices, and reduction of DC appliances prices by 10 %, 20 %, 30 % and 40 % till the prices of DC and existing AC appliances become identical. Figure 5.15 shows the life cycle cost profiles for all systems under this assumption. The reduction of DC appliances prices can lead to more saving opportunities.

When the prices of AC and DC appliances are the same, the DC-DC system is the cheapest.

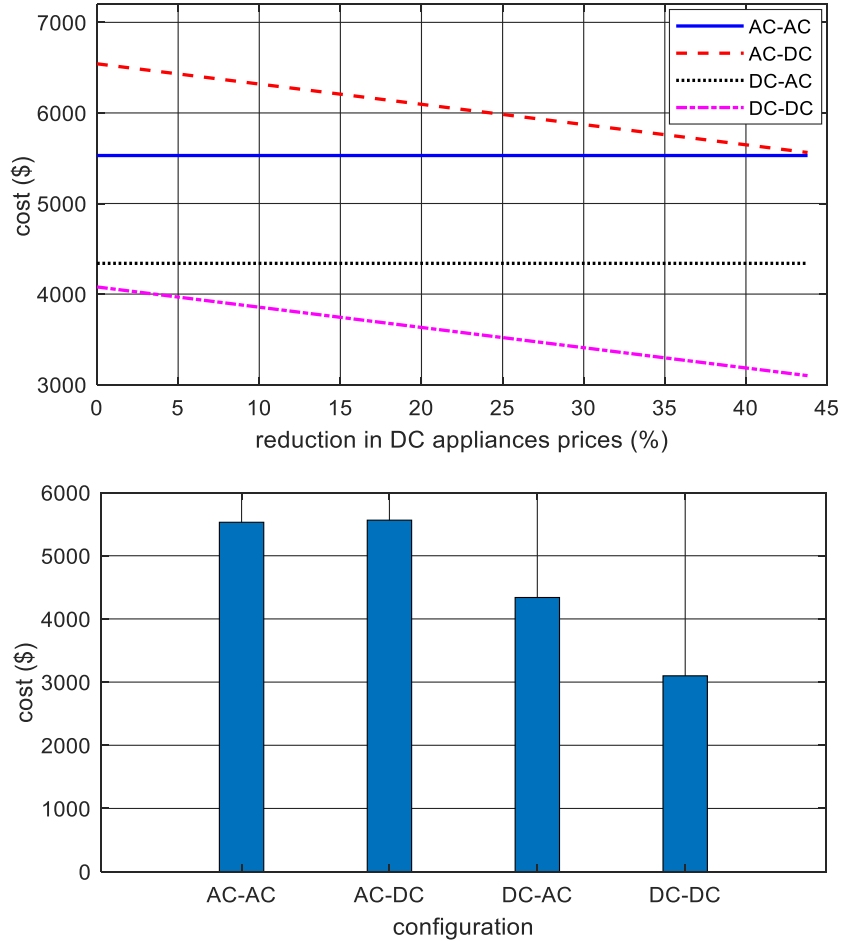


Figure 5.15: (a) Impact of reduction in DC appliances prices (b) life cycle costs at equal AC and DC appliances prices

5.9.2 Increasing Days of Autonomy for PV-Batteries Systems

All analyses presented previously were for an assumption of one autonomous day for estimating the required capacity of battery bank storage. Dhahran city is characterized by long sunshine hours in the summer with almost no or seldom cloudy days. In the winter, this city has several cloudy days but with the need for air conditioners due to the cold weather at this season. The selected battery bank capacity at the assumed one

autonomous day is expected to be still sufficient to supply the appliances with power even though at two or three days of autonomy in the winter. It is interesting to study the impact of two and three days of autonomy on the total life cycle cost of PV-batteries systems. Figure 5.16 demonstrates the impact of varying days of autonomy from 1 to 4. Increasing days of autonomy means that more energy storage capacity is required. The life cycle cost of PV-batteries system increases sharply at the increase in days of autonomy. The additional costs are included in the present worth of batteries replacements.

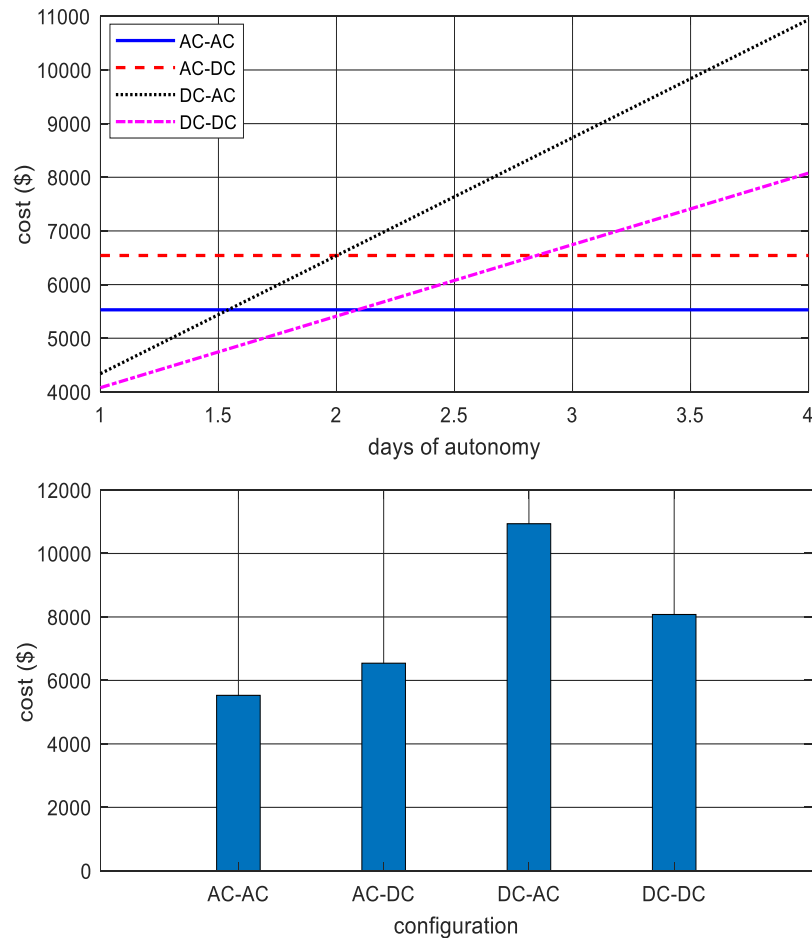


Figure 5.16: (a) Impact of days of autonomy variation (b) life cycle costs at four days of autonomy

5.9.3 Increasing Diesel Generator Lifespan

The lifespan of the diesel generator is basically dependent on several factors governed by the consumer behavior and the supplied load including regular O&M, oil changing, loading conditions and generator parts lubrication. It is assumed in the previous analysis that the lifespan of the diesel generator is two years based on data taken from [129]. In this subsection, the generator lifespan is increased to 5 years in steps of one year. Accordingly, the impact on life cycle cost of diesel generator systems is monitored. All parameters of PV-batteries systems are assumed unchanged. The responses of life cycle cost profiles for all systems are shown in Figure 5.17. At around generator lifespan of 4 years, the life cycle costs of AC-AC and DC-AC systems are identical. The life cycle cost of the AC-AC system then continues to decrease further. The DC-DC system is still the most economical system even at 5-year generator lifespan. The AC-DC system is still the most expensive network even with increasing the diesel generator lifespan.

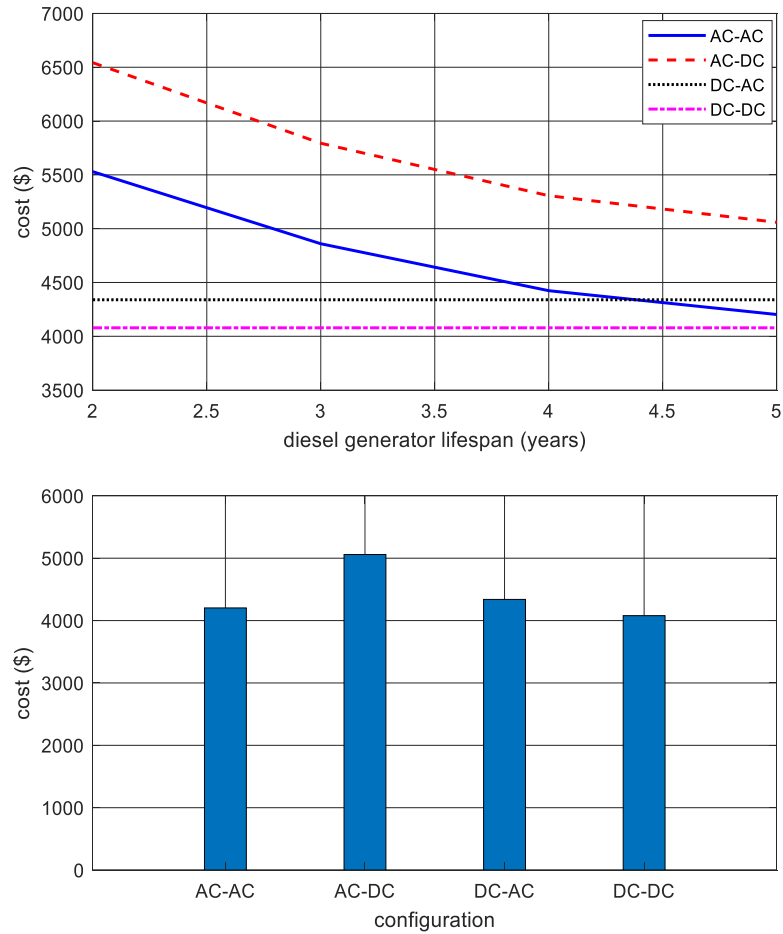


Figure 5.17: (a) Impact of diesel generator lifespan variation (b) life cycle costs at 5-year lifespan

5.10 Summary and Conclusions of the Chapter

By the end of this chapter, following are the main findings and conclusions obtained from all analyses presented in this chapter:

- Extensive analysis and investigation of various low voltage distribution schemes for a small standalone house are presented.
- The proposed schemes are represented by complete AC and DC networks, in addition to hybrid networks.

- In terms of energy saving, the DC system is the most energy saving system due to the integration of efficient and energy-saving new DC appliances.
- The DC appliances are too expensive resulting in high capital cost of the DC-DC system.
- In terms of total life cycle cost over 20 years, the DC system is considered as the most suitable configuration with an assumption of one day of autonomy and two-year diesel generator lifespan.
- Energy saving and cost reduction of the DC system could be more at a reduction in DC appliances prices.
- Increasing days of autonomy can sharply increase the cost of the DC system due to the requirement of more batteries.
- Increasing diesel generator lifespan leads to cheaper cost in the case of AC-AC system.
- The AC-DC network is not recommended due to its high life cycle cost even with DC appliances prices reduction and more diesel generator lifespan.

CHAPTER 6

MICROGRID DESIGN: SYSTEM

CONFIGURATIONS AND COMPARATIVE

STUDY

6.1 Introduction

This chapter discusses the design and analysis of a microgrid, incorporated with various sources and loads. Different situation is considered in this chapter as compared with the analysis presented in chapter 5. The chapter extends the idea of chapter 5 by designing a simple microgrid for a small town, rather than a single standalone house. The analysis in this chapter involves the design of a distribution network in which all cost analysis is based on the utility supply perspective. For example, the appliances costs are not considered in the costs calculations in this case. Also, the revenues are involved here in the calculations based on the recent electricity tariffs in Saudi Arabia. The required land for installing the generation sources is also accounted.

Four configurations are proposed to represent the entire network. The proposed configurations adopt a variety of AC and DC sources for the purpose of supplying the power to a residential area. The area represents a small town composed of 100 houses.

Two versions of the residential area are discussed; all AC load and all DC load; with each having a respective hourly load profile. The two load profiles are identical in terms of performing the task required by each AC or DC appliance. However, the load curves behaviors could be different due to the different electrical specifications between each AC appliance and its corresponding DC version.

The design considers a number of factors. These include system configurations, operating voltage selection, generation capacity and distribution voltage level selection. Converters efficiencies are also considered. The purpose is to investigate the impact of integrating the DC microgrid environment on the operation of the power generating units as well as the PV array and battery bank sizing. Another point of focus is the critical selection of the DC distribution voltage level that can mitigate the high losses caused by the high current resulting from the low DC appliances voltages, available at 12 V_{DC} and 48 V_{DC} voltage levels.

With regard to fuel consumption, the economic dispatch (ED) is usually used to estimate the fuel cost. Most of the previous research has concentrated on studying the ED problem under a fixed or dynamic load, without any consideration and attention to whether the supplied grid area is AC or DC. The emergence of the DC appliances into the market presented new challenges. In this chapter, the actual AC and DC load profiles proposed in chapter 5 are adopted, but are scaled to represent a small town of 100 houses. Each house is composed of the same appliances considered in chapter 5. Diesel generating units as well as PV array and batteries are employed in this chapter to represent AC and DC sources, respectively. Detailed cost analysis is carried out over an interval of 20 years in terms of capital costs, generation cost, revenues and overall total life cycle costs.

6.2 Design of the Power System Network under Study

This section discusses the components involved in the power system network under study. Various power generation sources and loads are incorporated to represent a microgrid system. Both generation and load sides comprise various components. All components that constitute the power network are identified with their operating voltages and detailed power characteristics.

6.2.1 Demand Side

The load area considered in this chapter represents a small town with 100 houses. Each house is assumed to have two identical rooms with same load profiles as suggested in chapter 5. For the AC house, the conventional distribution scheme is adopted. This comprises the 230 V_{AC} outlets distributed over the two rooms. All appliances are either connected directly to the source or via portable AC/DC converters.

For the DC case, each house is incorporated with a central DC/DC converter. A line is taken from the 48 V_{DC} feeder and converted via a DC/DC converter to 12 V_{DC}. This is distributed over the house to supply all other 12 V_{DC} appliances. Figure 6.1 depicts the configuration of the proposed DC house for a single room. The AC load profile is shown in Figure 6.2 with a peak of 200 kW at 12.00. The DC load profile is given in Figure 6.3. The peak demand in this case is around 120 kW at 12.00. The demand characteristics for the AC and DC load curves are different due to the different electrical specifications and power ratings between each AC appliance and its corresponding DC version.

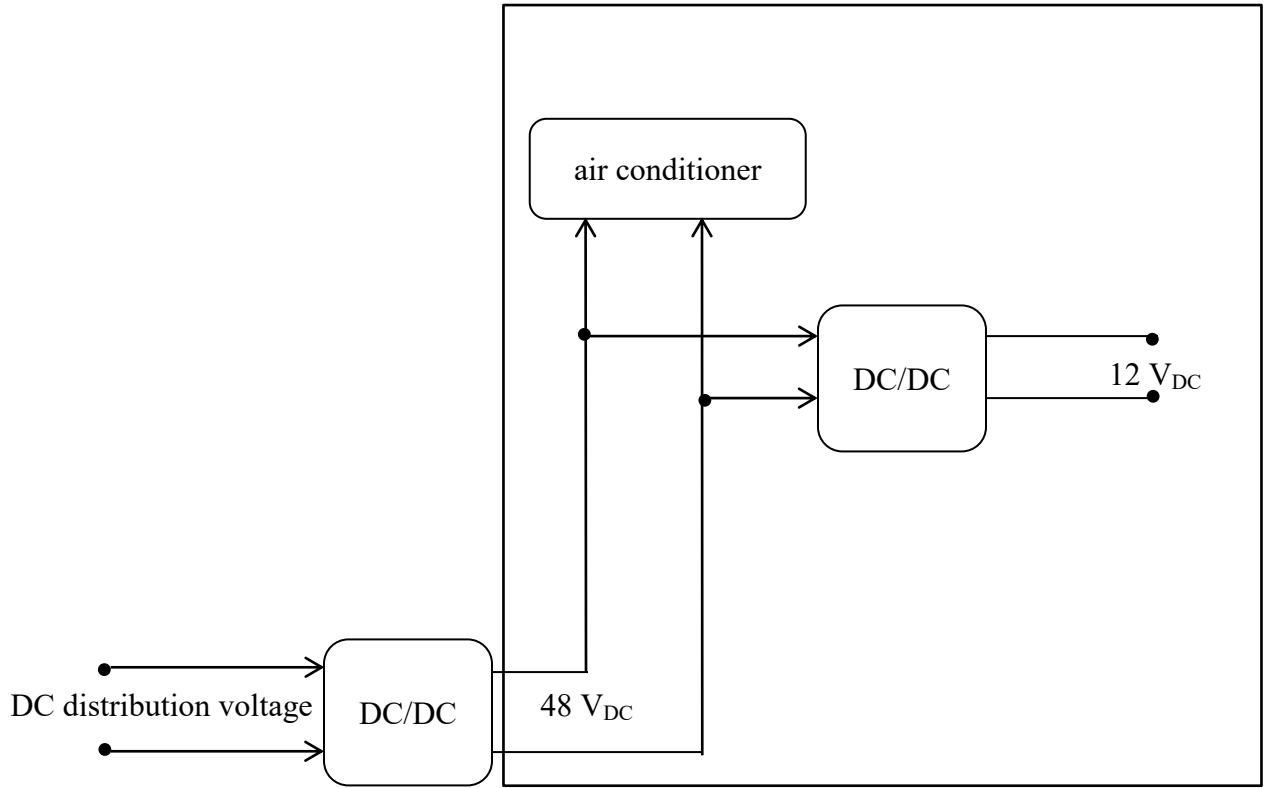


Figure 6.1: Electrical layout of the proposed DC house

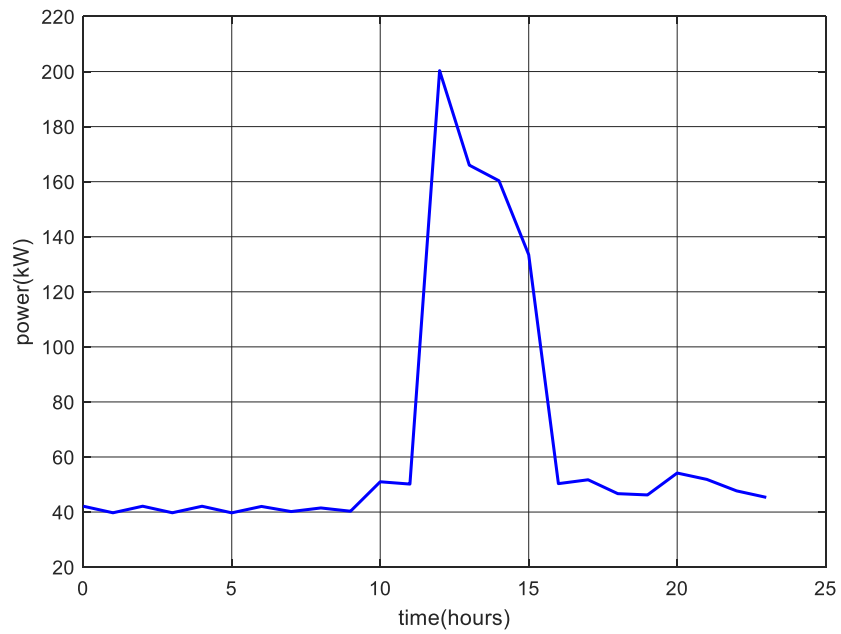


Figure 6.2: Hourly load profile of the AC load area

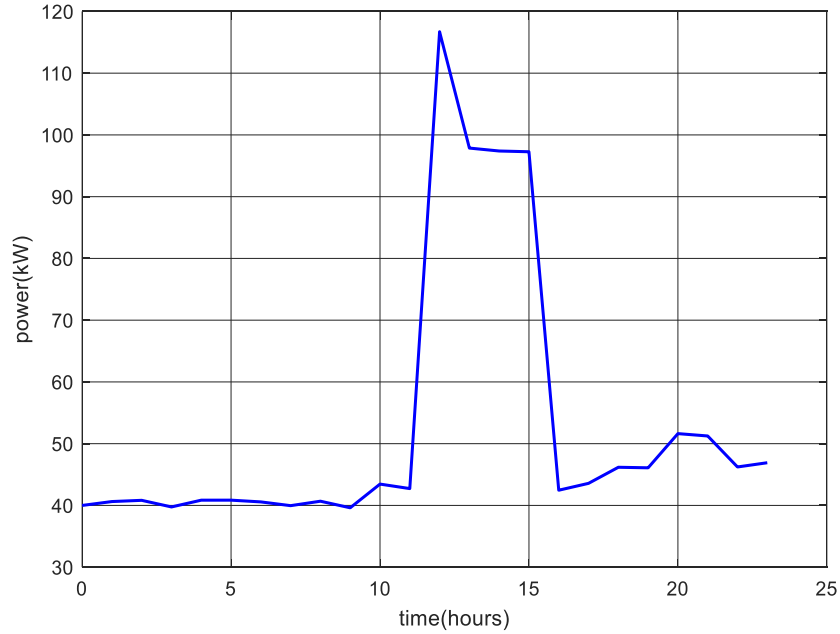


Figure 6.3: Hourly load profile of the DC load area

6.2.2 Supply Side

The power sources of the microgrid include various types of AC and DC sources. The diesel generator is selected to represent an AC source while PV and batteries represent the DC sources. In some schemes, conversion devices including AC/DC, DC/AC and DC/DC converters are required. The power ratings and specifications of such sources and converters are specified based on the connected load. The diesel generator is sized by the same approach discussed in chapter 5.

The selected PV array and battery bank are sized based on the connected load and the total energy consumed. The sizing procedure, followed in chapter 5, is employed in this chapter to evaluate the appropriate number and capacities of the required PV modules and batteries.

6.2.3 Selection of DC Grid Distribution Voltage

An appropriate DC distribution voltage has to be selected to compensate for the losses resulting from transmitting the power from generation station to the load. The generation station is assumed to be installed in the same area where the residential area is located. There is no standard DC distribution voltage yet available. Selection of low DC voltages at, for example, 24 V_{DC} or 48 V_{DC}, will significantly lead to high losses. Different research articles have suggested adopting distribution DC voltages of 380 V_{DC} and 750 V_{DC} [131-134]. Such voltage levels have proven to be efficient in reducing the current values and accordingly, needing for small cross-section area conductors. In addition, 380 V_{DC} is considered as a standard DC voltage for commercial and residential facilities by IEC [135] and by EMerge Alliance in the US [136]. In this chapter, 380 V_{DC} is selected as the DC distribution level for the proposed DC microgrid. Conventional three phase system with 400/230 V is selected for the AC microgrid.

By adopting 400 V_{AC(L-L)} for the AC microgrid and 380 V_{DC} for the DC microgrid, the maximum currents for both networks are around 500 A and 310 A, respectively. Further design arrangements are required to avoid such high current values. The main common bus at generation is sub-divided to several buses with same voltage level, with each supplying, for example, 10 or 20 houses. This point will be analyzed in the sections of power systems configurations analysis and design.

6.3 Proposed Network Schemes

This section combines all discussed generation sources and load area into a complete network with different configurations. The following four scenarios are considered in designing the proposed network:

- AC source supplying the AC grid area.
- AC source supplying the DC grid area.
- DC source supplying the AC grid area.
- DC source supplying the DC grid area.

6.3.1 System # 1: AC Source Supplying the AC Grid Area

This scheme adopts AC generating units to supply the AC grid residential area. This configuration is commonly adopted in all existing conventional AC power networks. Based on the proposed profile, the maximum load is 200 kW. The total generation capacity of 200 kW is required. Accordingly, a 200 kW diesel generator is selected. The generator specifications are listed in Table 6.1.

Table 6.1: Specifications of the selected 200 kW diesel generator

brand name	Huaquan
output type	AC three phase
rated power	200 kW
power factor	0.8

The 100 houses are divided to 5 groups. Each group is composed of 20 houses; with a maximum current of around 100 A. Figure 6.4 depicts the detailed layout of this

configuration. It is important to note that both sources and load area are AC. This scheme represents the base case conventional grid system.

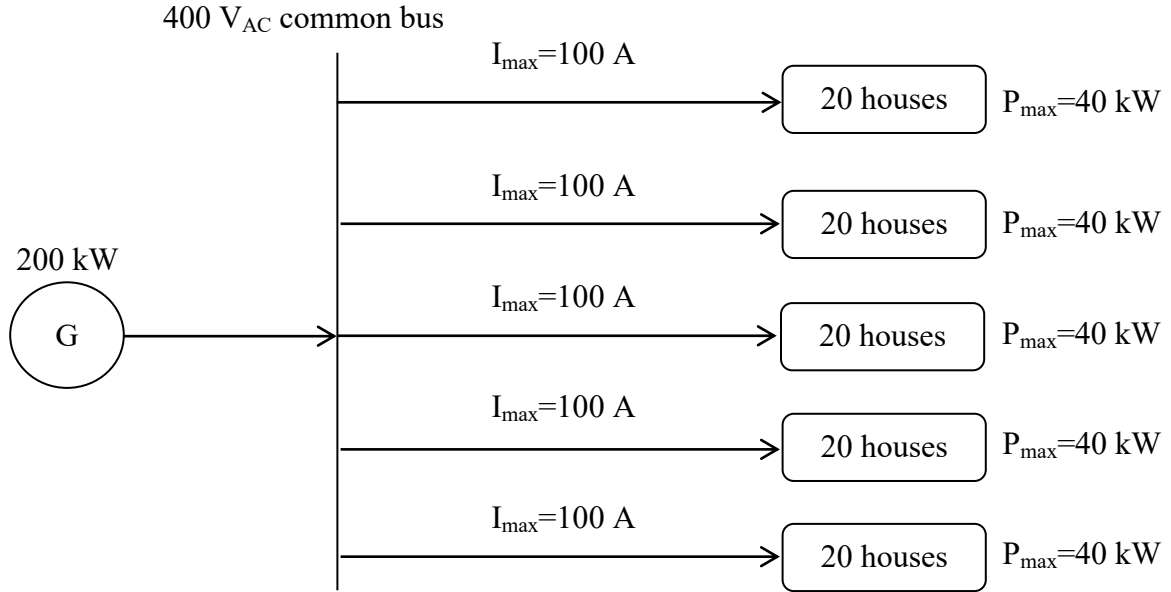


Figure 6.4: Layout of the diesel generator supplying the AC grid load area

6.3.2 System # 2: AC Source Supplying the DC Grid Area

DC grid load area with its respective load profile is considered in this configuration. The conversion losses caused by the AC/DC converter efficiency are accounted for this case. The maximum power for this scheme is around 120 kW. After accounting for converter losses, around 130 kW power is required from the generation plant. A 140 kW diesel generator is selected. The specifications of this generator are shown in Table 6.2.

Table 6.2: Specifications of the selected 140 kW diesel generator

brand name	YLFDJ
output type	AC three phase
rated power	140 kW
power factor	0.8

A 380 V_{DC} is selected for the DC distribution voltage level. The grid area is divided to 5 groups. Each feeder has a maximum current of around 63 A. The configuration of this scheme is demonstrated in Figure 6.5.

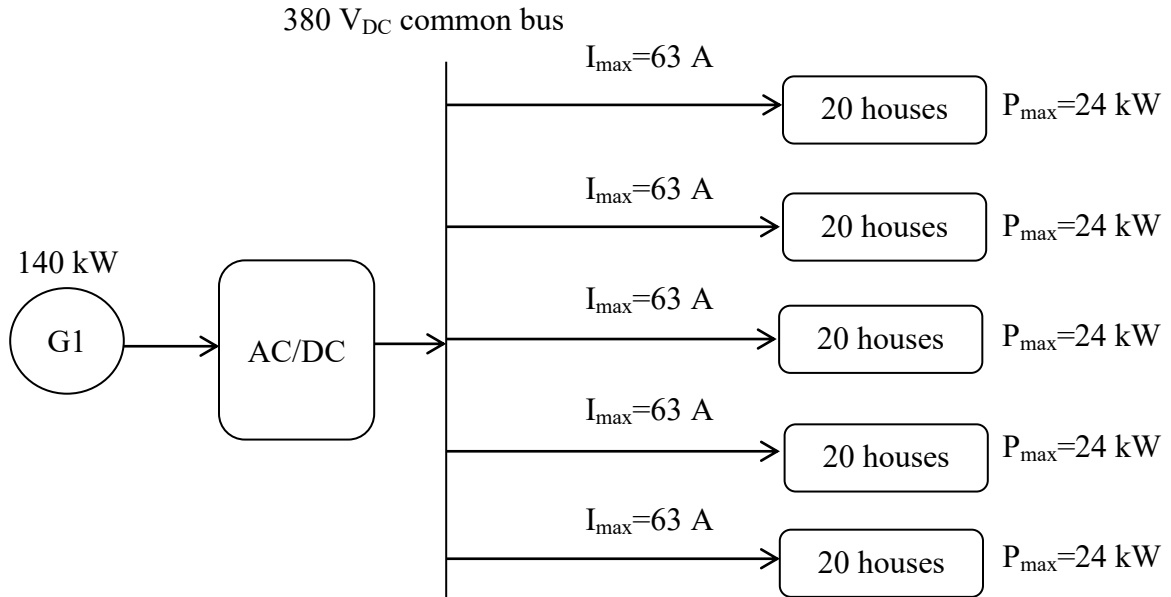


Figure 6.5: Layout of the diesel generator feeding the DC grid load area

6.3.3 System # 3: DC Source Supplying the AC Grid Area

PV array and battery bank are adopted to represent the DC source. A DC/AC converter is required for this system. The PV array and batteries are sized based on the approach discussed in chapter 5. For the typical day proposed in chapter 5, the total energy consumed by this scheme is calculated as 1565 kWh. A 350 kW PV array and about 7300 Ah of back up battery bank are required. The structure of this scheme is depicted in Figure 6.6.

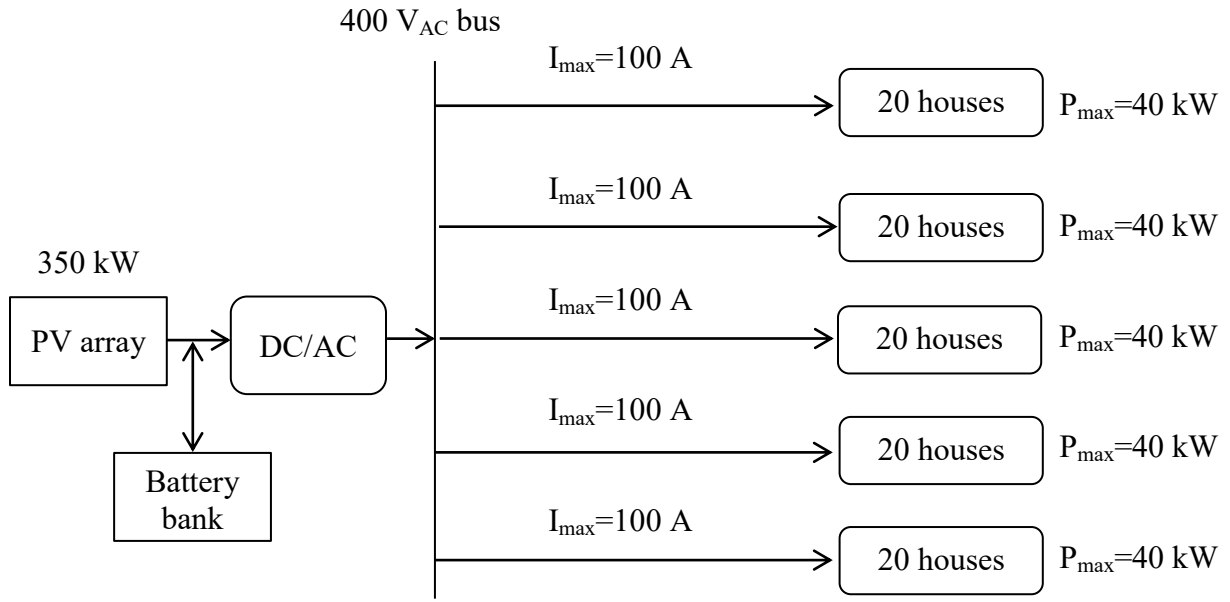


Figure 6.6: Layout of the PV array and battery bank supplying the AC grid load area

6.3.4 System # 4: DC Source Supplying the DC Grid Area

The entire residential AC grid load area is replaced by a corresponding DC grid. The DC load profile is adopted here. Figure 6.7 shows the structure of this scheme. Based on 1275 kWh total energy consumption, the required PV array and battery bank are 260 kW and 5300 Ah, respectively.

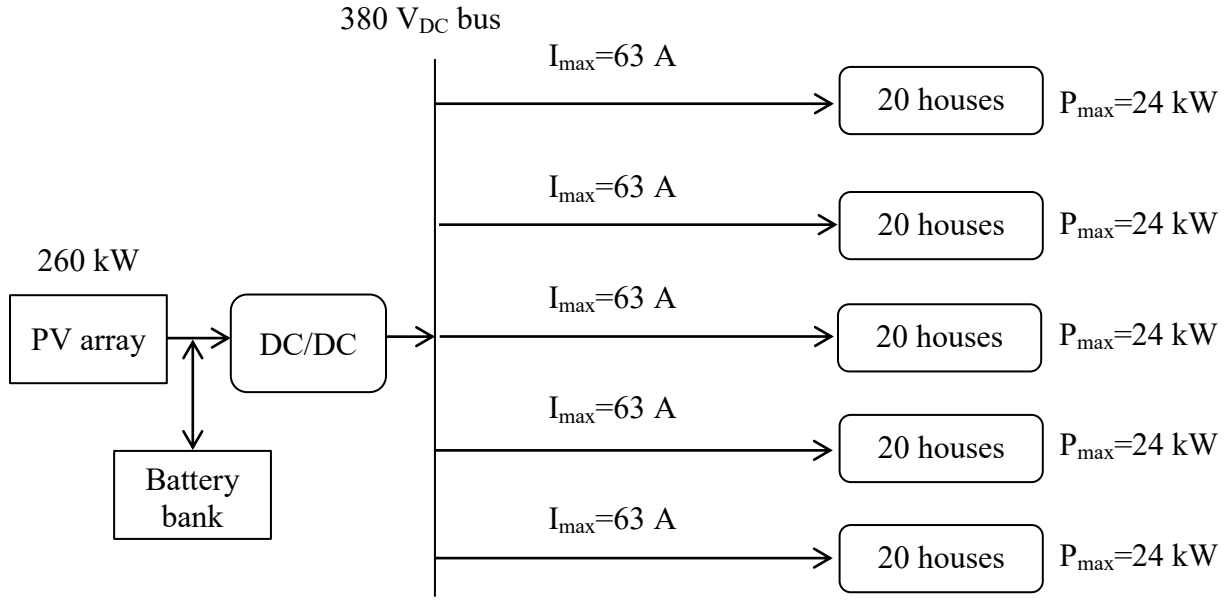


Figure 6.7: Layout of the PV array and battery bank feeding the DC grid load area

6.4 Cost Analysis of the Proposed Schemes

6.4.1 Cost of Generation Sources

System # 1 requires a 200 kW diesel generator while system # 2 requires a 140 kW diesel generator. For systems 3 and 4, a 250 W PV module and a 12 V, 250 Ah battery are selected. The difference is only in the estimated required number of such PV modules and batteries. In addition, several converters are needed according to the voltage levels and AC and DC distribution lines of the respective systems. In summary, the costs of all components in generation side for all configurations are listed in Table 6.3.

Table 6.3: Cost of all components of the AC and DC microgrids at supply side

	AC-AC (200 kW)	AC-DC (140 kW)	DC-AC (350 kW)	DC-DC (260 kW)
diesel generators	16,900	9,400	-	-
converters	-	3,250	5,200	3,650
PV array	-	-	125,280	92,160
batteries	-	-	201,600	147,840
total	16,900	12,650	332,100	243,650

Figure 6.8 compares the costs of the supply side components of all systems. The system with DC source supplying the AC microgrid is the most expensive system. This is due to the high costs of PV modules and batteries. The total energy consumed by the AC load area including the inverter losses is higher by around 23 % of that of the DC microgrid. Consequently, this has led to the requirements of more PV modules and batteries. The diesel generators have low cost as noticed from systems 1 and 2.

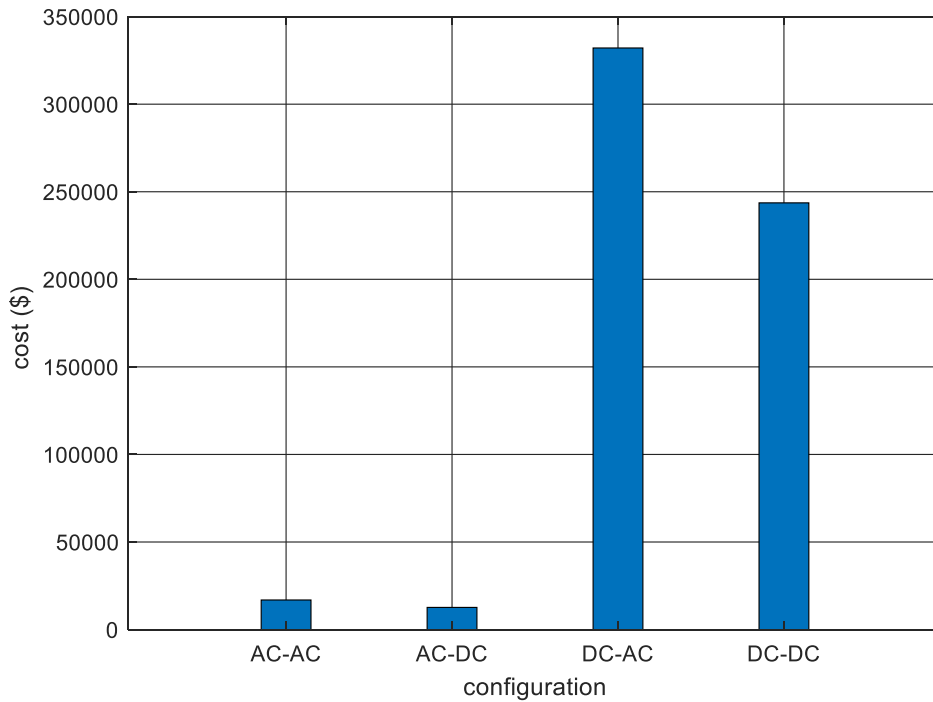


Figure 6.8: Cost comparisons of supply side components

6.4.2 Diesel Generator Fuel Consumption Estimation

The manufacturers of small diesel generators rated at few hundreds of kilowatts do not include the fuel consumption at different loading conditions [128]. A mathematical modeling approach was proposed by [128] for approximate fuel consumption estimation under variable loading conditions. The approach utilized an approximate fuel consumption chart presented by the Diesel Service & Supply Ltd [137]. This company, of more than 30 years of experience, has proposed an approximate look up table of the fuel consumption of diesel generators (20-200 kW) under the 0.25, 0.5, 0.75 and full loading conditions, shown in Table 6.4. [137]

Table 6.4: Approximate fuel consumption based on generator size and loading [137]

size (kW)	0.25 load (L/h)	0.5 load (L/h)	0.75 load (L/h)	full load (L/h)
20	2.73	4.09	5.91	7.27
30	5.91	8.18	10.91	13.18
40	7.27	10.46	14.55	18.18
60	8.18	13.18	17.28	21.82
75	10.91	15.46	20.91	27.73
100	11.82	18.64	26.37	33.64
125	14.09	22.73	32.28	41.37
135	15.00	24.55	34.55	44.55
150	16.37	26.82	38.19	49.55
175	18.64	30.91	44.10	57.74
200	21.37	35.00	50.00	65.46

Based on this table, a mathematical model of the fuel consumption as a function of power was formulated as: [128]

$$F = 3.252 \times 10^{-6} P^3 - 0.00101 P^2 + 0.391 P + 2.24 \quad (6.1)$$

Where F is fuel consumption in L/h and P is the load value in kW.

This model is used for fuel consumption estimation under the hourly AC and DC load profiles over a complete year.

6.4.3 O&M Costs

The O&M costs for the systems comprising diesel generators are 5 % of the diesel generator cost. The annual O&M for the PV arrays and batteries are assumed to be 1 % of the PV modules costs. Table 6.5 lists the O&M costs for all configurations for the first year.

Table 6.5: Cost of all components of the AC and DC microgrids at supply side

system	O&M cost (\$) for the first year
AC-AC	844.4
AC-DC	469.9
DC-AC	1252.8
DC-DC	921.6

6.4.4 Annual Load Profiles for the AC and DC Microgrids

In the previous analyses, the presented load profiles for the AC and DC microgrids are proposed based on the worst case, considering a typical day of June. In order to estimate the hourly generation cost of the diesel generators over one year, hourly load profile for the entire year is required. Residents' activities and some appliances power consumption behavior are different from season to season. To estimate the hourly load profile over one year, the hourly load profile for a residential substation in Dhahran for the year 2005 is used, as depicted in Figure 6.9 [138]. This profile is employed here as an indicator for evaluating the annual hourly load profiles for the presented AC and DC microgrids.

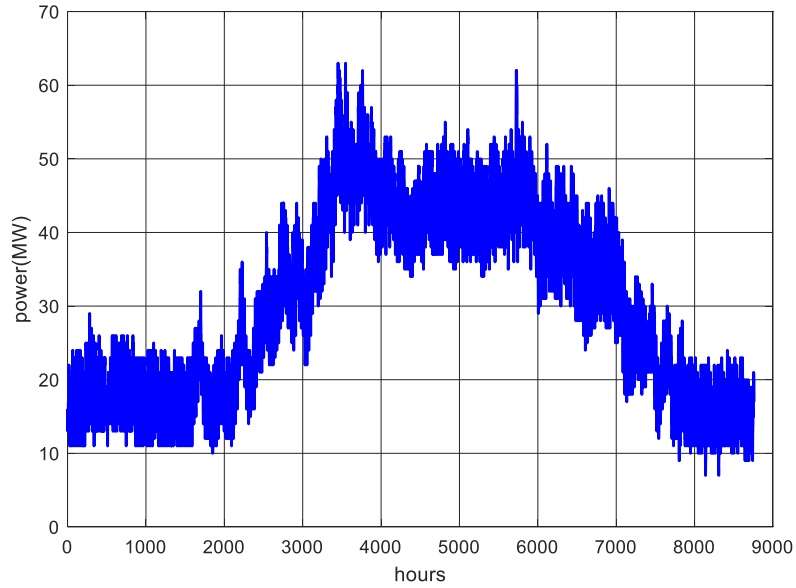


Figure 6.9: Hourly load profile for a residential area in Dhahran, 2005 [138]

The proposed load profile will be adjusted and scaled over the year by using the trend of Figure 6.9. The loads at hours 12.00 to 15.00 are used here as illustrative examples. The load values at the other hours follow the same approach. Figure 6.10 shows the extracted load profiles at the hours 12.00 to 15.00.

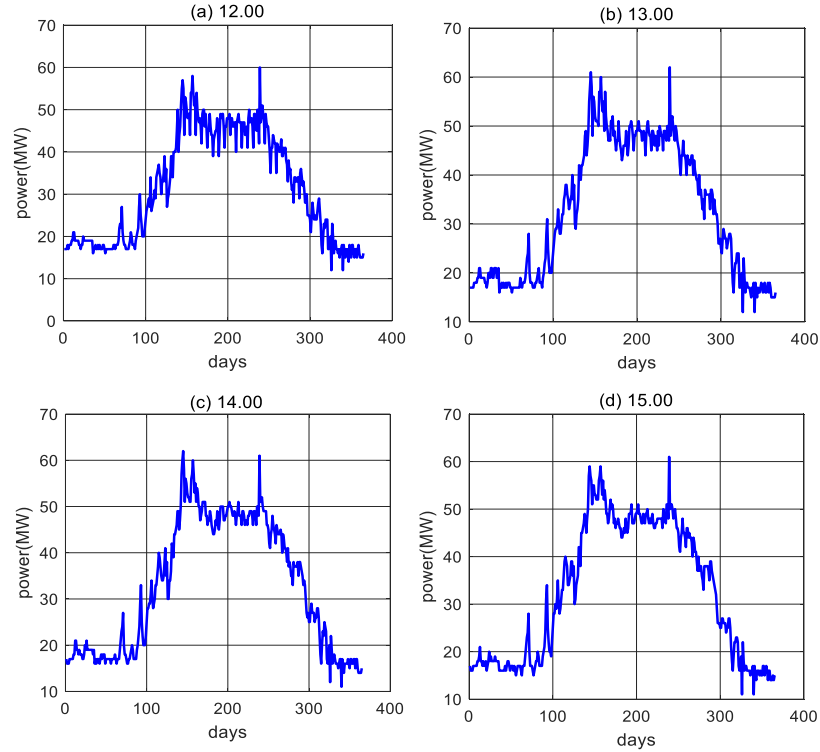


Figure 6.10: Load profiles at the designated hours for the area in Dhahran, 2005 [138]

For each hour, the value of the daily load is scaled as a percent with respect to the annual peak load at that hour. For example, at 14.00 hour, the entire curve shown in Figure 6.10(c) is now divided by the peak value of that curve. Figure 6.11 shows the percentage of all profiles at the designated hours over the year with respect to their respective peak values. The scaled profiles for the proposed AC and DC load profiles at the four hours are then evaluated and shown in Figure 6.12 and Figure 6.13, respectively. This operation is performed for all remaining hours. Finally, Figure 6.14 shows the complete hourly AC and DC load profiles that are adopted for evaluating the total generation costs over one year.

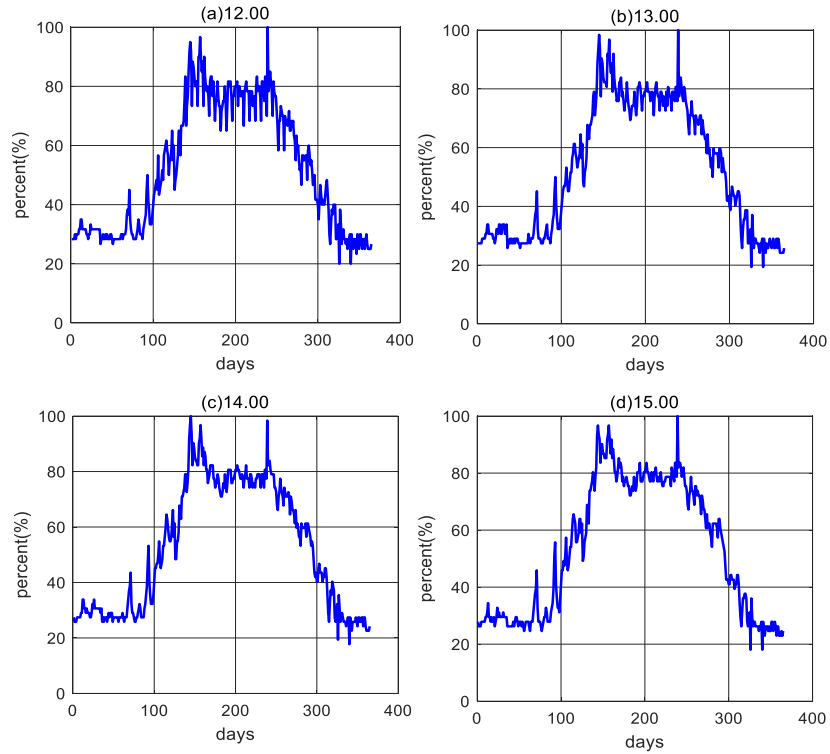


Figure 6.11: Percent profiles at hours 12.00-15.00 with respect to the peak load value

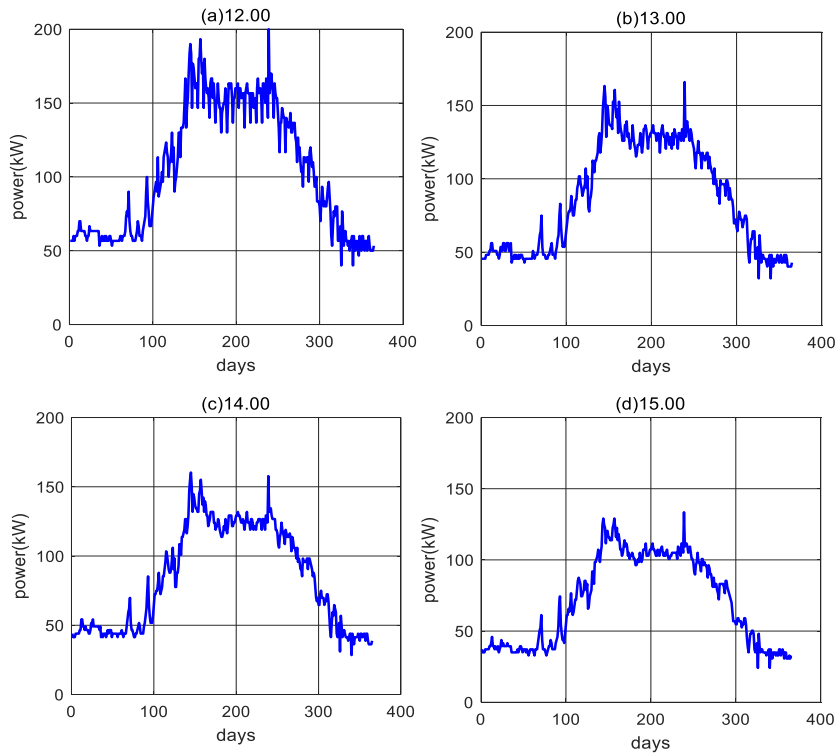


Figure 6.12: Scaled AC load profiles for the hours 12.00-15.00

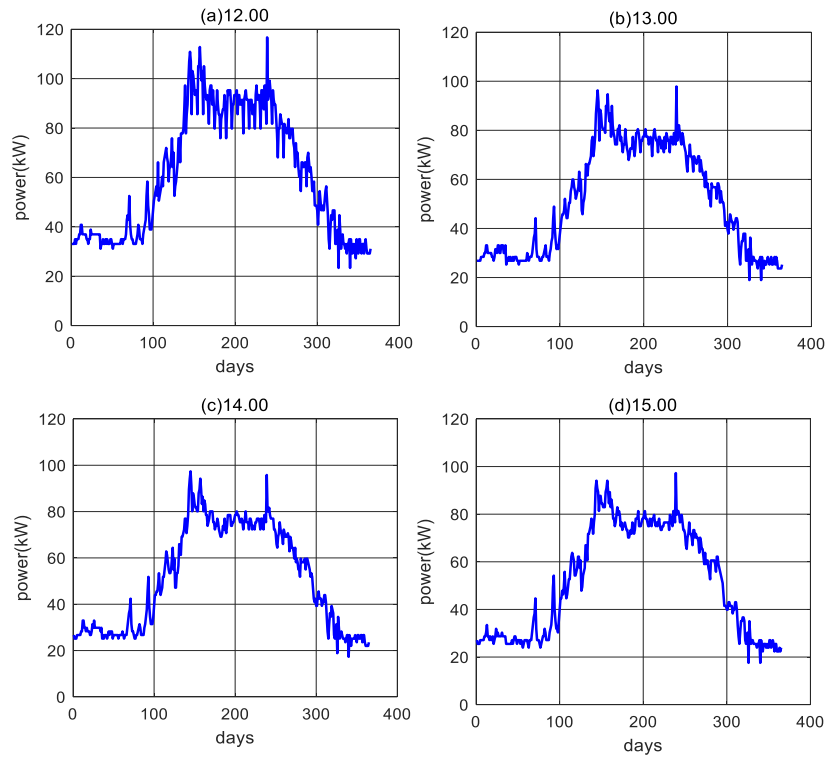


Figure 6.13: Scaled DC load profiles for the hours 12.00-15.00

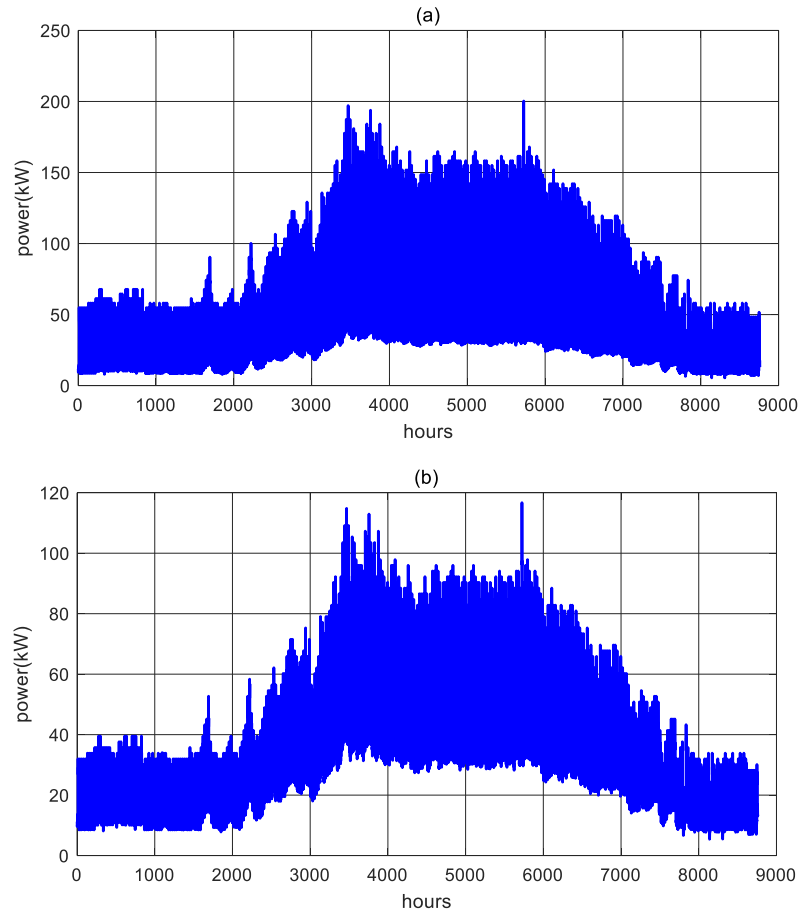


Figure 6.14: Final hourly load profiles over the year (a) AC town (b) DC town

To estimate the hourly generation costs over the year for systems 1 and 2, these profiles are used to calculate the fuel consumption. The conversion losses in system # 2 are accounted by dividing the DC load profile by 0.9, before processed to the model.

The evaluated total costs of generation for both systems for one year are demonstrated in Table 6.6. The diesel cost in Saudi Arabia as of 2018 is \$ 0.125 per liter. The generation cost of system # 1 is higher than system # 2. This is due to the low power consumption behavior of the DC appliances incorporated with system # 2.

Table 6.6: Total generation costs for systems 1 and 2 for the first year

	AC-AC	AC-DC
total generation cost (\$)	15,855	14,825

6.4.5 Required Land Area for PV Systems

The approximate land area for PV modules installation can be simply estimated by the product of the area of a single PV module and the total number of modules [139-141]. The selected PV module has an area of 1.7 m². The number of required PV modules for the DC-AC and the DC-DC systems are 1,392 and 1,024 modules, respectively. Therefore, the required land area for the DC-AC system is around 2,370 m² whereas the required land area for the DC-DC system is around 1,750 m².

6.5 Life Cycle Cost Analysis and Systems Comparisons

This section presents a comparative study between the four systems in terms of total life cycle cost analysis. The period of study is 20 years. All equations discussed in chapter 5 for total life cycle cost calculations are employed here as well. Table 6.7 and Table 6.8 show the values of all parameters involved in the total cost calculations for all proposed configurations. For revenues estimation, the energy of each scheme is sold at the same price. As of 2018, the electricity tariff in Saudi Arabia is \$ 0.048 per kWh. Unlike the small generators presented in chapter 5, the diesel generators rated at few hundreds of kW are assumed to be replaced every 7 years.

Table 6.7: Total life cycle cost calculations for systems 1 and 2

	AC-AC	AC-DC
generation side cost	\$ 16,888	\$ 12,647
PW of generator replacement	\$ 29,136	\$ 16,213
PW of O&M cost	\$ 14,582	\$ 8,114
PW of generation cost	\$ 273,797	\$ 255,982
revenue	\$ 254,383	\$ 207,317
total life cycle cost	\$ 80,020	\$ 85,640

Table 6.8: Total life cycle cost calculations for systems 3 and 4

	DC-AC	DC-DC
generation side cost	\$ 332,080	\$ 243,650
PW of batteries	\$ 323,466	\$ 237,209
PW of O&M cost	\$ 21,634	\$ 15,915
revenue	\$ 254,383	\$ 207,317
total life cycle cost	\$ 422,460	\$ 289,460

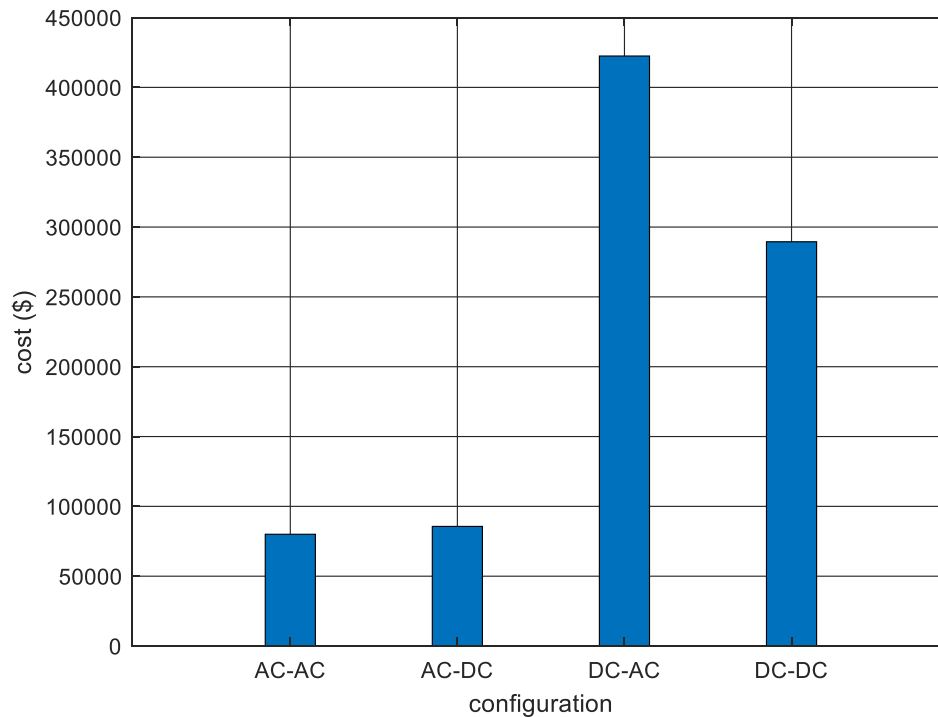


Figure 6.15: Life cycle costs comparison for all proposed configurations

The systems comprising PV arrays and batteries are the most expensive systems. The main factor contributing to such high cost is the cost of PV modules and batteries. The systems with diesel generators supplying AC and DC microgrids are the most economical solution with almost identical life cycle cost. This is mainly attributed to the low costs of the diesel generator. Although fuel is continuously consumed for system operation, the cost of diesel in Saudi Arabia is low which makes this factor to be insignificant in life cycle cost.

For comparison purposes, the study is extended to GCC countries with different diesel prices and electricity tariffs. Table 6.9 lists the electricity tariffs and the diesel prices per liter for the GCC countries in 2018 [142].

Table 6.9: Diesel prices of GCC countries in 2018 [142]

country	diesel price (\$/L)	electricity tariff (\$/kWh)
Saudi Arabia	0.125	0.048
Bahrain	0.42	0.0079
UAE	0.68	0.0204
Qatar	0.51	0
Kuwait	0.38	0.0248
Oman	0.63	0.0259

Assuming all components costs, load profiles and sizing results are same as of Saudi Arabia case, the life cycle costs are estimated here for each country by considering the respective diesel prices. This means that the DC-AC and DC-DC systems are kept unchanged. The impact of varying fuel prices from a country to another on the life cycle cost is investigated. Figure 6.16 compares the life cycle costs of GCC countries for the four configurations. For all other GCC countries, the systems with diesel generator have

high life cycle cost. The complete DC-DC system is the most economical system of four of the six GCC countries.

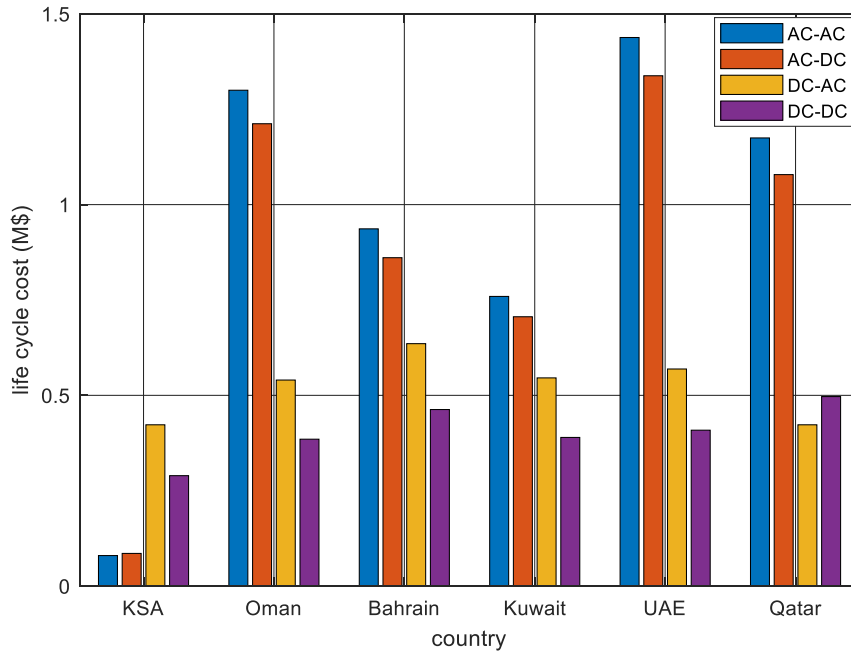


Figure 6.16: Life cycle cost comparisons for GCC countries for all proposed schemes

6.6 Summary and Conclusions of the Chapter

By the end of all analyses and discussions carried out in this chapter, the following points summarize the main topics addressed:

- Load profiles for AC and DC houses representing a small town of 100 houses are presented.
- All analysis presented in this chapter is considered according utility supply perspective, not from the consumer perspective.
- The profiles are proposed on the basis of actual implementation and measurements of various common appliances having both AC and DC versions.

- The main issue addressed in appliance selection is the choice of an appliance in which the required task is similar for both AC and DC versions, irrespective of their electrical parameters and specifications.
- Diesel generators are used to represent AC source while PV array and batteries are employed to represent DC sources.
- Four cases are considered for designing a microgrid: AC source supplying AC microgrid, AC source supplying DC microgrid, DC source supplying AC microgrid and DC source supplying DC microgrid.
- For cases 1 and 2, the fuel consumption in (L/h) is computed using a mathematical model of fuel consumption as a function of load value.
- For cases 3 and 4, the PV array and battery bank are sized based on the total energy consumed.
- The conventional complete AC system has the lowest capital investment due to the low capital cost of diesel generator.
- The systems with PV arrays and batteries are characterized by high capital cost due to the expensive PV modules and batteries.
- For a life cycle of 20 years, the AC-AC system is still the most economical solution in Saudi Arabia in 2018 due to the low prices of diesel.
- At the current situation of fuel and PV and batteries prices, it is not economical for the utility companies to implement completely DC systems.
- For all other remaining GCC countries, the DC-AC and DC-DC systems are more economical in this case.

CHAPTER 7

PROTECTION SCHEME FOR DC MICROGRID

7.1 Introduction

Rapid fault detection and location is a crucial issue in power system protection field. Extremely high current is generated when a fault occurs. Accordingly, the system components may be affected leading to negative impacts on the entire power system. If the fault is not detected and cleared rapidly, vital components in the power network may be damaged. An efficient method to detect and locate the faults, while protecting the power system against such faults is essential. Generally, the fault detecting and locating components must be efficient enough to protect the power system at the minimum possible time in order to enhance the system stability. This chapter proposes a methodology to detect and locate the faults in DC microgrid under variable loading conditions. The DC microgrid proposed in chapter 6 is adopted here for the analysis.

The chapter starts by briefly describing the DC microgrid under study including its components. This is followed by presenting the proposed methodology for detecting and locating the faults in the DC microgrid. The mathematical model for evaluating the fault distance with respect to the common DC bus is then proposed. The chapter is concluded by testing the model accuracy and assessing its application in online simulations for an efficient DC microgrid protection scheme design.

7.2 DC Microgrid System Description

The DC microgrid proposed in chapter 6 is employed in this chapter for protection scheme application and simulations. It consists of a 380 V_{DC} source supplying a residential DC microgrid with a maximum power of 120 kW. The 380 V_{DC} distribution line linking supply and demand sides is assumed to have a length of 200 m. The power is transmitted via five feeders with each having a 24 kW maximum power. Figure 7.1 depicts the power system configuration of the DC microgrid under study.

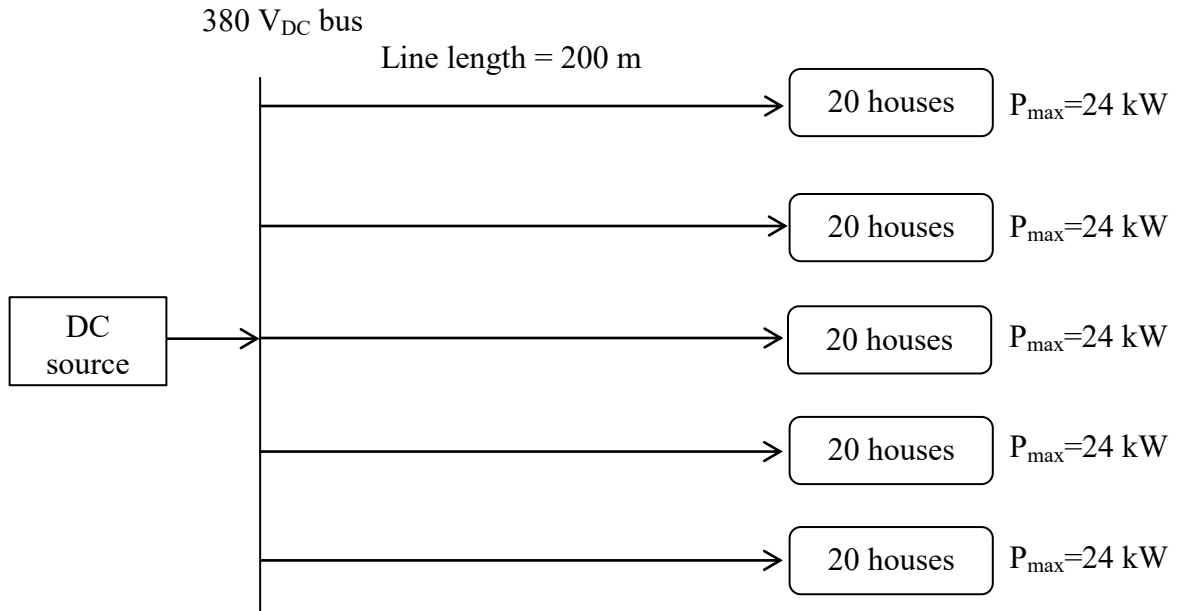


Figure 7.1: Layout of the DC microgrid under study

This system is modeled using SIMULINK in which the power supply is represented by a DC source of 380 V_{DC} . The parameters values of all system components are listed in Table 7.1. Figure 7.2 shows the single line diagram of one representative feeder of the DC microgrid under study. This system represents a DC microgrid built using actual DC home appliances as discussed in the previous chapters.

Table 7.1: Parameters values of the DC microgrid components

DC voltage source	380 V _{DC}
internal resistance	0.0013 Ω
line length	200 m
line resistance	0.0006 Ω/m
load resistance (at peak load)	5.94 Ω

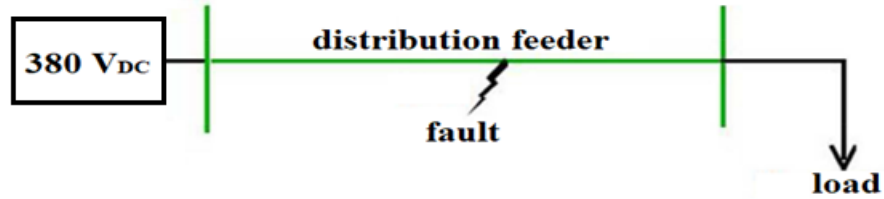


Figure 7.2: Single line diagram of the DC microgrid under study

7.3 Proposed Fault Detection and Locating Methodology and Resultant Mathematical Model

The proposed methodology for the detection and location of faults starts by simulating the SIMULINK model of the system shown in Figure 7.2 at various load values, various fault locations and various fault resistances. At each point, the sending end current at the instant of fault occurrence is recorded. This process is repeated for a representative range of distance values. The range of the varied parameters is as follows:

- Fault distance from the common DC bus: 0 m to 200 m in steps of 10 m.
- Fault resistance: 0.1 Ω to 1 Ω in steps of 0.1 Ω.
- Load: nine arbitrary selected values between 1 kW and 24 kW.

The data collected is composed of $21 \times 10 \times 9 = 1890$ points with each point having the fault resistance, supplied load and source current at fault as input variables, in addition to the corresponding fault distance as output variable. Sample data resulting from

SIMULINK simulations are listed in Table 7.2. For example, when the fault resistance is 0.1Ω , 70 m from the source while the load power is 1108.58 W, the sending end feeder current increases from 63 A to 2653.10 A.

Table 7.2: Sample data collected from SIMULINK simulations

$R_f (\Omega)$	I (A) (at fault)	d (m)
0.1	3753.94	0
0.1	3543.88	10
0.1	3356.08	20
0.1	3187.18	30
0.1	3034.47	40
0.1	2895.72	50
0.1	2769.11	60
0.1	2653.10	70
0.1	2546.42	80
0.1	2448.00	90
0.1	2356.89	100
0.1	2272.33	110
0.1	2193.62	120
0.1	2120.18	130
0.1	2051.50	140
0.1	1987.13	150
0.1	1926.68	160
0.1	1869.80	170
0.1	1816.18	180
0.1	1765.55	190
0.1	1717.66	200

The maximum normal operating current is around 63 A. The data collected from simulations have shown that the minimum sending end current value at fault is 341.21 A, which is more than 5 times the normal operating current. This makes the implementation of a protection scheme to be very essential. EUREQA software is utilized here as an

efficient mathematical formulation tool to build a precise model for the fault distance as a function of the pre-fault load value, fault resistance and the sending end current at fault.

To start building the mathematical model of the fault distance, the collected data are transferred to EUREQA software for the purpose of building a mathematical model of the form:

$$d = f(R_f, P_2, I_1) \quad (7.1)$$

Where d is the fault distance in meters, R_f is the fault resistance in Ω , P_2 is the pre-fault load value in Watt and I_1 is the sending end current at the time of the fault occurrence.

The final resulting model is:

$$d = \frac{633329}{I_1} + 0.0114P_2R_f^2 - 2.235 - 1666.5R_f - 1.28 \times 10^{-10} I_1 P_2^2 R_f^4 \quad (7.2)$$

In the on-line simulations, the purpose is to read the feeder sending end current at each instant of time. If this current is less than some predefined value, this model is deactivated and the output is forced to give a value indicating that the system is normal. In this system, 63 A is the maximum current value under 380 V_{DC} source and 24 kW load. Once the sending end current exceeds this value, the model shown in equation 7.2 is activated and starts to evaluate the fault distance by reading the aforementioned parameters. Model validation is presented in next section.

7.4 Simulation Results and Analysis

7.4.1 Model Accuracy Verification

The proposed model for locating the fault distance is tested by applying faults at the same DC microgrid SIMULINK model but at different test cases. Ten arbitrary fault locations at different fault resistances and load values are considered in this process. Table 7.3 compares the results obtained using the SIMULINK simulations and using the proposed model for evaluating the fault distance. The results have verified the effectiveness of the proposed model and its validity to be further used in online simulations for designing the protection scheme of the DC microgrid.

Table 7.3: Results of model testing at new input data

R_f (Ω)	P (W)	I (A)	SIMULINK	model	difference (m)
			d (m)	d (m)	
0.312	8824.77	1185.55	21.33	21.34	-0.01
0.696	10754.61	488.52	192.38	192.35	0.03
0.672	1866.79	568.49	0.927	0.933	-0.006
0.205	1305.03	1273.43	154.98	154.96	0.02
0.163	1098.88	1449.10	163.46	163.43	0.03
0.523	6116.32	615.23	173.74	173.73	0.001
0.962	1751.37	394.96	16.89	16.88	0.01
0.373	2089.13	903.34	79.96	79.96	0
0.606	18534.87	639.44	51.97	52.01	-0.04
0.263	2809.99	1059.61	160.01	160.02	-0.01

7.4.2 Online Monitoring and Simulations of the Proposed Protection Scheme

The model will be employed here for the purpose of building an efficient protection scheme for the proposed DC microgrid. This includes online fault detecting and locating, as well as instant isolation of the faulty feeders. The DC microgrid SIMULINK model

incorporated with the proposed protection scheme for a representative feeder is demonstrated in Figure 7.3. This figure comprises all components and algorithms required for building the protection scheme.

IGBT-based circuit breakers are implemented at both ends of the feeder. IGBTs have been widely used in low voltage DC systems due to their ability to operate in a few milliseconds [143]. Moreover, IGBTs are characterized by high withstanding capability against short circuit currents [144]. Various studies have adopted IGBTs as circuit breakers in different DC systems [143], [145-148].

The fault resistance in the on-line simulations is evaluated by dividing the voltage across the fault by the fault current:

$$R_f = \frac{V_f}{I_f} \quad (7.3)$$

Where V_f is the voltage across the fault and I_f is the fault current. These two parameters cannot be measured online since there is no prior knowledge about fault location. Alternatively, from the data collected for building the fault distance, a mathematical model for the fault resistance can be formulated as a function of sending end current, I_1 , load current, I_2 and load voltage, V_2 as follows:

$$R_f = 5.69 \times 10^{-5} I_2 + 1.84 \times 10^{-7} V_2 I_2 + 6 \times 10^{-7} I_2^2 + \frac{V_2}{I_1 - 0.003 V_2 I_2} - 3.63 \times 10^{-8} I_2 I_1 \quad (7.4)$$

The variables of this equation can be measured in online simulations and the fault resistance can be then easily evaluated.

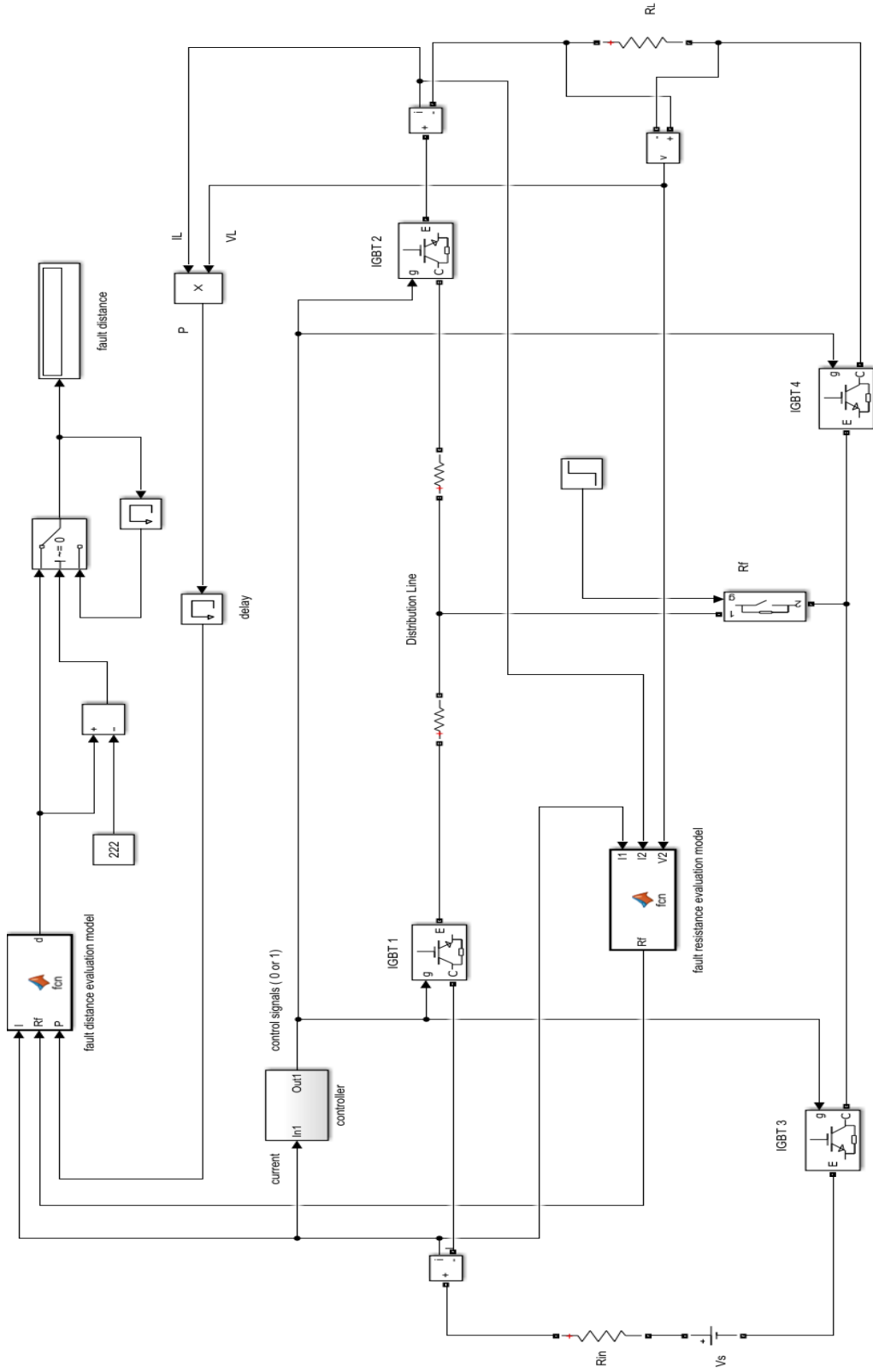


Figure 7.3: SIMULINK model of the DC microgrid protection scheme for one feeder

The IGBTs control block shown in the figure is responsible for generating signals for opening or closing the IGBTs. The algorithm of this block is depicted in Figure 7.4. The feeder sending end current is compared with the normal operating current. If this value is less than 63 A, the output signal is “1” and the IGBTs act as short circuit and the power is continuously delivered to the load. The mathematical model block in this case gives an arbitrary constant value of “222” indicating that the system is working properly without any faults.

On the other hand, as the sending end current value exceeds 63 A, the IGBTs control block algorithm is executed and “0” value is generated to the IGBTs to act as open circuit and isolate the faulty feeder instantly. At the same time, the mathematical model is now activated and evaluated which gives the fault distance in meters as measured from the common DC bus. The faulty feeder is also identified during the same process. The faulty feeder is then isolated without affecting the loads supplied by the other feeders.

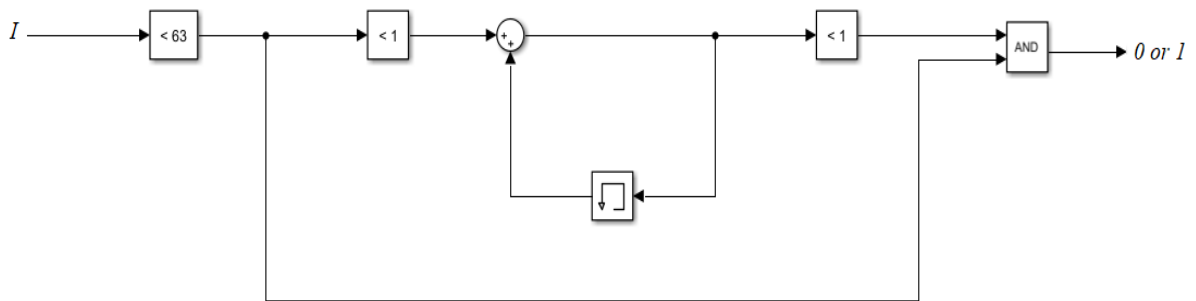


Figure 7.4: Algorithm of the IGBTs switching and controlling block

Figure 7.5 shows the steps of fault detecting and locating, as well as the faulty feeders isolation process. The complete DC microgrid SIMULINK model including all feeders incorporated with the proposed protection algorithm is depicted in Figure 7.6. Each feeder has its own protection scheme by the same method of the discussed scheme for the

representative feeder. In addition, the indicators displayed in the figure show the feeder number and the fault location through the feeder with respect to the common DC bus.

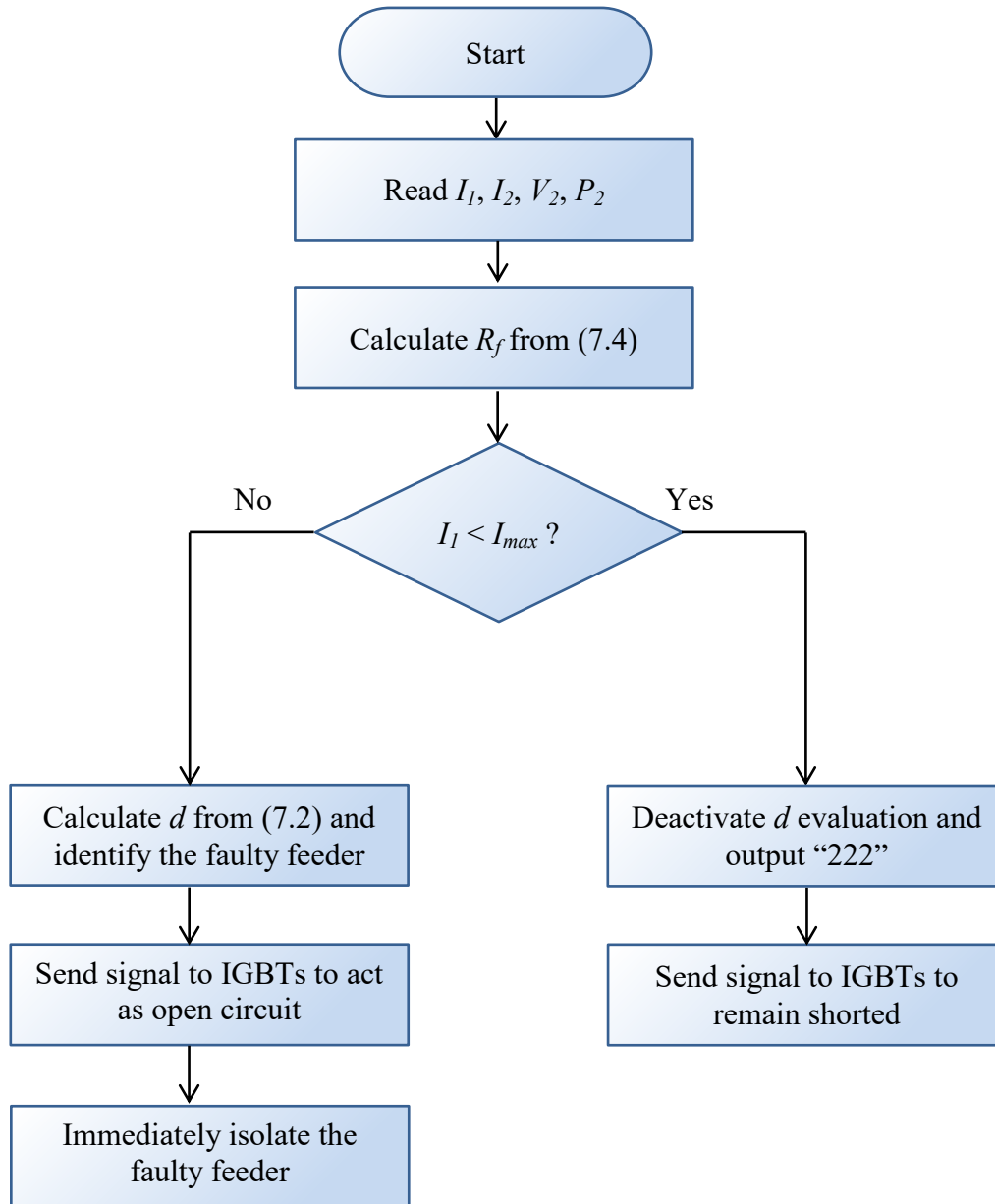


Figure 7.5: Proposed protection scheme process

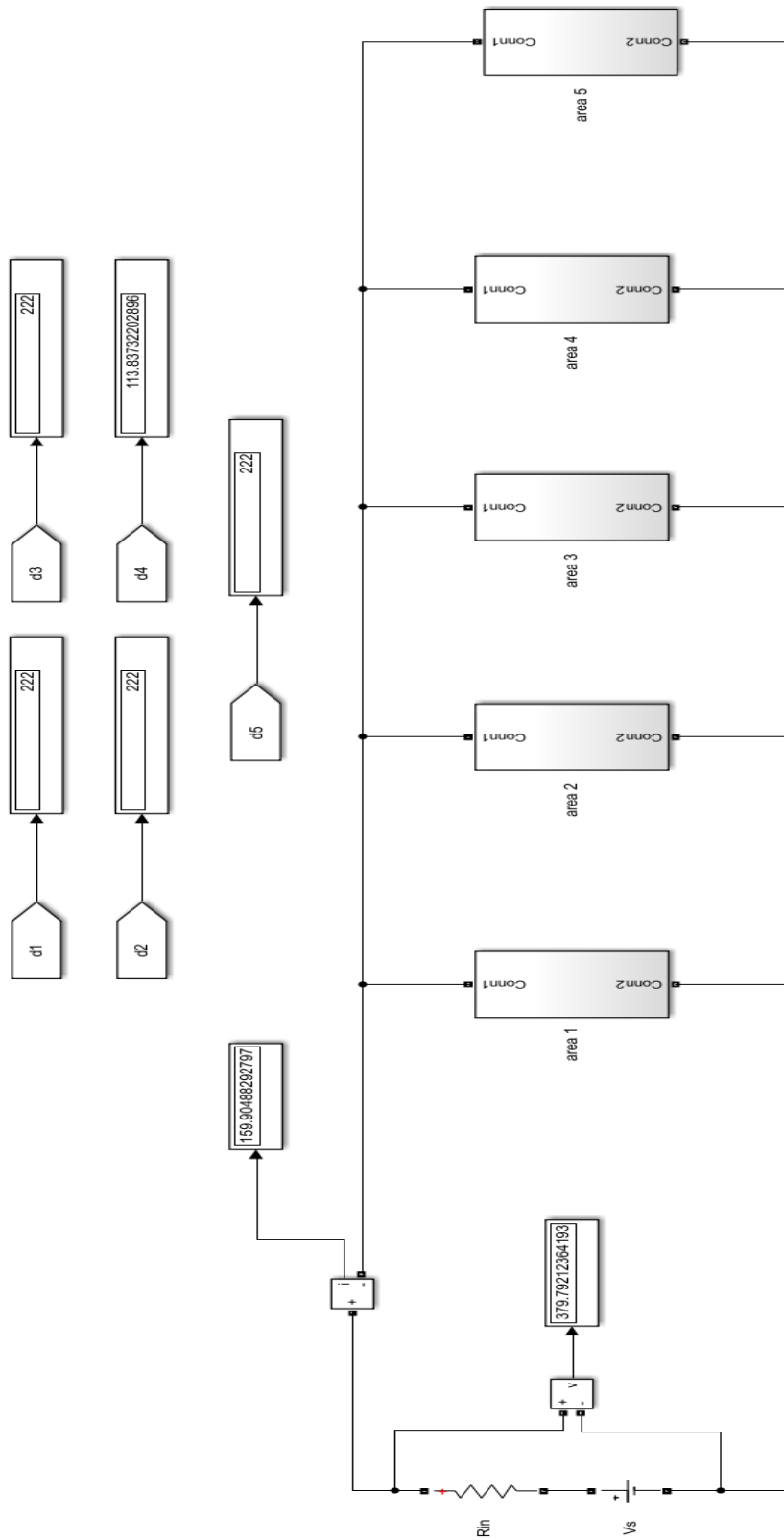


Figure 7.6: Complete DC microgrid incorporated with proposed protection scheme

7.4.3 System Simulations and Performance under Different Fault Conditions

In this subsection, the system shown in Figure 7.6 is subjected to faults at various locations. Two cases are considered in this analysis under ten-second simulations:

- **Case #1:** fault with 0.815Ω resistance at the second 6 at a distance 113.5 m of feeder # 4 supplying 10 kW load. The loads at feeders 1, 2, 3 and 5 are 20 kW, 6 kW, 17.5 kW and 15.6 kW, respectively.
- **Case #2:** two sequential faults: the first fault is applied at the second 3.5 at a distance 192 m of feeder # 5 supplying 17.2 kW load. Then, another fault is applied at the second 8.25 at a distance 8 m of feeder # 2 supplying 8.2 kW load. The fault resistances of the faults at feeders # 5 and 2 are 0.279Ω and 0.547Ω , respectively. The loads at feeders 1, 3 and 4 are 16.7 kW, 6.4 kW and 22 kW, respectively.

For each case, the response of all parameters to the fault is presented including the load power, breakers performance and feeder and distance evaluation capability.

7.4.3.1 Case # 1: fault at feeder # 4

The DC microgrid in this case is exposed to a fault at feeder # 4. The fault resistance is 0.815Ω . The distance of the fault to the common $380 V_{DC}$ bus is 113.5 m. The system is operating normally before it is subjected to that fault at $t = 6$ sec. Figure 7.7 shows the response of the proposed mathematical model for fault distance evaluation. The number “222” designates the normal operating conditions of the respective feeder. The figure also indicates that all other feeders are not subjected to any fault. The faulty feeder is also

designated by “222” up to just prior to the time of the fault. Once the fault is applied at 6 sec, the fault distance with respect to the common bus is evaluated.

The output signal profiles of the IGBT’s control block are displayed in Figure 7.8 for all feeders. As long as the system is normal, the signal is always “1” and the IGBTs are accordingly closed. Once feeder # 4 is subjected to a fault, the signal is changed to “0” giving the IGBT’s a command to open and isolate the load connected to the faulty feeder. All IGBTs incorporated with the other feeders are not affected by that fault.

The load power values for all areas are depicted in Figure 7.9. The power is cut off from the faulty line immediately at the time of the fault. The loads supplied by other feeders are not affected and all respective connected loads are supplied by power properly. High source current is noticed at the time of fault after being suppressed by rapid disconnection of the faulty line. This can validate the value and effectiveness of the proposed protection scheme. The total power is shown in Figure 7.10.

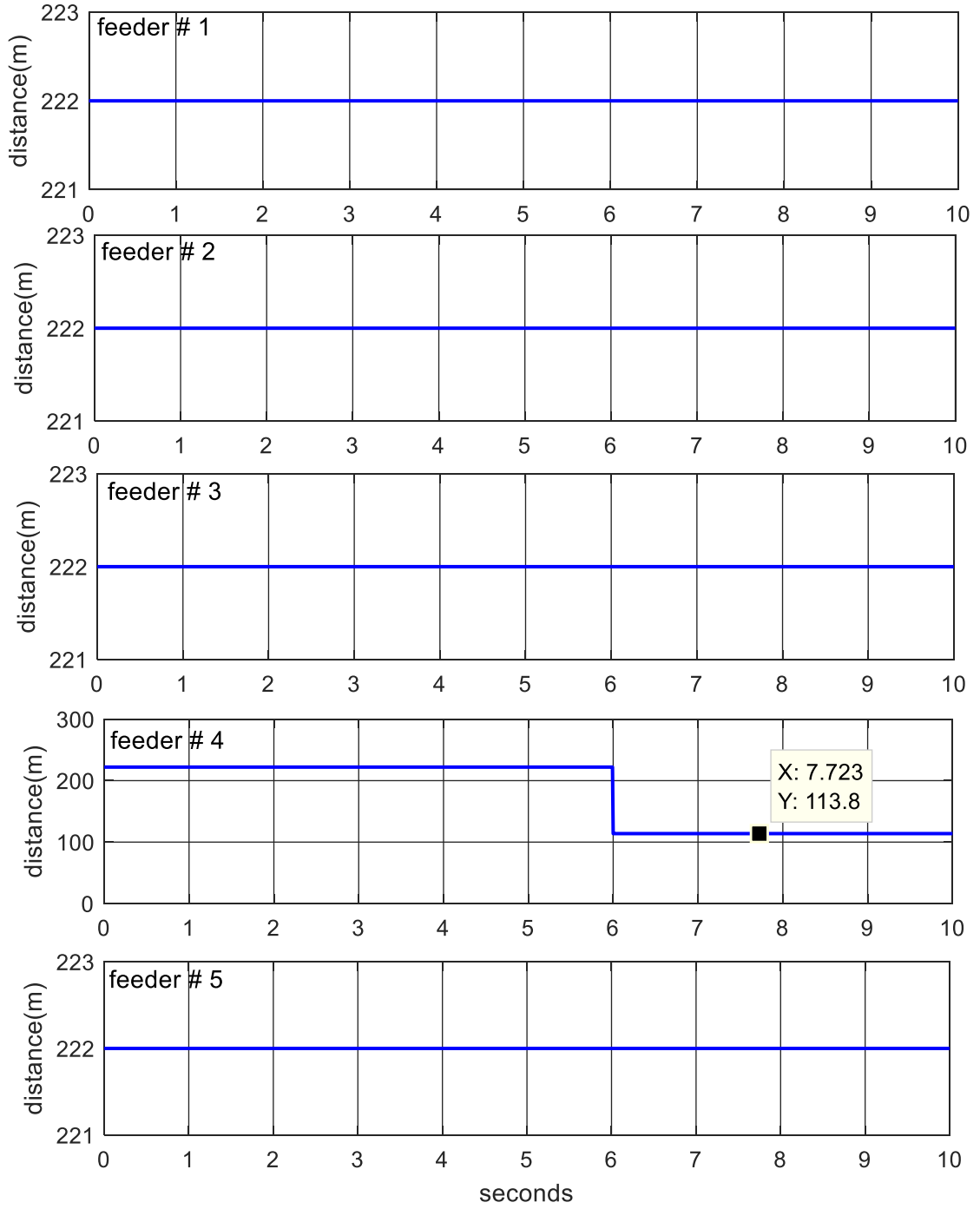


Figure 7.7: Fault distance evaluation under fault at feeder # 4 (case # 1)

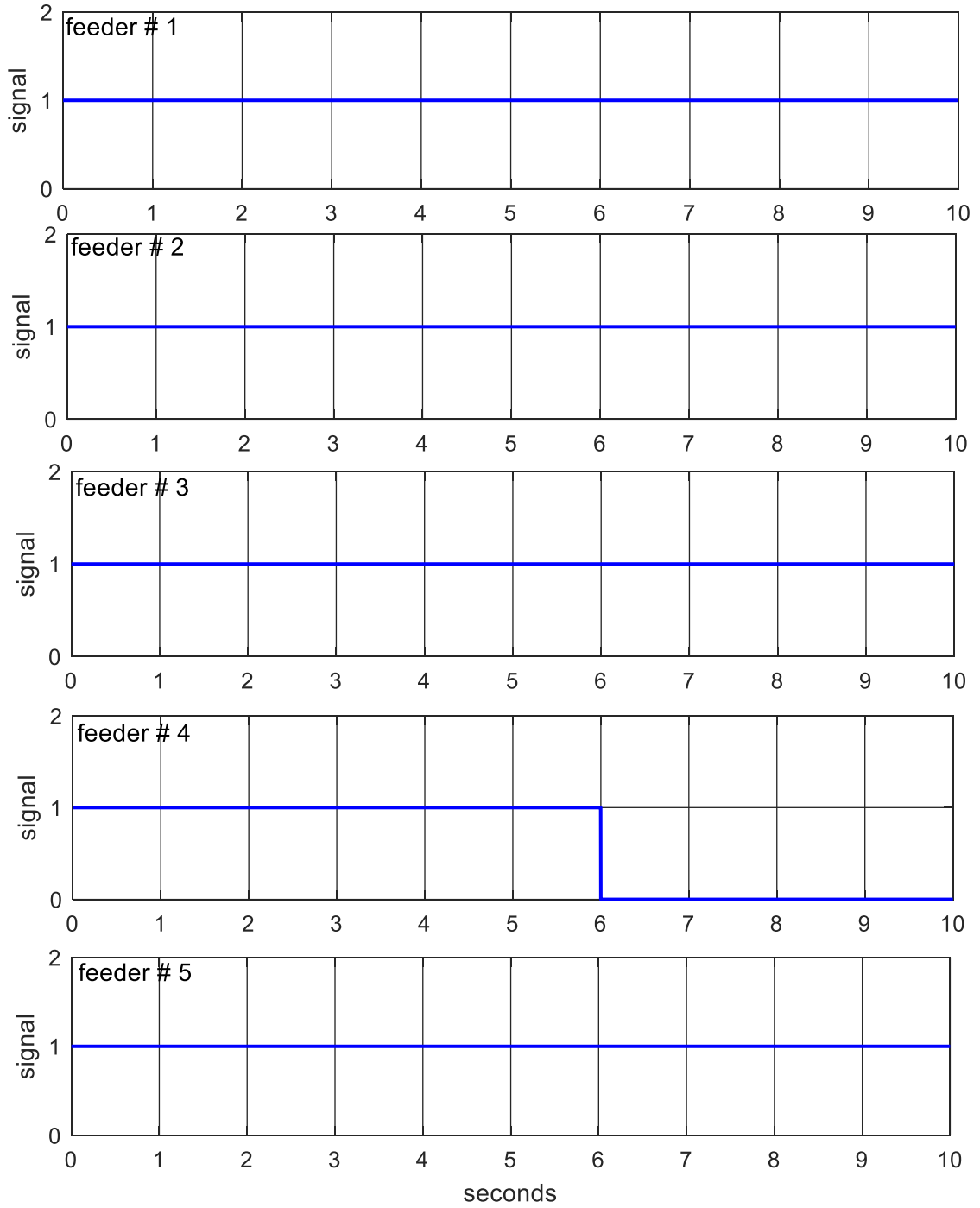


Figure 7.8: Response of the signals sent to the IGBT's (case # 1)

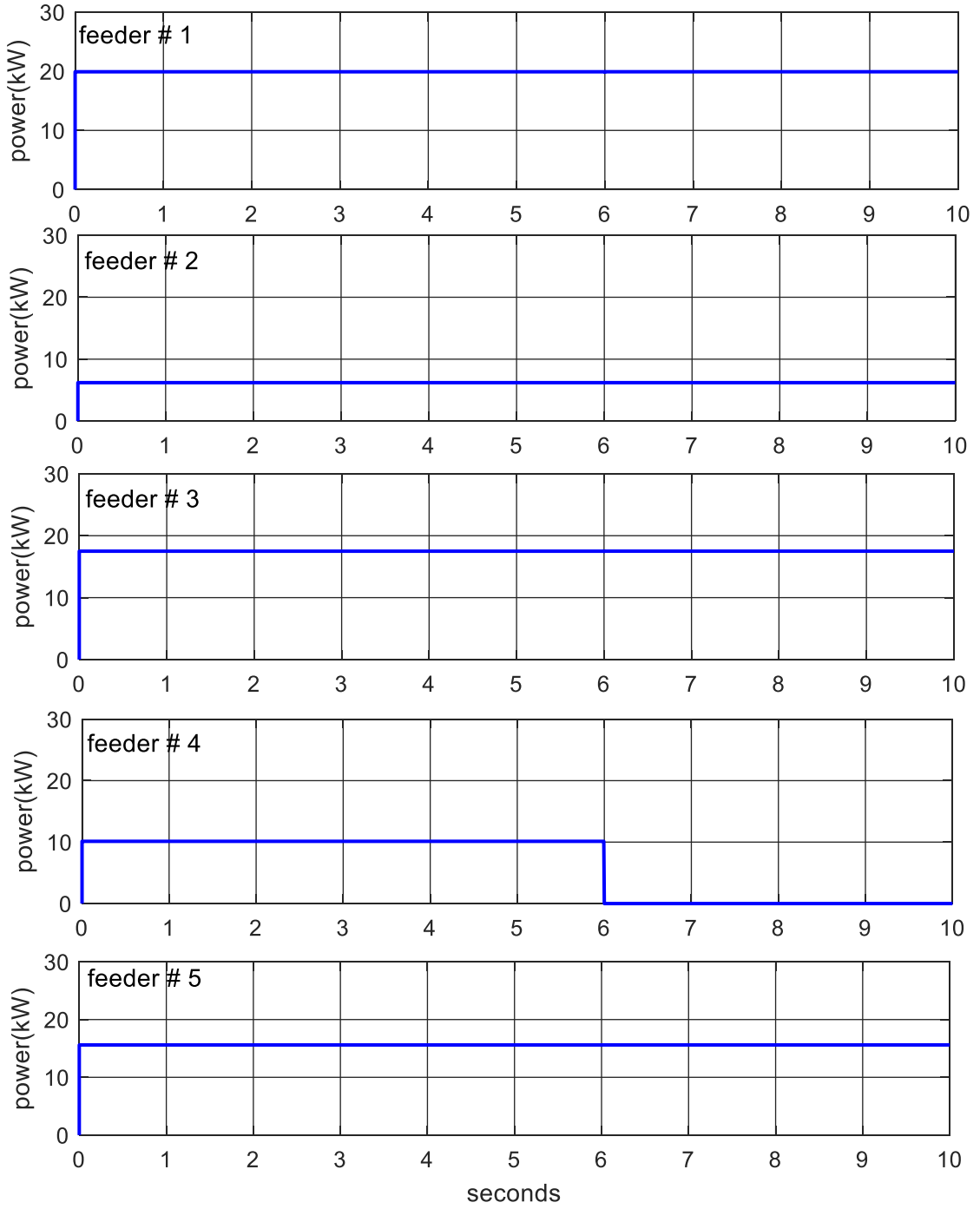


Figure 7.9: Load supplied by each feeder (case # 1)

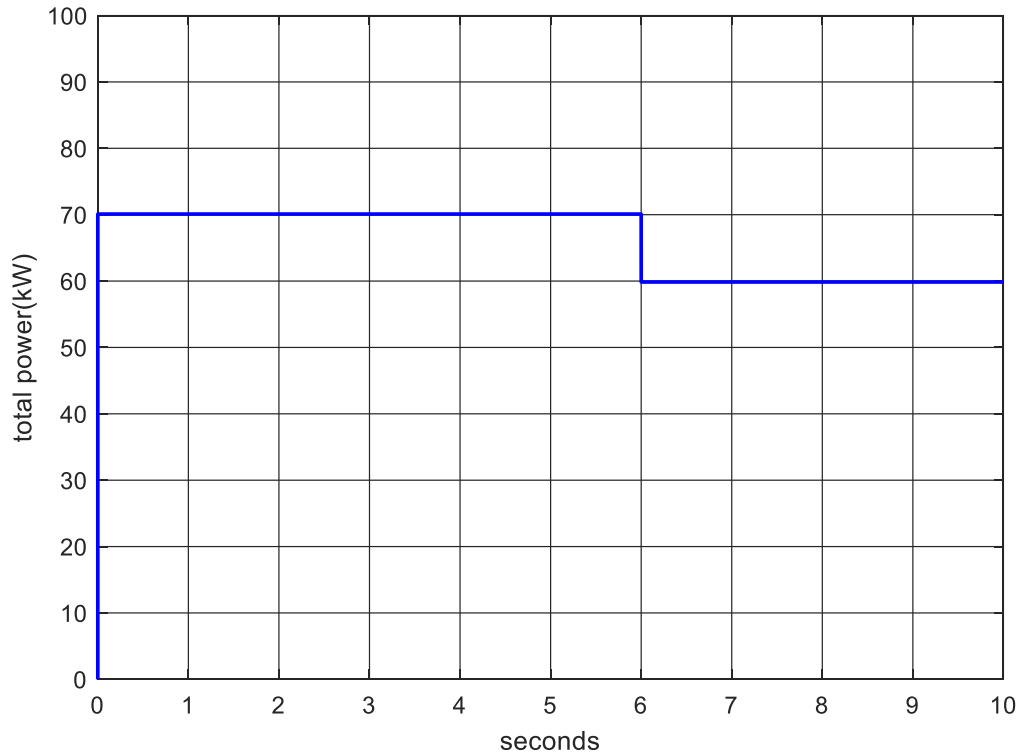


Figure 7.10: Total load supplied by the main generation source (case # 1)

7.4.3.2 Case # 2: sequential faults at feeders # 5 and 2

In this case, the system is subjected to two different faults at different locations, different fault resistances and times. At 3.5 s, feeder # 5 is subjected to a fault with a resistance of 0.279 Ω and 192 m away from the common DC bus. Another fault with 0.547 Ω resistance is applied at the feeder # 2 at 8 m from the common DC bus at 8.25 s. Figure 7.11 to Figure 7.13 show the response of distance evaluation, signals sent to the IGBTs and the supplied loads, respectively. The total supplied power is demonstrated in Figure 7.14. The complete protection scheme has shown efficient performance for fault detecting, locating and rapid isolating of the faulty line without affecting the other feeders.

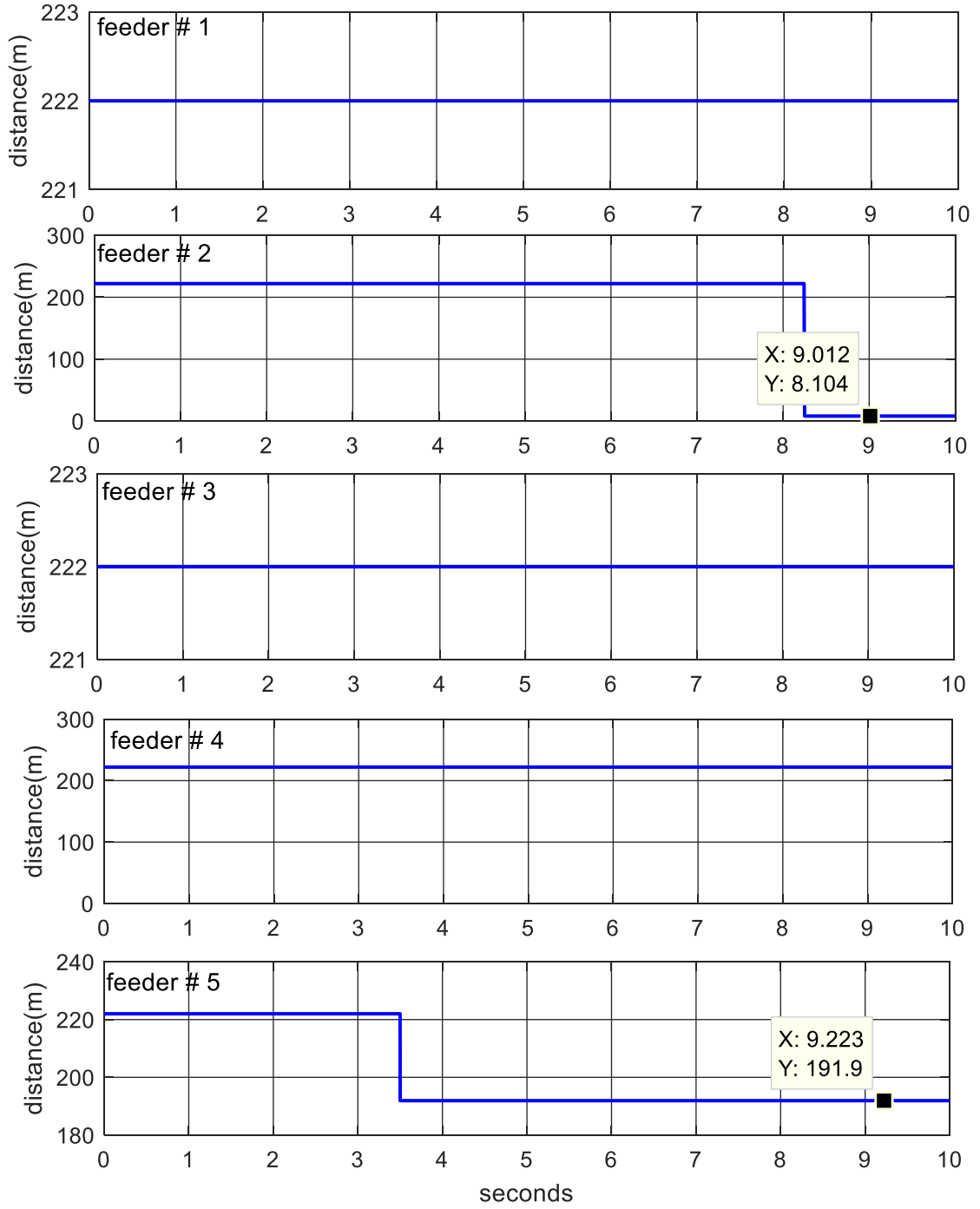


Figure 7.11: Fault distance evaluation under faults at feeders # 2 and 5 (case # 2)

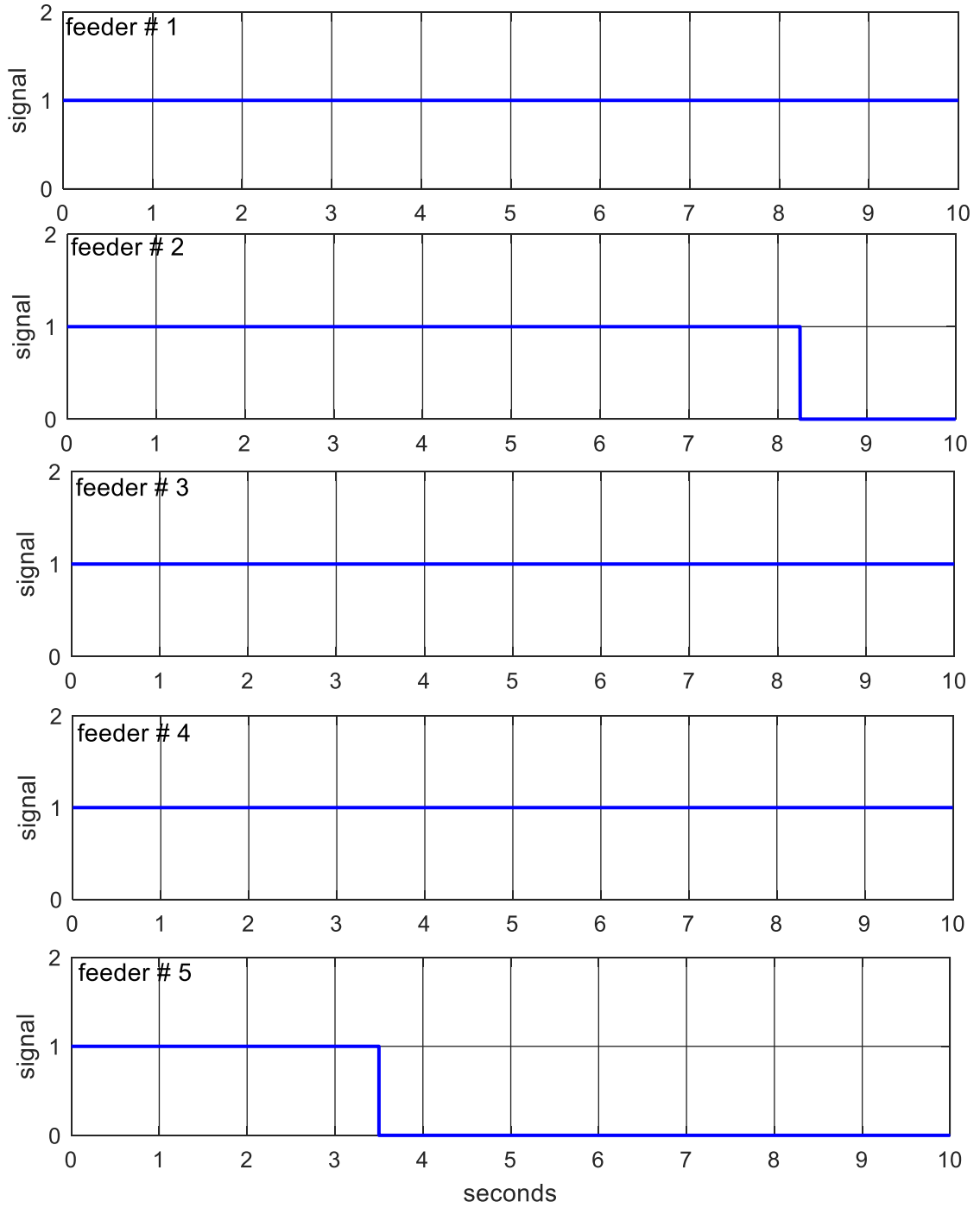


Figure 7.12: Response of the signals sent to the IGBTs (case # 2)

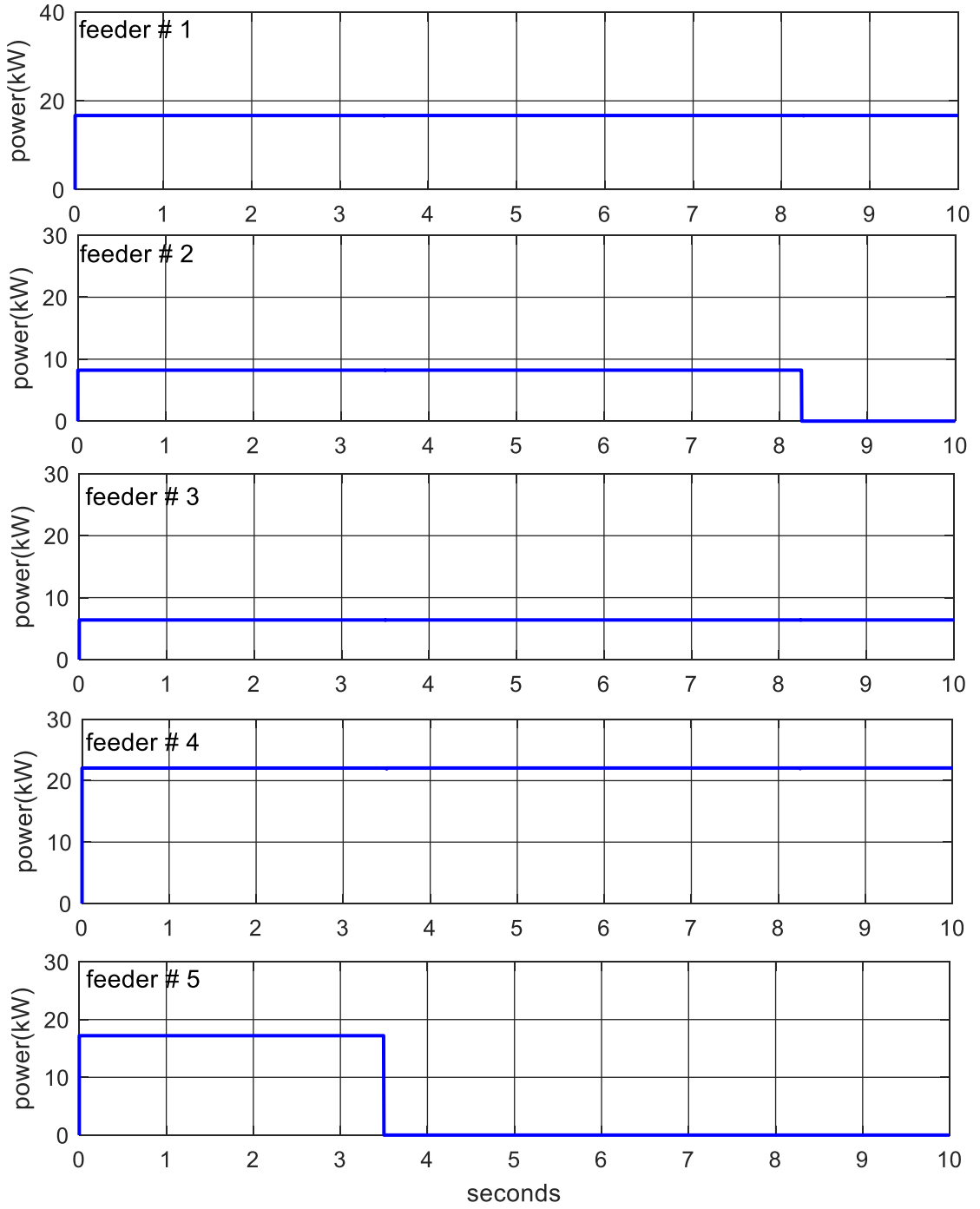


Figure 7.13: Load supplied by each feeder (case # 2)

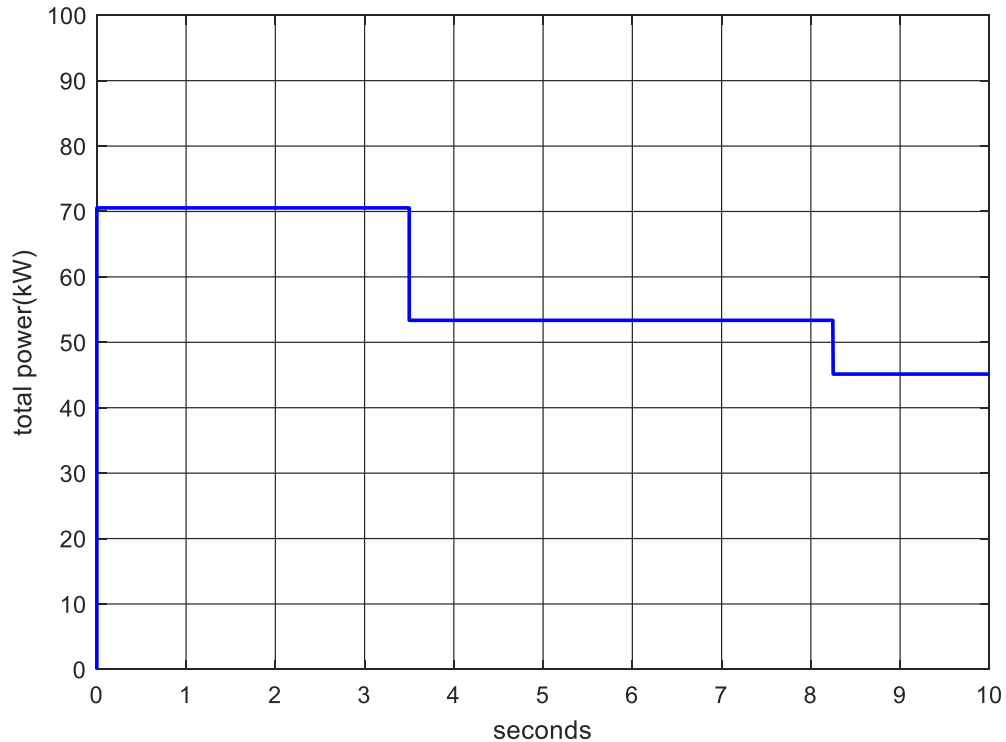


Figure 7.14: Total load supplied by the main generation source (case # 2)

7.5 Summary and Conclusions of the Chapter

The following points summarize the main outcomes and findings concluded from this chapter:

- The DC microgrid presented in chapter 6 is adopted in this chapter for the purpose of proposing an efficient protection scheme.
- An effective methodology for the DC microgrid protection is proposed.
- The protection scheme can be employed effectively to detect, locate and clear the faults occurring at any point in the DC microgrid under variable loading conditions.

- A mathematical model is proposed to identify the faulty feeder and estimate the fault location.
- IGBTs are employed to act as DC breakers controlled by a control block of “0” or “1” output signals based on the system operating conditions.
- The protection scheme performance is tested by applying faults at different points of the feeders, different loading conditions, different fault resistances and different fault times.
- The results have verified the effectiveness of the proposed protection scheme for rapid detection, faulty feeder identification, fault distance evaluation and faulty feeder isolation without affecting the loads connected to other feeders.

CHAPTER 8

CONCLUSIONS AND FUTURE WORK

8.1 Conclusions

In light of this dissertation, the work presented has explored various aspects concerned with DC systems including design, modeling, cost analysis, energy assessment and DC microgrid protection. The main outcomes of this dissertation are presented in the following subsections.

8.1.1 Modeling and Control of One of the Essential DC Sources: PV System

Models for predicting the characteristics of PV modules under variable weather conditions were proposed in this study. The main features of the proposed models are:

- Ability to generate the I-V curves of any PV modules by just knowledge of weather conditions and module technical specifications at STC.
- The estimation of PV circuit model parameters is not required.
- No need for a special software for models computations.
- Efficient evaluation capability by obtaining similar results to SIMULINK simulations and experimental data.
- Best performance as compared with other seven recent reported algorithms, in terms of both execution time and estimation accuracy with respect to actual data.

- Similar results when compared with other two commonly used algorithms for achieving MPPT for PV systems.

8.1.2 Modeling of Major AC and DC Home Appliances

Having modeled the DC source, it is important to develop models for major AC and DC household appliances. Two approaches were proposed in this dissertation for modeling analysis. The proposed models are characterized by:

- Ability for studying and modeling each appliance individually, rather than modeling a complete residential area or an entire substation.
- Efficient modeling capability of the appliances under study when compared with the experimental data.
- Ability to represent the electrical characteristics of the appliances under study in on-line simulations using MATLAB/SIMULINK.
- Modeling the new DC appliances available currently in the market. These new appliances have not assessed and modeled before.
- Opening opportunities for further analysis of the proposed models including simulating AC and DC houses, performing more energy assessments and carrying out load flow analysis and short circuit studies.

8.1.3 Energy and Cost Assessments for a Standalone House Configurations

One of the issues needed to be explored, as recommended by previous research, is to design a complete system comprising DC components, and to compare its performance with a corresponding conventional AC and hybrid AC/DC systems. In this dissertation, a complete DC system has been experimentally implemented. A small standalone house

was designed comprising the major household appliances. The cost analysis adopted in this part was conducted based on the costs of all components in the house, including generating sources, converters and appliances. The outcomes of the energy assessments and cost comparisons are as follows:

- The complete DC system is the most energy saving system due to the integration of efficient and energy-saving new DC appliances.
- Around 35 % energy saving is achieved when compared with the conventional AC system.
- The DC appliances are too expensive which results in high capital cost of the DC system.
- In terms of total life cycle cost over 20 years, the DC system is considered as the most suitable configuration with an assumption of one day of autonomy and two-year diesel generator lifespan.
- Energy saving and cost reduction of the DC system could be more at a reduction in DC appliances prices.
- Increasing days of autonomy can sharply increase the cost of the DC system due to the requirement of more batteries.
- Increasing diesel generator lifespan leads to cheaper life cycle cost in the case of AC-AC system.
- It is not recommended to implement the AC-DC network due to its high life cycle cost even with DC appliances prices reduction and more diesel generator lifespan.

8.1.4 Proposing a Microgrid with Different Configurations for Analysis and Study

The concept of the small standalone house was then extended to represent an entire microgrid area. The microgrid was represented by a small town comprising 100 houses. In this part, the analysis carried out was in terms of utility supply perspective. The main findings of this chapter are summarized as:

- 380 V_{DC} distribution voltage is selected in order to mitigate the losses that result from transmitting the power at lower voltages.
- The conventional AC system has the lowest capital investment due to the low capital cost of the diesel generator.
- The systems with PV arrays and batteries (DC-AC and DC-DC systems) are characterized by high capital cost due to the expensive PV modules and batteries.
- For a life cycle of 20 years, the AC-AC system is still the most economical solution in Saudi Arabia as of 2018 due to the low prices of diesel in the Kingdom.
- At the current situation of fuel and PV and batteries prices, it is not economical for the utility companies to implement completely DC systems.
- For all other GCC countries, the DC-AC and DC-DC systems are more economical than diesel generator systems.

8.1.5 Designing a Simple and Efficient Protection Scheme for DC Microgrid

After the DC microgrid has been designed, it was modeled using SIMULINK. A new simple and efficient protection scheme was proposed using a mathematical model. The main features of the proposed scheme are:

- Ability to detect, locate and clear the faults occurring at any point in the DC microgrid under variable loading conditions and fault resistance values.
- Ability for successful identification of the faulty feeder and estimation of the fault distance.
- Successful implementation of the IGBTs employed as DC breakers controlled by a control block of “0” or “1” output signals based on the system operating conditions.
- Efficient response of the proposed protection scheme for rapid detection and instant faulty feeder isolation without affecting the loads connected to other feeders.

8.2 Future Work

During the course of this study, it has been observed that it is worth to direct the related future work to the following points:

- In this study, diesel generator, PV system and battery bank are employed to represent the DG sources. Other DG sources can be also presented in the future including fuel cells as a DC source, as well as wind energy systems.

- More DC appliances are emerging now in the market including DC iron, DC kettle, DC washing machine and DC vacuum cleaner. All these appliances are manufactured to work based on 12 V_{DC}. These appliances can be integrated with the appliances presented in this dissertation to represent larger system with more appliances.
- The proposed modeling approaches can be applied also to model the DC appliances not considered in this study, as well as all other remaining AC household appliances such as kitchen appliances, washing machine and dryer.
- The proposed appliances models can be connected together to represent actual DC house considered as a typical test system for carrying out various studies. The models can be controlled upon the researcher preferences including selecting the number of each appliance in the house, in addition to controlling and changing the operation intervals and the load profiles.
- The study presented here was for residential application. Another field of possible application of DC system is the industrial sector. VSDs are widely used in the industrial facilities. It is of interest to carry out similar cost analysis and energy assessments of the feasibility of removing the rectification stage and coupling the DC bus directly to the input of the inverter.
- It is of interest to study and investigate the performance of DC system at medium voltage networks rather than low voltage DC network adopted in this study.

REFERENCES

- [1] M. H. Rashid, *Power electronics handbook*: Butterworth-Heinemann, 2017.
- [2] *First International Conference on DC microgrids USA*, 2015.
- [3] *Second International Conference on DC microgrids Germany*, 2017.
- [4] B. Zahedi and L. E. Norum, "Efficiency analysis of shipboard dc power systems," in *Industrial Electronics Society, IECON 2013-39th Annual Conference of the IEEE*, 2013, pp. 689-694.
- [5] B. Zahedi and L. E. Norum, "Modelling and simulation of hybrid electric ships with DC distribution systems," in *Power Electronics and Applications (EPE), 2013 15th European Conference on*, 2013, pp. 1-10.
- [6] W. Zhu, J. Shi, and S. Abdelwahed, "End-to-end system level modeling and simulation for medium-voltage DC electric ship power systems," *International Journal of Naval Architecture and Ocean Engineering*, vol. 10, pp. 37-47, 2018.
- [7] X. Feng, K. L. Butler-Purry, and T. Zourntos, "Real-time electric load management for DC zonal all-electric ship power systems," *Electric Power Systems Research*, vol. 154, pp. 503-514, 2018.
- [8] A. Shekhar, L. Ramírez-Elizondo, and P. Bauer, "DC microgrid islands on ships," in *DC Microgrids (ICDCM), 2017 IEEE Second International Conference on*, 2017, pp. 111-118.
- [9] B. Zahedi, L. E. Norum, and K. B. Ludvigsen, "Optimized efficiency of all-electric ships by dc hybrid power systems," *Journal of power sources*, vol. 255, pp. 341-354, 2014.
- [10] R. E. Brown, R. Brown, E. Masanet, B. Nordman, B. Tschudi, A. Shehabi, *et al.*, "Report to congress on server and data center energy efficiency: Public law 109-431," Ernest Orlando Lawrence Berkeley National Laboratory, Berkeley, CA (US)2007.
- [11] M. Salato, A. Zolj, D. J. Becker, and B. Sonnenberg, "Power system architectures for 380V DC distribution in telecom datacenters," in *Telecommunications Energy Conference (INTELEC), 2012 IEEE 34th International*, 2012, pp. 1-7.

- [12] D.-H. Kim, T. Yu, H. Kim, H. Mok, and K.-S. Park, "300V DC feed system for Internet data center," in *Power Electronics and ECCE Asia (ICPE & ECCE), 2011 IEEE 8th International Conference on*, 2011, pp. 2352-2358.
- [13] DC Power Distribution Cuts Data Center Energy Use. Available: <http://www.energy.ca.gov/2008publications/CEC-500-2008-042/CEC-500-2008-042-FS.PDF>
- [14] S. Rajagopalan, B. Fortenbery, and D. Symanski, "Power quality disturbances within DC data centers," in *Telecommunications Energy Conference (INTELEC), 32nd International*, 2010, pp. 1-7.
- [15] D. Fregosi, S. Ravula, D. Brhlik, J. Saussele, S. Frank, E. Bonnema, *et al.*, "A comparative study of DC and AC microgrids in commercial buildings across different climates and operating profiles," in *DC Microgrids (ICDCM), 2015 IEEE First International Conference on*, 2015, pp. 159-164.
- [16] D. L. Gerber, V. Vossos, W. Feng, C. Marnay, B. Nordman, and R. Brown, "A simulation-based efficiency comparison of AC and DC power distribution networks in commercial buildings," *Applied Energy*, vol. 210, pp. 1167-1187, 2018.
- [17] R. Panguloori, P. Mishra, and U. Boeke, "Economic viability improvement of solar powered Indian rural banks through DC grids," in *India Conference (INDICON), 2011 Annual IEEE*, 2011, pp. 1-4.
- [18] E. Iannone, *Telecommunication networks*: CRC Press, 2017.
- [19] T. Tanaka, N. Hanaoka, A. Takahashi, K. Asakimori, T. Iwato, A. Sakurai, *et al.*, "Concept of new power supply system topology using 380 V and 48 V DC bus for future datacenters and telecommunication buildings," in *Telecommunications Energy Conference (INTELEC), 2015 IEEE International*, 2015, pp. 1-6.
- [20] W. Rahman, "A feasibility study of low voltage DC distribution system for LED lighting in building," in *Innovations in Power and Advanced Computing Technologies (i-PACT)*, India, 2017.
- [21] J. Qureshi, T. Lie, R. Hasan, and T. Mujtaba, "Impact of efficient DC loads: LED lighting as equivalent to large power generation plant," in *Power Electronics Conference (SPEC), IEEE Annual Southern*, 2016, pp. 1-5.

- [22] A. Jhunjhunwala, K. Vasudevan, P. Kaur, B. Ramamurthi, S. Bitra, and K. Uppal, "Energy efficiency in lighting: AC vs DC LED lights," in *Sustainable Green Buildings and Communities (SGBC), International Conference on*, 2016, pp. 1-4.
- [23] M. Das and V. Agarwal, "A novel control strategy for stand-alone solar PV systems with enhanced battery life," in *Applied Power Electronics Conference and Exposition (APEC), 2014 Twenty-Ninth Annual IEEE*, 2014, pp. 2880-2887.
- [24] S. Agarwal and M. Jamil, "A comparison of photovoltaic maximum power point techniques," in *India Conference (INDICON), 2015 Annual IEEE*, 2015, pp. 1-6.
- [25] J. Ma, K. L. Man, T. Ting, H. Lee, T. Jeong, J.-K. Sean, *et al.*, "Insight of Direct Search Methods and Module-Integrated Algorithms for Maximum Power Point Tracking (MPPT) of Stand-Alone Photovoltaic Systems," in *IFIP International Conference on Network and Parallel Computing*, 2012, pp. 463-471.
- [26] S. Lalouni and D. Rekioua, "Optimal control of a grid connected photovoltaic system with constant switching frequency," *Energy Procedia*, vol. 36, pp. 189-199, 2013.
- [27] S. Ma, M. Chen, J. Wu, W. Huo, and L. Huang, "Augmented Nonlinear Controller for Maximum Power-Point Tracking with Artificial Neural Network in Grid-Connected Photovoltaic Systems," *Energies*, vol. 9, p. 1005, 2016.
- [28] M. Mahfouz, "On-Line Maximum Power Point Tracking for Photovoltaic System Grid Connected Through DC-DC Boost Converter and Three Phase Inverter," *Fundamentals of Renewable Energy and Applications*, vol. 5, pp. 1-5, 2015.
- [29] M. Elsharty and H. Ashour, "Realization of DC-bus sensor-less MPPT technique for a single-stage PV grid-connected inverter," in *Proceedings of the 23rd International Conference and Exhibition on Electricity Distribution, Lyon, France*, 2015, pp. 15-18.
- [30] M. Wattenberg and M. Pfof, "Optimal Power Point tracking for PV-systems with retrofitted Energy Storage Systems," in *Signals, Circuits and Systems (ISSCS), 2017 International Symposium on*, 2017, pp. 1-4.
- [31] E. Moshksar and T. Ghanbari, "A model-based algorithm for maximum power point tracking of PV systems using exact analytical solution of single-diode equivalent model," *Solar Energy*, vol. 162, pp. 117-131, 2018.
- [32] S. Handoko and T. Sukmadi, "Maximum power point tracking simulation for a photovoltaic system," in *Information Technology, Computer, and Electrical*

Engineering (ICITACEE), 2015 2nd International Conference on, 2015, pp. 266-270.

- [33] F. Khosrojerdi, S. Taheri, and A.-M. Cretu, "An adaptive neuro-fuzzy inference system-based MPPT controller for photovoltaic arrays," in *Electrical Power and Energy Conference (EPEC), 2016 IEEE*, 2016, pp. 1-6.
- [34] F. El Aamri, H. Maker, A. Mouhsen, and M. Harmouchi, "A new MPPT using Gradient Method for grid-connected PV inverter," in *Renewable and Sustainable Energy Conference (IRSEC), 2014 International*, 2014, pp. 197-202.
- [35] N. Femia, G. Petrone, G. Spagnuolo, and M. Vitelli, "A technique for improving P&O MPPT performances of double-stage grid-connected photovoltaic systems," *IEEE transactions on industrial electronics*, vol. 56, pp. 4473-4482, 2009.
- [36] M. A. Elgendy, B. Zahawi, and D. J. Atkinson, "Assessment of perturb and observe MPPT algorithm implementation techniques for PV pumping applications," *IEEE transactions on sustainable energy*, vol. 3, pp. 21-33, 2012.
- [37] M. Abido, M. S. Khalid, and M. Y. Worku, "An efficient ANFIS-based PI controller for maximum power point tracking of PV systems," *Arabian Journal for Science and Engineering*, vol. 40, pp. 2641-2651, 2015.
- [38] R. Sridhar, S. Jeevananthan, and B. S. Pranahita, "Investigations on Multidimensional Maximum Power Point Tracking in Partially Shaded Photovoltaic Arrays with PSO and DE Algorithms," in *Artificial Intelligence and Evolutionary Computations in Engineering Systems*, ed: Springer, 2016, pp. 1113-1125.
- [39] N. Marks, T. Summers, and R. Betz, "Current sensor-less control of a cascaded h-bridge photovoltaic system," in *Renewable Energy Research and Application (ICRERA), 2014 International Conference on*, 2014, pp. 212-217.
- [40] S. Khani, L. Mohammadian, S. H. Hosseini, and K. R. Milani, "Application of embedded Z-Source inverters in Grid connected photovoltaic systems," in *Electrical Power Distribution Networks (EPDC), 2013 18th Conference on*, 2013, pp. 1-5.
- [41] R. Kadri, J.-P. Gaubert, and G. Champenois, "An improved maximum power point tracking for photovoltaic grid-connected inverter based on voltage-oriented control," *IEEE transactions on industrial electronics*, vol. 58, pp. 66-75, 2011.

- [42] O. Abdel-Rahim and H. Funato, "Model predictive control based maximum power point tracking technique applied to ultra step-up boost converter for PV applications," in *Innovative Smart Grid Technologies-Asia (ISGT Asia), 2014 IEEE*, 2014, pp. 138-142.
- [43] D. Yu, Y. Li, Y. Zhou, X. Shi, H. Liu, and M. Huo, "Fuzzy control of photovoltaic MPPT based on current perturbation," in *Proceedings of the 2017 IEEE 2nd Advanced Information Technology, Electronic and Automation Control Conference (IAEAC), Chongqing, China, 2017*, pp. 25-26.
- [44] S. Surendran, S. Ajayan, and S. Sruthi, "Advanced topology to minimize leakage current grid-tied PV systems," in *Circuit, Power and Computing Technologies (ICCPCT), 2017 International Conference on*, 2017, pp. 1-5.
- [45] M. Al-Dhaifallah, A. M. Nassef, H. Rezk, and K. S. Nisar, "Optimal parameter design of fractional order control based INC-MPPT for PV system," *Solar Energy*, vol. 159, pp. 650-664, 2018.
- [46] Y. Wu, J. Li, and C. Li, "Study of the improved INC MPPT algorithm for PV systems," in *Control Science and Systems Engineering (ICCSSE), 2017 3rd IEEE International Conference on*, 2017, pp. 412-415.
- [47] J. Ahmed and Z. Salam, "An Enhanced Adaptive P&O MPPT for Fast and Efficient Tracking Under Varying Environmental Conditions," *IEEE Transactions on Sustainable Energy*, 2018.
- [48] A. I. Ali, M. A. Sayed, and E. E. Mohamed, "Modified efficient perturb and observe maximum power point tracking technique for grid-tied PV system," *International Journal of Electrical Power & Energy Systems*, vol. 99, pp. 192-202, 2018.
- [49] U. Yilmaz, A. Kircay, and S. Borekci, "PV system fuzzy logic MPPT method and PI control as a charge controller," *Renewable and Sustainable Energy Reviews*, vol. 81, pp. 994-1001, 2018.
- [50] L.-L. Li, G.-Q. Lin, M.-L. Tseng, K. Tan, and M. K. Lim, "A maximum power point tracking method for PV system with improved gravitational search algorithm," *Applied Soft Computing*, vol. 65, pp. 333-348, 2018.
- [51] K. S. Tey, S. Mekhilef, M. Seyedmahmoudian, B. Horan, A. M. T. Oo, and A. Stojcevski, "Improved Differential Evolution-based MPPT Algorithm using SEPIC for PV Systems under Partial Shading Conditions and Load Variation," *IEEE Transactions on Industrial Informatics*, 2018.

- [52] T. S. Babu, J. P. Ram, T. Dragičević, M. Miyatake, F. Blaabjerg, and N. Rajasekar, "Particle swarm optimization based solar PV array reconfiguration of the maximum power extraction under partial shading conditions," *IEEE Transactions on Sustainable Energy*, vol. 9, pp. 74-85, 2018.
- [53] S. Duman, N. Yorukeren, and I. H. Altas, "A novel MPPT algorithm based on optimized artificial neural network by using FPSOGSA for standalone photovoltaic energy systems," *Neural Computing and Applications*, vol. 29, pp. 257-278, 2018.
- [54] K. Sundareswaran and S. Palani, "Application of a combined particle swarm optimization and perturb and observe method for MPPT in PV systems under partial shading conditions," *Renewable Energy*, vol. 75, pp. 308-317, 2015.
- [55] Q. Fu and N. Tong, "A new fuzzy control method based on PSO for Maximum Power Point Tracking of photovoltaic system," in *Computer Science and Network Technology (ICCSNT), 2011 International Conference on*, 2011, pp. 1487-1491.
- [56] Y.-Y. Hong, A. A. Beltran, and A. C. Paglinawan, "A robust design of maximum power point tracking using Taguchi method for stand-alone PV system," *Applied Energy*, vol. 211, pp. 50-63, 2018.
- [57] R. Subha and S. Himavathi, "MPPT of PV systems under partial shaded conditions using flower pollination algorithm," in *Innovations in Electrical, Electronics, Instrumentation and Media Technology (ICEEIMT), 2017 International Conference on*, 2017, pp. 206-210.
- [58] A. Oshaba, E. Ali, and S. A. Elazim, "MPPT control design of PV system supplied SRM using BAT search algorithm," *Sustainable Energy, Grids and Networks*, vol. 2, pp. 51-60, 2015.
- [59] N. Fumo and M. R. Biswas, "Regression analysis for prediction of residential energy consumption," *Renewable and Sustainable Energy Reviews*, vol. 47, pp. 332-343, 2015.
- [60] M. E.-N. Jahromi and M. T. Ameli, "Measurement-based modelling of composite load using genetic algorithm," *Electric Power Systems Research*, vol. 158, pp. 82-91, 2018.
- [61] C.-L. Tsai, W. T. Chen, and C.-S. Chang, "Polynomial-Fourier series model for analyzing and predicting electricity consumption in buildings," *Energy and Buildings*, vol. 127, pp. 301-312, 2016.

- [62] Y. Ge, C. Zhou, and D. M. Hepburn, "Domestic electricity load modelling by multiple Gaussian functions," *Energy and Buildings*, vol. 126, pp. 455-462, 2016.
- [63] E. Polykarpou, M. Asprou, and E. Kyriakides, "Dynamic load modelling using real time estimated states," in *PowerTech, 2017 IEEE Manchester*, 2017, pp. 1-6.
- [64] P. Regulski, D. Vilchis-Rodriguez, S. Djurović, and V. Terzija, "Estimation of composite load model parameters using an improved particle swarm optimization method," *IEEE Transactions on Power Delivery*, vol. 30, pp. 553-560, 2015.
- [65] A. J. Collin, G. Tsagarakis, A. E. Kiprakis, and S. McLaughlin, "Development of low-voltage load models for the residential load sector," *IEEE Transactions on Power Systems*, vol. 29, pp. 2180-2188, 2014.
- [66] A. Rouhani and A. Abur, "Real-time dynamic parameter estimation for an exponential dynamic load model," *IEEE Transactions on Smart Grid*, vol. 7, pp. 1530-1536, 2016.
- [67] A. S. Carneiro, L. F. Araujo, J. L. R. Pereira, P. A. Garcia, I. D. Melo, and M. B. Amaral, "Static load modeling based on field measurements," in *PowerTech, 2017 IEEE Manchester*, 2017, pp. 1-5.
- [68] N. Ashraf, A. Polycarpou, Y. Ioannides, M. Lestas, and M. A. Michael, "Linear static parametric models for online parameter identification of power load models," in *PowerTech, 2017 IEEE Manchester*, 2017, pp. 1-5.
- [69] K. S. Metallinos, T. A. Papadopoulos, and C. A. Charalambous, "Derivation and evaluation of generic measurement-based dynamic load models," *Electric Power Systems Research*, vol. 140, pp. 193-200, 2016.
- [70] V. Vignesh, S. Chakrabarti, and S. C. Srivastava, "Load modeling under unbalanced disturbances," *IEEE Transactions on Power Systems*, vol. 31, pp. 1661-1662, 2016.
- [71] A. Bokhari, A. Alkan, R. Dogan, M. Diaz-Aguiló, F. De Leon, D. Czarkowski, *et al.*, "Experimental determination of the ZIP coefficients for modern residential, commercial, and industrial loads," *IEEE Transactions on Power Delivery*, vol. 29, pp. 1372-1381, 2014.
- [72] Y. Wei, X. Zhang, Y. Shi, L. Xia, S. Pan, J. Wu, *et al.*, "A review of data-driven approaches for prediction and classification of building energy consumption," *Renewable and Sustainable Energy Reviews*, vol. 82, pp. 1027-1047, 2018.

- [73] N. Fumo, "A review on the basics of building energy estimation," *Renewable and Sustainable Energy Reviews*, vol. 31, pp. 53-60, 2014.
- [74] V. Harish and A. Kumar, "A review on modeling and simulation of building energy systems," *Renewable and Sustainable Energy Reviews*, vol. 56, pp. 1272-1292, 2016.
- [75] K. Amasyali and N. M. El-Gohary, "A review of data-driven building energy consumption prediction studies," *Renewable and Sustainable Energy Reviews*, vol. 81, pp. 1192-1205, 2018.
- [76] L. Suganthi and A. A. Samuel, "Energy models for demand forecasting—A review," *Renewable and sustainable energy reviews*, vol. 16, pp. 1223-1240, 2012.
- [77] C. Deb, F. Zhang, J. Yang, S. E. Lee, and K. W. Shah, "A review on time series forecasting techniques for building energy consumption," *Renewable and Sustainable Energy Reviews*, vol. 74, pp. 902-924, 2017.
- [78] M. Alluhaidan and I. Almutairy, "Modeling and Protection for Low-Voltage DC Microgrids Riding Through Short Circuiting," *Procedia Computer Science*, vol. 114, pp. 457-464, 2017.
- [79] Q. Yang, J. Li, S. Le Blond, and C. Wang, "Artificial Neural Network Based Fault Detection and Fault Location in the DC Microgrid," *Energy Procedia*, vol. 103, pp. 129-134, 2016.
- [80] G. Patil, M. Satarkar, and G. Abande, "New Scheme for Protection of DC Micro grid," *International Journal of Innovative Research in Science, Engineering and Technology*, vol. 3, 2014.
- [81] J. Aswani and P. Kanakasabapathy, "Protection of a low-voltage DC ring microgrid system," in *Energy Efficient Technologies for Sustainability (ICEETS), 2016 International Conference on*, 2016, pp. 17-22.
- [82] A. Abdali, K. Mazlumi, and R. Noroozian, "Fast fault detection and isolation in low-voltage DC microgrids using fuzzy inference system," in *Fuzzy and Intelligent Systems (CFIS), 2017 5th Iranian Joint Congress on*, 2017, pp. 172-177.
- [83] D. Wang, A. Emhemed, and G. Burt, "A novel protection scheme for an LVDC distribution network with reduced fault levels," in *DC Microgrids (ICDCM), 2017 IEEE Second International Conference on*, 2017, pp. 69-75.

- [84] J. P. Ram, T. S. Babu, and N. Rajasekar, "A comprehensive review on solar PV maximum power point tracking techniques," *Renewable and Sustainable Energy Reviews*, vol. 67, pp. 826-847, 2017.
- [85] A. T. Elsayed, A. A. Mohamed, and O. A. Mohammed, "DC microgrids and distribution systems: An overview," *Electric Power Systems Research*, vol. 119, pp. 407-417, 2015.
- [86] Ö. GÜL, "Smart AC/DC low voltage distribution system for building with distributed generation and electric vehicles," *International Journal of Electrical Engineering & Technology*, vol. 5, pp. 1-16, 2014.
- [87] S. F. Porter, D. Denkenberger, C. Mercier, E. P. May-Ostendorp, and P. Turnbull, "Reviving the War of Currents: Opportunities to Save Energy with DC Distribution in Commercial Buildings," ed: ECOVA, 2014.
- [88] M. C. Kinn, "An exploration of the technical and economic feasibility of a low powered DC voltage mains power supply in the domestic arena," in *Green Building Power Forum 01-03 June 2009 Anaheim California Proceedings*, 2009.
- [89] B. Glasgo, I. L. Azevedo, and C. Hendrickson, "How much electricity can we save by using direct current circuits in homes? Understanding the potential for electricity savings and assessing feasibility of a transition towards DC powered buildings," *Applied Energy*, vol. 180, pp. 66-75, 2016.
- [90] K. Garbesi, "Optimizing energy savings from direct-DC in US residential buildings," 2012.
- [91] W. Li, X. Mou, Y. Zhou, and C. Marnay, "On voltage standards for DC home microgrids energized by distributed sources," in *Power Electronics and Motion Control Conference (IPEMC), 2012 7th International*, 2012, pp. 2282-2286.
- [92] J. Han, Y.-S. Oh, G.-H. Gwon, D.-U. Kim, C.-H. Noh, T.-H. Jung, *et al.*, "Modeling and analysis of a low-voltage DC distribution system," *Resources*, vol. 4, pp. 713-735, 2015.
- [93] M. A. V. Evans, "Why Low Voltage Direct Current Grids?," Citeseer, 2013.
- [94] F. Dastgeer, "Direct current distribution systems for residential areas powered by distributed generation," Victoria University, 2011.
- [95] S. M. Frank, *Optimal design of mixed AC-DC distribution systems for commercial buildings*: Colorado School of Mines, 2013.

- [96] M. C. Kinn, *Benefits of direct current electricity supply for domestic application*: University of Manchester, 2011.
- [97] O. Alarfaj, "Modeling and Control of Low-Voltage DC Microgrid With Photovoltaic Energy Resources," University of Waterloo, 2014.
- [98] K. P. Vijayaragavan, "Feasibility of DC microgrids for rural electrification," ed, 2017.
- [99] M. Schmidt and H. Lipson, "Distilling free-form natural laws from experimental data," *science*, vol. 324, pp. 81-85, 2009.
- [100] M. Schmidt and H. Lipson, "Eureqa (version 0.98 beta)[software]," *Nutonian, Somerville, Mass, USA*, 2013.
- [101] I. Bormann, "Digitizelt (version 1.5. 7)[Computer software]," *Braunschweig, Germany: Bormisoft*, 2003.
- [102] H. S. Sahu and S. K. Nayak, "Estimation of maximum power point of a double diode model photovoltaic module," *IET Power Electronics*, vol. 10, pp. 667-675, 2017.
- [103] H. S. Sahu and S. K. Nayak, "Numerical approach to estimate the maximum power point of a photovoltaic array," *IET Generation, Transmission & Distribution*, vol. 10, pp. 2670-2680, 2016.
- [104] A. Kulaksız, "ANFIS-based parameter estimation of one-diode equivalent circuit model of PV modules," in *Computational Intelligence and Informatics (CINTI), 2011 IEEE 12th International Symposium on*, 2011, pp. 415-420.
- [105] G. Sybille, "SimPowerSystem user's guide, version 4," ed: Nattick, MA: Hydro-Quebec/The MathWorks, 2004.
- [106] G.-E. Subtirelu, M. Dobriceanu, and M. Linca, "Power quality analyzer," in *Advanced Topics in Electrical Engineering (ATEE), 2017 10th International Symposium on*, 2017, pp. 909-914.
- [107] J. Geppert, "Modelling of domestic refrigerators' energy consumption under real life conditions in Europe," 2011.
- [108] J. Hedengren, "APMonitor Optimization Suite. 28," 2013.

- [109] G. M. Masters, *Renewable and efficient electric power systems*: John Wiley & Sons, 2013.
- [110] M. A. Ramli, H. Boucekara, and A. S. Alghamdi, "Optimal Sizing of PV/wind/diesel hybrid microgrid system using multi-objective self-adaptive differential evolution algorithm," *Renewable Energy*, 2018.
- [111] M. Azab, "A new maximum power point tracking for photovoltaic systems," *WASET. ORG*, vol. 34, pp. 571-574, 2008.
- [112] C. W. Tan, T. C. Green, and C. A. Hernandez-Aramburo, "Analysis of perturb and observe maximum power point tracking algorithm for photovoltaic applications," in *Power and Energy Conference, 2008. PECon 2008. IEEE 2nd International*, 2008, pp. 237-242.
- [113] A. Chel, G. Tiwari, and A. Chandra, "Simplified method of sizing and life cycle cost assessment of building integrated photovoltaic system," *Energy and Buildings*, vol. 41, pp. 1172-1180, 2009.
- [114] F. Spertino, P. Di Leo, V. Cocina, and G. M. Tina, "Storage sizing procedure and experimental verification of stand-alone photovoltaic systems," in *Energy Conference and Exhibition (ENERGYCON), 2012 IEEE International*, 2012, pp. 464-468.
- [115] R. Dufo-López, J. M. Lujano-Rojas, and J. L. Bernal-Agustín, "Comparison of different lead–acid battery lifetime prediction models for use in simulation of stand-alone photovoltaic systems," *Applied Energy*, vol. 115, pp. 242-253, 2014.
- [116] T. Markvart, A. Fragaki, and J. Ross, "PV system sizing using observed time series of solar radiation," *Solar Energy*, vol. 80, pp. 46-50, 2006.
- [117] A. Q. Jakhriani, A.-K. Othman, A. R. H. Rigit, S. R. Samo, and S. A. Kamboh, "A novel analytical model for optimal sizing of standalone photovoltaic systems," *Energy*, vol. 46, pp. 675-682, 2012.
- [118] A. Yoza, A. Yona, T. Senjyu, and T. Funabashi, "Optimal capacity and expansion planning methodology of PV and battery in smart house," *Renewable Energy*, vol. 69, pp. 25-33, 2014.
- [119] C. B. Salah, K. Lamamra, and A. Fatnassi, "New optimally technical sizing procedure of domestic photovoltaic panel/battery system," *Journal of Renewable and Sustainable Energy*, vol. 7, p. 013134, 2015.

- [120] A. Mellit, S. A. Kalogirou, and M. Drif, "Application of neural networks and genetic algorithms for sizing of photovoltaic systems," *Renewable Energy*, vol. 35, pp. 2881-2893, 2010.
- [121] P. Nikhil and D. Subhakar, "Sizing and parametric analysis of a stand-alone photovoltaic power plant," *IEEE journal of photovoltaics*, vol. 3, pp. 776-784, 2013.
- [122] G. Ahmad, "Photovoltaic-powered rural zone family house in Egypt," *Renewable Energy*, vol. 26, pp. 379-390, 2002.
- [123] M. Buresch, "Photovoltaic energy systems: Design and installation," 1983.
- [124] N. D. Nordin and H. A. Rahman, "A novel optimization method for designing stand alone photovoltaic system," *Renewable Energy*, vol. 89, pp. 706-715, 2016.
- [125] S. S. Rashwan, A. M. Shaaban, and F. Al-Suliman, "A comparative study of a small-scale solar PV power plant in Saudi Arabia," *Renewable and Sustainable Energy Reviews*, vol. 80, pp. 313-318, 2017.
- [126] A. Chel, G. Tiwari, and A. Chandra, "Sizing and cost estimation methodology for stand-alone residential PV power system," *International journal of agile Systems and management*, vol. 4, pp. 21-40, 2009.
- [127] L. Al-Hadhrami and S. Rehman, "Study of a solar pvedieselebattery hybrid power system for a remotely located," *Energy*, vol. 35, pp. 4986-4995, 2010.
- [128] L. K. Gan, J. K. Shek, and M. A. Mueller, "Hybrid wind–photovoltaic–diesel–battery system sizing tool development using empirical approach, life-cycle cost and performance analysis: A case study in Scotland," *Energy Conversion and Management*, vol. 106, pp. 479-494, 2015.
- [129] W. M. Amutha and V. Rajini, "Techno-economic evaluation of various hybrid power systems for rural telecom," *Renewable and Sustainable Energy Reviews*, vol. 43, pp. 553-561, 2015.
- [130] K. Kusakana and H. Vermaak, "Hybrid Diesel Generator-battery systems for offgrid rural applications," in *Industrial Technology (ICIT), 2013 IEEE International Conference on*, 2013, pp. 839-844.
- [131] J. Kaiser, K. Gosses, L. Ott, Y. Han, B. Wunder, M. März, *et al.*, "Grid behavior under fault situations in±380 V DC distribution systems," in *DC Microgrids (ICDCM), 2017 IEEE Second International Conference on*, 2017, pp. 139-144.

- [132] C. Strobl, L. Ott, J. Kaiser, M. Streck, F. Nothnagel, F. Berger, *et al.*, "Resonant electric arcs in DC microgrids with low system impedance in the VLF-band," in *DC Microgrids (ICDCM), 2017 IEEE Second International Conference on*, 2017, pp. 1-7.
- [133] G. AlLee and W. Tschudi, "Edison redux: 380 Vdc brings reliability and efficiency to sustainable data centers," *IEEE Power and Energy Magazine*, vol. 10, pp. 50-59, 2012.
- [134] M. Mobarrez, D. Fregosi, G. Jalali, S. Bhattacharya, and M. Bahmani, "A novel control method for preventing the PV and load fluctuations in a DC microgrid from transferring to the AC power grid," in *DC Microgrids (ICDCM), 2017 IEEE Second International Conference on*, 2017, pp. 352-359.
- [135] IEC SG4, "LVDC distribution systems up to 1500V DC," 2009.
- [136] D. Symanski, "Residential and commercial use of DC power," presented at the Low Voltage Direct Current Workshop, 2011.
- [137] D. S. Supply. *Approximate Diesel Fuel Consumption Chart*. Available: http://www.dieselserviceandsupply.com/Diesel_Fuel_Consumption.aspx
- [138] A. A. Al-Harbi, "Residential Saudi load forecasting using analytical model and Artificial Neural Networks," King Fahd University of Petroleum and Minerals (Saudi Arabia), 2012.
- [139] M. A. H. Mondal and A. S. Islam, "Potential and viability of grid-connected solar PV system in Bangladesh," *Renewable energy*, vol. 36, pp. 1869-1874, 2011.
- [140] I. Nawaz and G. Tiwari, "Embodied energy analysis of photovoltaic (PV) system based on macro-and micro-level," *Energy Policy*, vol. 34, pp. 3144-3152, 2006.
- [141] S. Rehman, M. Ahmed, M. H. Mohamed, and F. A. Al-Sulaiman, "Feasibility study of the grid connected 10 MW installed capacity PV power plants in Saudi Arabia," *Renewable and Sustainable Energy Reviews*, vol. 80, pp. 319-329, 2017.
- [142] *Diesel prices around the world*. Available: https://www.globalpetrolprices.com/diesel_prices/
- [143] I. Almutairy and M. Alluhaidan, "Fault Diagnosis Based Approach to Protecting DC Microgrid Using Machine Learning Technique," *Procedia Computer Science*, vol. 114, pp. 449-456, 2017.

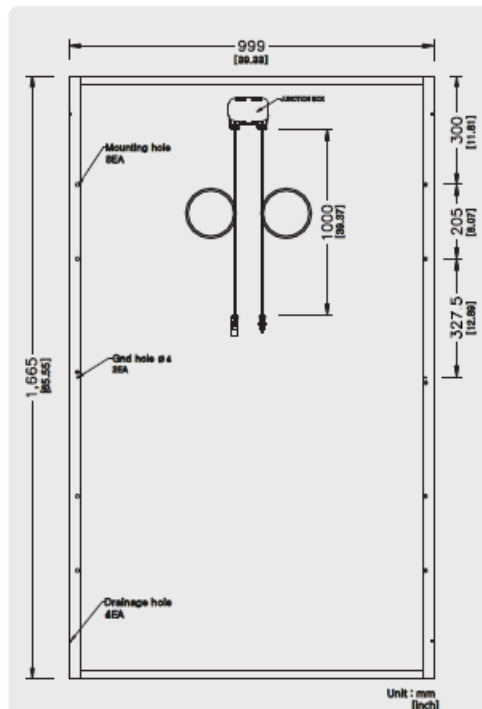
- [144] E. L. Wellner and A. R. Bendre, "IGCTs vs. IGBTs for circuit breakers in advanced ship electrical systems," in *Electric Ship Technologies Symposium, 2009. ESTS 2009. IEEE*, 2009, pp. 400-405.
- [145] J.-D. Park, J. Candelaria, L. Ma, and K. Dunn, "DC ring-bus microgrid fault protection and identification of fault location," *IEEE transactions on Power delivery*, vol. 28, pp. 2574-2584, 2013.
- [146] J.-D. Park and J. Candelaria, "Fault detection and isolation in low-voltage DC-bus microgrid system," *IEEE transactions on power delivery*, vol. 28, pp. 779-787, 2013.
- [147] S. Munasib and J. C. Balda, "Short-circuit protection for low-voltage DC microgrids based on solid-state circuit breakers," in *Power Electronics for Distributed Generation Systems (PEDG), 2016 IEEE 7th International Symposium on*, 2016, pp. 1-7.
- [148] G. Patil and M. Satarkar, "Autonomous protection of low voltage DC microgrid," in *Power, Automation and Communication (INPAC), 2014 International Conference on*, 2014, pp. 23-26.

APPENDIX

SM-255PC8 60 cell-series Polycrystalline PV Module

Electrical Characteristics

STC (Irradiance 1000W/m ² , module temperature 25°C, AM=1.5)	SM-240PC8	SM-245PC8	SM-250PC8	SM-255PC8
Rated power (P _{max})	240W	245W	250W	255W
Voltage at P _{max} (V _{mp})	30.0V	30.4V	30.8V	30.8V
Current at P _{max} (I _{mp})	8.02A	8.08A	8.14A	8.28A
Warranted minimum P _{max}	240W	245W	250W	255W
Short-circuit current (I _{sc})	8.58A	8.63A	8.67A	8.82A
Open-circuit voltage (V _{oc})	37.3V	37.4V	37.5V	37.9V
Module efficiency	14.42%	14.72%	15.03%	15.33%
Operating module temperature	-40°C to +85°C			
Maximum system voltage	600VDC (UL) / 1000VDC (IEC)			
Maximum series fuse rating	15A			
Maximum reverse current	20.25A			
Power tolerance	0 ~ +5 W			

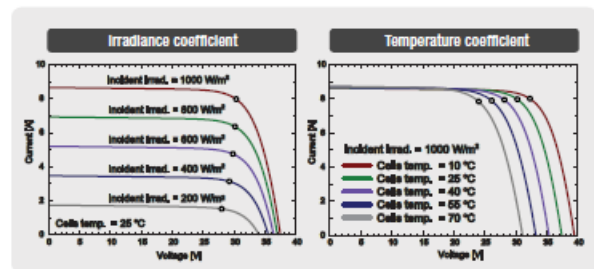


Temperature Characteristics

Temperature coefficient of I _{sc}	0.052%/°C
Temperature coefficient of V _{oc}	-0.312%/°C
Temperature coefficient of power	-0.429%/°C
NOCT (Air 20°C; Sun 0.8kW/m ² ; Wind 1m/s)	45±3°C

Packing Configuration

Container	40' H/C
Modules per pallet	20 pcs
Pallets per container	26 pallets
Modules per container	520 pcs



Remarks :

P_{max} measurement tolerance : ±3%
 S-Energy uses triple A class simulator.
 Specification subject to change without prior notice. S-Energy reserves the rights of final interpretation.

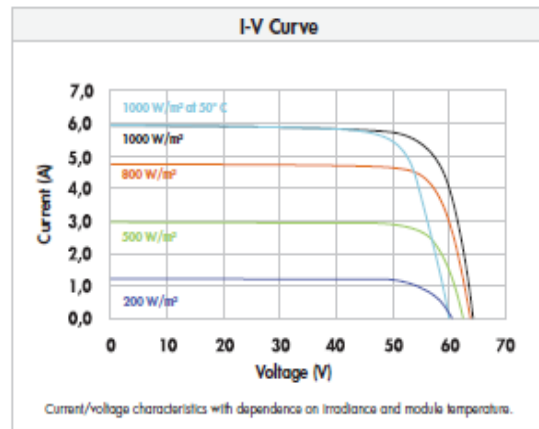
SUNPOWER

305 SOLAR PANEL

EXCEPTIONAL EFFICIENCY AND PERFORMANCE

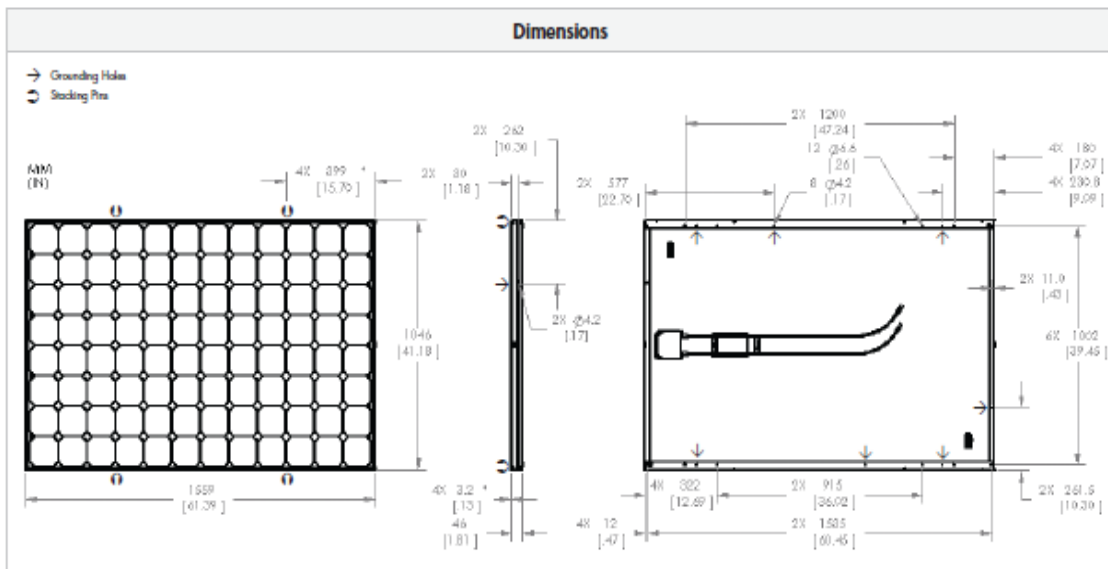
Electrical Data		
Measured at Standard Test Conditions (STC): Irradiance of 1000W/m ² , AM 1.5, and cell temperature 25° C		
Peak Power (+/-5%)	P _{max}	305 W
Rated Voltage	V _{mpp}	54.7 V
Rated Current	I _{mpp}	5.58 A
Open Circuit Voltage	V _{oc}	64.2 V
Short Circuit Current	I _{sc}	5.96 A
Maximum System Voltage	UL	600 V
Temperature Coefficients		
	Power	-0.38% / K
	Voltage (V _{oc})	-176.6mV / K
	Current (I _{sc})	3.5mA / K
NOCT		45° C +/-2° C
Series Fuse Rating		15 A

Mechanical Data	
Solar Cells	96 SunPower all-back contact monocrystalline
Front Glass	high transmission tempered glass
Junction Box	IP-65 rated with 3 bypass diodes Dimensions: 32 x 155 x 128 (mm)
Output Cables	1000mm length cables / MultiContact (MC4) connectors
Frame	Anodized aluminum alloy type 6063 (silver); stacking pins
Weight	41 lbs. (18.6 kg)

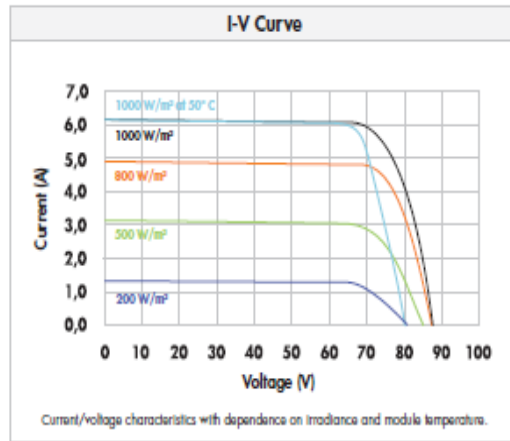


Tested Operating Conditions	
Temperature	-40° F to +185° F (-40° C to + 85° C)
Max load	50 psf 245 kg/m ² (2400 Pa) front and back – e.g. wind
Impact Resistance	Hail 1 in (25 mm) at 52mph (23 m/s)

Warranties and Certifications	
Warranties	25 year limited power warranty 10 year limited product warranty
Certifications	Tested to UL 1703. Class C Fire Rating



Electrical Data		
Measured at Standard Test Conditions (STC): Irradiance of 1000W/m ² , AM 1.5, and cell temperature 25° C		
Peak Power (+/-5%)	P _{max}	425 W
Efficiency	η	19.7 %
Rated Voltage	V _{mpp}	72.9 V
Rated Current	I _{mpp}	5.83 A
Open Circuit Voltage	V _{oc}	85.6 V
Short Circuit Current	I _{sc}	6.18 A
Maximum System Voltage	UL	600 V
Temperature Coefficients	Power (P)	-0.38% / K
	Voltage (V _{oc})	-235.5mV / K
	Current (I _{sc})	3.5mA / K
NOCT		45° C +/-2° C
Series Fuse Rating		15 A
Mechanical Data		
Solar Cells	128 SunPower all-back contact monocrystalline	
Front Glass	High transmission tempered glass with anti-reflective (AR) coating	
Junction Box	IP-65 rated with 3 bypass diodes Dimensions: 32 x 155 x 128 (mm)	
Output Cables	1000 mm length cables/ MultiContact (MC4) connectors	
Frame	Anodized aluminum alloy type 6063 (silver); stacking pins	
Weight	56.0 lbs. (25.4 kg)	

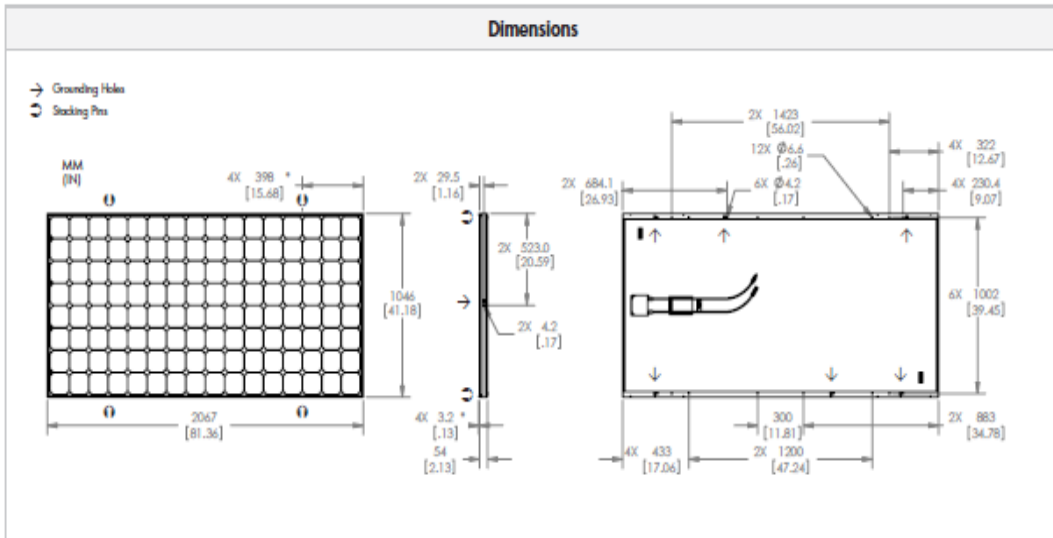


Tested Operating Conditions

Temperature	-40° F to +185° F (-40° C. to + 85° C)
Max load	50 psf (245 kg/m ²) (2400 Pa) front and back – e.g. wind
Impact Resistance	Hail 1 in (25 mm) at 52mph (23 m/s)

Warranties and Certifications

Warranties	25 year limited power warranty
	10 year limited product warranty
Certifications	Tested to UL 1703. Class C Fire Rating



VITAE

Name: Ahmad Abdulaziz Mubaireek Al-Subhi Al-Harbi

Date of Birth: 1982

Place of Birth: Badr (Madinah Munawrah Region)

Education: **Sep 2000 – May 2005: Bachelors in Electrical Engineering**
King Fahd University of Petroleum and Minerals

Sep 2008 – May 2012: Masters in Electrical Engineering
King Fahd University of Petroleum and Minerals

Sep 2013 – May 2018: PhD in Electrical Engineering
King Fahd University of Petroleum and Minerals

Experience: **Aug 2005 – March 2006:** Electrical Engineer at Royal Commission of Yanbu (Parsons Company).

March 2006 – Oct 2006: Instructor at Yanbu Technical College.

Oct 2006 – Aug 2007: Electrical Engineer at Saudi Electricity Company (SEC) in city of Badr.

Aug 2007 – Aug 2008: Instructor at Yanbu Industrial College, Royal Commission of Yanbu.

June 2012 – Aug 2013: Lecturer at Yanbu Industrial College, Royal Commission of Yanbu.

May 2018 – present: Assistant Professor at Yanbu Industrial College, Royal Commission of Yanbu.

Email subhi@rcyci.edu.sa, shaheed107@yahoo.com.

Address Saudi Arabia, Madinah region, Badr, 46357

Publications from this dissertation:

Conference papers:

- [1] **Ahmad Al-Subhi** and Ibrahim El-Amin, "Optimal Duty Cycle Modeling for Maximum Power Point Tracking of Photovoltaic System," *9th IEEE GCC Conference and Exhibition*, Bahrain, 8-11 May, 2017.
- [2] **Ahmad Al-Subhi** and Ibrahim El-Amin, "Experimental Performance Analysis of Existing Conventional AC Air Conditioner and Corresponding New Pure DC Air Conditioner," *IEEE Second International Conference on DC Microgrids (ICDCM)*, Germany, 2017, pp. 330-336.
- [3] **Ahmad Al-Subhi**, Ibrahim El-Amin and Sami Al-Alwani, "Mathematical-Based Accurate Prediction Model of Output AC Power for Grid-Connected Photovoltaic System." *Smart Grid (SASG)*, IEEE, Saudi Arabia, 10-12 December, 2017.
- [4] **Ahmad Al-Subhi**, Ibrahim El-Amin and Sami Al-Alwani, "Mathematical Models for Characterization of Photovoltaic Panel Performance under Diverse Environmental Conditions." *Smart Grid (SASG)*, IEEE, Saudi Arabia, 10-12 December, 2017.
- [5] **Ahmad Al-Subhi**, Mohammed Alsumiri and Sami Al-Alwani, "Novel MPPT Algorithm for Low Cost Wind Energy Conversion Systems." *In: Advanced Control Circuits Systems (ACCS) Systems & 2017 Intl Conference on New Paradigms in Electronics & Information Technology (PEIT)*, IEEE, Egypt, 2017, pp. 144-148.
- [6] **Ahmad Al-Subhi** and Ibrahim El-Amin, "Maximum Power Point Tracking of Photovoltaic Systems by Accurate Prediction of Maximum Power Voltage," *Smart Cities Symposium*, IET, Bahrain, 22-23 April, 2018.
- [7] **Ahmad Al-Subhi** and Ibrahim El-Amin, "Feasibility Study of a Standalone DC House: Energy Savings Opportunities and Capital Costs Assessment," *Smart Cities Symposium*, IET, Bahrain, 22-23 April, 2018.

Journal papers:

- [1] **Ahmad Al-Subhi** and Ibrahim El-Amin, “Development of Measurement-Based Models for Major AC and DC Home Appliances,” considered by: *Journal of Building Engineering*, Elsevier.
- [2] **Ahmad Al-Subhi** and Ibrahim El-Amin, “Efficient Mathematical Based Models for Maximum Power Point Tracking of Photovoltaic Systems,” *Canadian Journal of Electrical and Computer Engineering*, under review.
- [3] **Ahmad Al-Subhi** and Ibrahim El-Amin, “Efficient Predictive Models for Characterization of Photovoltaic Module Performance,” *Sustainable Energy Technologies and Assessments*, Elsevier, under review.